POWER REACTOR TECHNOLOGY

A Quarterly Technical Progress Review

Prepared for DIVISION OF TECHNICAL INFORMATION, USAEC, by
W. H. ZINN and J. R. DIETRICH, GENERAL NUCLEAR ENGINEERING CORPORATION

March 1962

● VOLUME 5

● NUMBER 2

TECHNICAL PROGRESS REVIEWS

To meet the needs of industry for concise summaries of current atomic developments, the Atomic Energy Commission is publishing this series, Technical Progress Reviews. Issued quarterly, each of the reviews digests and evaluates the latest findings in a specific area of nuclear technology and science.

The four journals published in this series are:

Nuclear Safety, W. B. Cottrell, Editor, W. H. Jordan, Advisory Editor, and associates, Oak Ridge National Laboratory

Power Reactor Technology, W. H. Zinn and J. R. Dietrich, General Nuclear Engineering Corporation

Reactor Materials, R. W. Dayton, E. M. Simons, and associates, Battelle Memorial Institute

Reactor Fuel Processing, Stephen Lawroski and associates, Chemical Engineering Division, Argonne National Laboratory

Each journal may be purchased ($2.00 per year for subscription and individual issues $0.55) from the Superintendent of Documents, U. S. Government Printing Office, Washington 25, D. C. See back cover for remittance instructions and foreign postage requirements.

Availability of Reports Cited in This Review

Unclassified AEC reports are available for inspection at AEC depository libraries and are sold by the Office of Technical Services, Department of Commerce, Washington 25, D. C. Some of the reports cited are not available owing to their preliminary nature; however, the information contained in them will eventually be made available in formal progress or topical reports.

Unclassified reports issued by other Government agencies or private organizations should be requested from the originator.

Unclassified British and Canadian reports may be inspected at AEC depository libraries. British reports are sold by the British Information Service, 45 Rockefeller Plaza, New York, N. Y.; Canadian reports (AECL series) are sold by the Scientific Document Distribution Office, Atomic Energy of Canada, Ltd., Chalk River, Ontario, Canada.

Classified U. S. and foreign reports identified in this journal as Classified may be purchased by properly cleared Access Permit Holders from the Division of Technical Information Extension, U. S. Atomic Energy Commission, P. O. Box 1001, Oak Ridge, Tenn. Such reports may be inspected at classified AEC depository libraries.

POWER REACTOR TECHNOLOGY

A REVIEW OF RECENT DEVELOPMENTS

Prepared for DIVISION OF TECHNICAL INFORMATION, USAEC,
by W. H. ZINN and J. R. DIETRICH,
GENERAL NUCLEAR ENGINEERING CORPORATION

● MARCH 1962

● VOLUME 5

● NUMBER 2

Foreword

This quarterly review of reactor development has been prepared at the request of the Division of Technical Information of the U. S. Atomic Energy Commission. Its purpose is to assist interested organizations in the task of keeping abreast of new results in reactor technology for civilian application.

Power Reactor Technology contains reviews of selected recently published reports that are judged noteworthy, in the fields of power-reactor research and development, power-reactor applications, design practice, and operating experience. It is not meant to be a comprehensive abstract of all material published during the quarter, nor is it meant to be a treatise on any part of the subject. However, related articles are often treated together to yield reviews having some breadth of scope, and from time to time background material is added to place recent developments in perspective.

The intention is to cover the various areas of reactor development from the general viewpoint of the reactor designer rather than from the more detailed points of view of specialists in the individual areas. To whatever extent the coverage of *Power Reactor Technology* may occasionally overlap the fields of the other Technical Progress Reviews, the overlaps will be motivated by this objective of viewing current progress through the eyes of the reactor designer.

A degree of critical appraisal and some interpretation of results are often necessary to define the significance of reported work. Any such appraisals or interpretations represent only the opinions of the reviewers and the editor of *Power Reactor Technology*, who are General Nuclear Engineering Corporation personnel. Readers are urged to consult the original references in order to obtain all the background of the work reported and to obtain the interpretation of the results given by the original authors.

W. H. ZINN, President
J. R. DIETRICH, Vice President and Editor
General Nuclear Engineering Corporation

Contents

Issued quarterly by the U. S. Atomic Energy Commission. Use of funds for printing this publication approved by the Director of the Bureau of the Budget on November 1, 1960.

Section

I

Power Reactor Technology

Reactor Physics

Critical and Exponential Experiments

The Physical Constants Testing Reactor (PCTR) at Hanford Atomic Products Operation (HAPO) has been used to perform experiments[1] in which lattice parameters for a 2.50-in.-diameter fuel element of natural enrichment were determined. The experiments provided measurements of infinite multiplication factor (k_∞), thermal utilization factor (f), resonance escape probability (p), and fast-fission factor (ϵ) for a $10^1/_2$-in. graphite lattice which uses both water and air in the coolant channel. The four-factor formula was then used to calculate a value of η. The December 1961 issue of *Power Reactor Technology*, Vol. 5, No. 1, contains a review of similar experiments, which were performed to obtain measurements of the same lattice parameters for a tubular natural-uranium fuel element (inside diameter, 2.00 in.; outside diameter, 2.50 in.).

Four-foot-long exponential piles were used at HAPO to measure[2] the material bucklings for various lattice arrays of hollow-tube and rod-in-tube, natural-enrichment, aluminum-clad fuel elements. The hollow-tube fuel elements had an outside diameter of 2.5 in. and an inside diameter of 1.6 in. The same tubes, along with concentric rods of 1.17-in. diameter, were used to make the rod-in-tube fuel elements. Experiments were performed with both water and air in the coolant channels. Measurements were obtained for the following lattice spacings: $8^3/_8$, $10^3/_8$, $12^3/_8$, and $14^9/_{16}$ in. Volume ratios of carbon to uranium varied from 15 to 70. A water-to-uranium volume ratio of 1.286 was used for the hollow-tube fuel-element experiments; however, a water-to-uranium volume ratio of 0.628 was used for rod-in-tube fuel-element experiments.

The Zero Power Reactor III (ZPR-III), located at the Argonne National Laboratory facilities in Idaho (at the National Reactor Testing Station), was used to perform critical studies of a dilute oxide fast-reactor core.[3] An oxide fuel was simulated by the use of uranium metal and alumina (Al_2O_3). The alumina served as the source of oxygen and was so distributed as to provide an oxygen-to-uranium atomic ratio of 1:1. Stainless steel and metallic aluminum were also included in the core. Measurements were made of the critical mass and fission ratio (measured average fission cross section for a given fissile material divided by the average measured fission cross section for U^{235}). The reactivity worths of various materials that were placed in the center of the core, the reactivity worths of distributed materials, and the average neutron lifetime were also measured. In both this and a previous set of experiments (uranium-to-oxygen atomic ratio of 1:2), there was a notable discrepancy between the calculated and the measured critical masses. Although no explanation of this discrepancy is given, it is concluded in reference 3 that the discrepancy in the calculation of the critical mass is not due to the oxygen in the fuel.

The ZPR-III was also used to conduct a set of similar experiments[4] in which uranium carbide was the simulated fuel. The uranium was 30.7 per cent enriched in U^{235}, and the over-all uranium-to-carbon atomic ratio was 0.946. A critical mass of 503.01 kg of U^{235} was required. The parameters measured in the dilute uranium carbide studies were the same as those determined in the dilute uranium oxide experiments, namely, critical mass, fission cross-section ratios, central reactivity coefficients, hetero-

geneity effects, reactivity worth of distributed materials, and prompt-neutron lifetime.

Experiments were performed in two critical assemblies to provide data[5] in support of the preliminary design study for the Argonne High-Flux Reactor (AHFR). The two assemblies were used to simulate an end-of-cycle AHFR core and a cold clean core. The latter contained 34.34 kg of evenly distributed stainless steel to simulate a burnable poison. Each core was composed of an internal parallelepiped thermal column of H_2O (12.7 by 12.7 by 50.8 cm), surrounded by a 100-liter fuel zone. A radial reflector of 90 vol.% beryllium and 10 vol.% water and Plexiglas was used. The end reflectors were pure water. Forty fuel clusters that contained 3.64 kg of highly enriched uranium were used for the end-of-cycle core. The 40 fuel clusters in the cold clean core contained 7.25 kg of highly enriched uranium. Measurements were made of flux distributions; cadmium ratios; temperature and void coefficients; and control rod, beam hole, and reflector reactivity worths.

Critical experiments[6] were performed at the Special Power Excursion Reactor Test (SPERT) facility to determine the degree of accuracy obtained in the use of a four-group diffusion-theory calculational method. These experiments used close-packed lattices of SPERT-III, highly enriched, plate type, stainless-steel-clad fuel assemblies. Slab geometry was used for all the experiments. In some of the arrays a central, water-filled, square-shaped control rod was fully inserted into the core. Since reactor control was accomplished by varying the water-moderator height, criticality data were obtained for partial water-height cores.

A brief review of the Multi-region Reactor Lattice Studies Program, conducted by the Westinghouse Atomic Power Department, was given in *Power Reactor Technology*, Vol. 5, No. 1. Final compilations of the analytic and experimental procedures and results from two of the four phases of the investigation are presented in references 7 and 8.

Reference 7 is concerned with the methods and results of measurements and calculations of the microscopic parameters and modified conversion ratios (phase four of the over-all program) in single-region and multiregion cores containing stainless-steel-clad, low-enrichment, UO_2 fuel rods. Chapter III of reference 7 contains a discussion of the experimental methods used to measure the following:

1. The U^{238} cadmium ratio that is used to calculate the ratio of resonance capture in U^{238} to thermal capture in U^{238}
2. The U^{235} cadmium ratio that is used to calculate the ratio of resonance fission in U^{235} to thermal fission in U^{235}
3. The ratio of fissions in U^{238} to those in U^{235} from which ϵ, the fast-fission factor, is calculated
4. A modified form of the conversion ratio, i.e., the ratio of total capture in U^{238} to total fission in U^{235}

Also included are discussions of the measurements made to determine the possible effects of lattice perturbations due to the presence of cadmium and the random and systematic errors that may be associated with activation measurements.

The calculational methods, and results thereof, used to analyze the experimental data are discussed in Chapter IV of reference 7. Multigroup computer codes (MUFT-SOFOCATE and MUFT-Repetitious-SOFOCATE), with supplementary resonance information provided by Monte Carlo calculations, were used in the calculation of the macroscopic lattice parameters.

Chapter V contains a detailed comparison of the results from the theoretical analyses and the experimental investigations. Possible sources of error associated with theory and experiment are discussed. In Chapter II the agreement between theory and experiment is concluded to be relatively good except when measurements are made near a region interface in a multiregion core. It is further concluded that perturbations are introduced into the lattice if cadmium is used in the measurement of a reaction rate. If the cadmium ratio is close to unity, the effect of these perturbations is accentuated in the process of analyzing the experimental data, and the resulting correlation between theory and experiment is poor.

Reference 8 presents detailed accounts of the experimental and analytic methods used to determine reactivity values and spatial neutron and source distributions for moderating ratios of 2.4:1 and 4.5:1 (phase three of the Multiregion Reactor Lattice Studies Program). The light-water-moderated single-region and multi-

region cores contained stainless-steel-clad UO_2 fuel rods with enrichments of 1.6, 2.7, and 3.7 per cent U^{235}.

The agreement between theory and experiment in the determination of criticality and source and flux distributions was concluded to be excellent. Both diffusion-theory and transport-theory IBM-704 codes were used in the analyses, and note is made of the conditions under which one or the other method provided better agreement with the experiments. The analyses resulted in the formation of a consistent computational scheme that may be directly used in the nuclear design of multiregion cores.

The material bucklings for two different lattice arrays of fuel assemblies that are identical to those which will be used in the Swedish R-3/Adam reactor were determined experimentally[9] in the Process Development Pile at the Savannah River Laboratory (SRL).* The natural-uranium oxide fuel rods were 1.70 cm in diameter and were clad in Zircaloy-2 tubes (inside diameter, 1.72 cm; outside diameter, 1.86 cm). Nineteen such fuel rods, arranged in the form of a hexagon, constituted a fuel assembly. Interassembly pitches of 9.33 and 12.22 in. were used for the experiments performed in the lattices, which were moderated by D_2O. The material bucklings were determined by means of a critical substitution technique wherein an unknown lattice (in this case the lattices made up of R-3/Adam type elements) is compared to a reference lattice. The reference lattices for these experiments were composed of 31-rod clusters of $\frac{1}{2}$-in.-diameter UO_2 fuel pellets which were contained in aluminum tubes. When necessary, copper rods were used as a poison in the reference lattices in order to determine a range of material bucklings.

To aid in the specification of the fuel enrichment for the Hallam Nuclear Power Facility, exponential experiments[10] that used uranium-molybdenum fuel elements were conducted. The fuel enrichment was 3.448 wt.% U^{235}. The geometry and composition of the 18-rod clusters used as fuel assemblies in the exponentials were described in *Power Reactor Technology*, Vol. 5, No. 1. A graphite-moderated square lattice and three graphite-moderated hexagonal lattices of different pitches were employed. The hexagonal arrays investigated in these experiments had lattice pitches of 13, 16, and 19 in. The square-lattice pitch was 9.5 in. Values of the material bucklings for each array were inferred from measurements of the gross horizontal and vertical neutron-flux distributions made with and without the fuel. The thermal utilization factors were determined for the hexagonal lattices from detailed measurements of the neutron flux within the lattice cells. The ratio of resonance to thermal-capture probability in U^{238} and the ratio of U^{238} fissions to U^{235} fissions were also determined from measurements in the hexagonal lattices.

*A report of buckling measurements on R-3/Adam lattices, at elevated temperatures, in the Pressurized Subcritical Experiment at SRL is Report DP-613, PSE Measurements on R-3/Adam Lattices, by N. P. Baumann. This report will be reviewed in the next issue of this journal.

Neutron Rethermalization

The initial Hanford investigation of neutron rethermalization, in the vicinity of a temperature discontinuity in the moderator, was reviewed in the June 1960 issue of *Power Reactor Technology*, Vol. 3, No. 3, page 1, and is described in reference 11. Reference 12 is an account of later work in the same program, which has introduced substantial improvements in the experimental techniques and in the technique of analysis. As before, the measurements were made in the PCTR, but the geometry of the moderator region was changed from a finite slab geometry to a cylindrical geometry; specifically, an annular ring of fuel elements surrounded an annular region of graphite, which in turn enclosed a thermally insulated cylinder of graphite. The temperatures of the inner cylinder and the surrounding graphite annulus could be adjusted independently. For the experiments with water, the inner cylinder of graphite was replaced by an annulus which provided, at its center, for a 6.8-cm-diameter thermally insulated cylinder of H_2O. In the graphite experiments rethermalization cross sections were determined for (1) neutrons at various temperatures incident upon graphite at a fixed temperature of 300°K and (2) neutrons at a fixed temperature of 300°K incident upon graphite at various temperatures. The water rethermalization experiments yielded rethermalization cross sections for neutrons of various temperatures incident upon H_2O at 300°K.

The temperature discontinuity occurred between the annulus of graphite and the inner cylinder. As in previous analyses[11] neutrons in equilibrium with each moderator region were assumed to lie in a thermal-energy spectrum with the Maxwellian distribution characteristic of the physical temperature of the moderator. Neutrons diffusing from one moderator region to the other were assumed to be transferred from their original spectrum to the spectrum characteristic of the new region in, effectively, single collisions whose probability is described by the rethermalization cross section, Σ_{reth}. The cross sections were determined by fitting theoretical curves, consistent with this two-thermal-group picture, to the experimental activation curves for $1/v$ detector traverses of the two moderator regions. A bivariant iteration process was employed to determine those rethermalization cross sections for both regions which would provide the best agreement between the theoretical and experimental activation traverses. The analysis differed from that previously reported[11] in that the temperature dependence of the graphite diffusion coefficient was taken into account and the upscattering and downscattering probabilities were not assumed to be equal. The results for rethermalization in graphite were substantially different from those previously reported; much of this difference is attributable to the more detailed analytical method.

The experimentally determined rethermalization cross sections, relaxation lengths (L_{reth}), and effective masses (M_{eff}) of the scattering centers are given, for graphite and water, in Tables I-1 and I-2. The definitions of the important quantities are as follows:

$$L_{reth}\ (T_n,\ T_g) = [D\ (T_n,\ T_g)/\Sigma_{reth}\ (T_n,\ T_g)]^{1/2}$$

$$M_{eff}\ (T_n,\ T_g) = 2\,\Sigma_s\ (T_n,\ T_g)/\ \Sigma_{reth}\ (T_n,\ T_g)$$

where T_n = neutron temperature in the thermal group before rethermalization (T_n is equal to T_1 for neutrons from region 1 being rethermalized in region 2, and T_n is equal to T_2 for neutrons from region 2 being rethermalized in region 1)

T_g = moderator temperature

$D\ (T_n,\ T_g)$ = diffusion constant for neutrons of temperature T_n in moderator of temperature T_g, etc.

Cross Sections

Two 19-level sets of cross sections are presented in reference 13; one set is for beryllium, which includes the $(n,2n)$ and (n,α) reactions in beryllium, and the other set is for U^{235}. These cross-section sets can be used with diffusion-theory codes of General Electric's Aircraft Nuclear Propulsion Department (GE ANPD) to produce analytical results within ±1 per cent of the experimental multiplication constant for beryllium oxide-reflected systems having thermal-fission fractions between 5 and 51 per cent. Also described in the reference are several critical experiments that were specifically designed for theory-experiment correlation of beryllium- and beryllium oxide-moderated systems. Five such experiments were performed at Livermore and six at GE ANPD. These experiments were analyzed using a 19-group neutron-diffusion code and were used to evaluate several sets of beryllium cross sections. Calculations of beryllium- and beryllium oxide-moderated reactors which are made using isotropic scattering cross sections for beryllium, and which neglect the $(n,2n)$ reaction, yield multiplication constants that are as much as 10 per cent too low; much of this discrepancy is attributed to the omission of the $Be(n,2n)$ reaction. When the $(n,2n)$ cross sections established by these studies were used with a revised set of U^{235} cross sections, the above-mentioned very good agreement on multiplication constants was obtained.

Reference 14 describes a comparison between the Westcott[15] scheme* for obtaining thermal-group effective cross sections and the MUFT-SOFOCATE cross-section schemes. MUFT is a multigroup Fourier transform code, developed at Westinghouse Atomic Power Department (WAPD), which calculates the energy distribution of neutrons slowing down from a fission source, and, by use of this distribution, calculates average thermal-group constants by first computing the Wigner-Wilkins flux spectrum and then averaging the constants over that spectrum. The MUFT-SOFOCATE method was developed for the typical H_2O-moderated reactor, which employed enriched fuel and which had a relatively important epithermal component of

*The most recent compilation of effective cross sections by Westcott is listed as reference 16.

Table I-1 RETHERMALIZATION PROPERTIES OF GRAPHITE[12]

Experiment	Temp. of cylinder, °K	Temp. of annulus, °K	Properties of graphite at T_1 for neutrons at T_2				Properties of graphite at T_2 for neutrons at T_1			
			Diffusion coefficient, cm	Rethermalization cross section,* cm^{-1}	Relaxation length, cm	Effective mass, amu	Diffusion coefficient, cm	Rethermalization cross section,* cm^{-1}	Relaxation length, cm	Effective mass, amu
	T_1	T_2	D	$\Sigma_{2\to1}$	$L_{2\to1}$	M_{eff}	D	$\Sigma_{1\to2}$	$L_{1\to2}$	M_{eff}
A	144	283	0.849	0.0092	9.60	83.2	0.900	0.0157	7.58	49.1
C	523	299	0.828	0.0468	4.21	16.4	0.794	0.0435	4.28	17.7
D	690	308	0.828	0.0665	3.53	12.0	0.782	0.0446	4.19	17.3
E	828	315	0.825	0.0691	3.46	11.1	0.776	0.0408	4.36	18.9

Graphite density = 1.614 g/cm^3.
Theoretical gaseous graphite: $\Sigma_{2\to1} = 0.0665\ cm^{-1}$; $L_{2\to1} = 3.53$ cm; $M_{eff} = 12.011$ amu.
*All cross sections have an uncertainty of ±10 per cent. Macroscopic scattering cross section of graphite = $0.399\ cm^{-1}$.

Table I-2 RETHERMALIZATION PROPERTIES[12] OF WATER AT 300°K

Experiment	Neutron temp., °K	Diffusion coefficient, cm	Rethermalization cross section, cm^{-1}	Relaxation length, cm	Effective mass, amu
B	410	0.1749	1.25	0.37	4.96
E	558	0.2112	1.27	0.41	4.53
D	720	0.2290	0.74	0.56	7.30

Water density = 1.0 g/cm^3.
Macroscopic scattering cross section of water = $3.38\sqrt[4]{T_0/T}\ cm^{-1}$.
Theoretical effective mass of H_2O = 18.016 amu.

neutron absorption; the Westcott scheme was intended for well-moderated systems, typified by the D_2O-moderated, natural-uranium reactor, and the existence of limits to its applicability has always been recognized.

It is perhaps not surprising that the two methods predict different reactivity lifetimes for a given reactor. However, reference 14 shows also that the two methods differ substantially in predicting the reactivity of relatively small, aqueous homogeneous critical assemblies fueled with plutonium and that the Westcott scheme, in these cases, gives better agreement with experiment. The resolution of these differences, for the purpose of improving reactivity lifetime calculations, is the motivation for the work described in the reference. Two critical plutonium cores, a plutonium-fueled Materials Testing Reactor (MTR) loading, and various reactivity measurements on irradiated UO_2 at the MTR Reactivity Measurement Facility were analyzed using constants determined by MUFT-SOFOCATE and by the Westcott scheme. Also, the effective cross sections given by the two schemes were compared with recent microscopic cross-section data. The following conclusions were drawn:[14]

1. Westcott's method yields better agreement with plutonium experiments for well-moderated reactors than does the MUFT-SOFOCATE method with the presently used cross sections, the main reason being a 3 per cent higher value of the thermal eta for Pu^{239} in Westcott's method, which is in better agreement with recent cross-section measurements.

2. The Wigner-Wilkins flux spectrum of SOFOCATE represents the spectrum when a large amount of thermal resonance material is present much better than a hardened Maxwellian spectrum, as in Westcott.

3. MUFT does allow variation of the effective resonance integrals with dilution, but neither the Westcott scheme nor the usual fast-fitted CANDLE (a WAPD lifetime code that was used with MUFT-SOFOCATE cross sections for burnup calculations) scheme allows for changes in the effective resonance integrals during lifetime.

4. The epithermal α values used by Westcott seem to be too small and hence lead to too optimistic an estimate of lifetime for the drier, more epithermal, lattices.

In short, the conclusion appears to be that the discrepancies exhibited by the MUFT-SOFOCATE system are not fundamental but are traceable to the microscopic data used, and, in the case of reactivity lifetime calculations, to the handling of the effective cross sections in the lifetime calculation proper. Recommendations are made for improving these shortcomings.

Reference 17 is of interest in connection with the Westcott formulation. The reference gives effective cross sections for Pu^{239}, U^{235}, and U^{233}, which were derived by use of the experimentally measured spectrum in a Calder Hall lattice of natural uranium and graphite, as functions of the moderator temperature. These effective cross sections are compared with similar data published by Westcott,[16] which used the same experimental neutron spectrum but different calculational methods to obtain the effective cross sections. The two sets of data were in almost complete agreement. It is pointed out that the neutron spectrum was measured in the moderator of a graphite-uranium system, and that, strictly speaking, the effective cross sections apply for reaction rates in the moderator.

The low-energy total neutron cross section of Pu^{241} has been measured from 0.02 ev to 2 kev and is reported in reference 18. The cross section was determined from the measured neutron transmission in PuO_2 which was enriched to 81 per cent in Pu^{241}. Measurements were made using the MTR fast-neutron chopper. A study to determine the extent of the Doppler distortion of the resonances in Pu^{241} below 11 ev, at temperatures ranging from 0 to 2000°C, was also made and is discussed in the reference.

Reference 19 reports a consistent set of energy-dependent U^{235} partial cross sections, i.e., σ_γ, σ_f, σ_s, and σ_t, from 10^{-3} to 10^7 ev, that have been compiled for use in the analysis of thermal or intermediate reactor systems. An attempt has been made to present these data in the form most useful for reactor analyses: the cross sections are given in detailed graphic form for the energy range from 10^{-3} to 60 ev; quarter-lethargy-group cross sections averaged over a constant lethargy flux are graphed for the energy range from 0.414 to 10^7 ev, and 100 energy points are tabulated from 10^{-3} to 2.5 ev. The cross sections were obtained by analytical extensions of the existing experimental data. The partial cross sections that are presented were compared with integral experiments reported in the literature: specifically,

they were checked against reported measured values for the fission- and capture-resonance integrals of U^{235} and reported integral and monoenergetic measurements of α for U^{235}. In general, good agreement was observed.

In reference 20 a quite extensive treatment of the energy-dependent cross sections is made for U^{233}, U^{234}, U^{235}, U^{236}, Np^{239}, Pu^{239}, Pu^{240}, Pu^{241}, Pu^{242}, the fission-product aggregates of U^{233}, U^{235}, and Pu^{239}, and certain specific fission products. The data are given at 100 energy points over the range from 0.005 to 2.5 ev, a form suitable for the thermalization codes in use at General Atomics. The cross sections were derived from several sources, including direct experimental data, information recorded in BNL-325 and its supplement, calculations using the Breit-Wigner single-level formula with appropriate resonance parameters, results of a multilevel treatment by Vogt, and from the fission-products work of Garrison and Roos. Comparisons of several measured and calculated spectra are given in the reference; these comparisons demonstrate the current success of theoretical efforts to reproduce the experimental results of neutron thermalization. Examples of thermal spectra, the associated spectrum-average cross section, and "effective" cross sections for carbon: U^{235} atom ratios between 2819 and 10,000, with moderator temperatures ranging from 300 to 2400°K, are also recorded.

References 21 and 22 give cross sections for Th^{232} and Pu^{240}, which include the effects of target temperature. Total, scattering, and radiative-capture cross sections for Th^{232} are presented by reference 21 in both graphic and tabular form as functions of energy from 0.0253 to 0.999 ev and for thorium temperatures from 0.0253 to 500 ev. The total, scattering, radiative-capture, and a portion of the fission cross sections are similarly given in reference 22 for Pu^{240} as functions of neutron energy between 0.0253 and 120 ev and for Pu^{240} temperatures in the range 0.253 to 0.2 ev. Cross sections in these two references were calculated by use of the Breit-Wigner single-level formula, using several experimental sources for level parameters and radiation widths, and the Breit-Wigner analysis was folded into a Maxwellian velocity distribution.

The calculation of thermal average cross sections by means of Maxwellian averages is reviewed in reference 23. A numerical integration scheme for calculating the average over the Maxwellian energy distribution is used, and an IBM-704 program for computing these averages is described.

References

1. D. E. Wood and E. Z. Block, Lattice Parameters for a 2.5-Inch Natural Uranium Fuel Element, in Physics Research Quarterly Report, October, November, December, 1960, USAEC Report HW-68389, pp. 59–74, Hanford Atomic Products Operation, Jan. 20, 1961.
2. G. W. R. Endres and D. E. Wood, Material Bucklings of Large Diameter Fuel Elements in Graphite Lattices, in Physics Research Quarterly Report, January, February, March, 1961, USAEC Report HW-69475, pp. 40–55, Hanford Atomic Products Operation, Apr. 20, 1961.
3. P. I. Amundson et al., Critical Studies of a Dilute Oxide Fast Reactor Core (ZPR-III Assembly 30), USAEC Report ANL-6337, Argonne National Laboratory, May 1961.
4. R. J. Huber et al., Critical Studies of Dilute Carbide Fast Reactor Core. ZPR-III Assembly 34, USAEC Report ANL-6401, Argonne National Laboratory, May 1961.
5. J. W. de Villiers (Ed.), Critical Experiments for the Preliminary Design of the Argonne High Flux Reactor, USAEC Report ANL-6357, Argonne National Laboratory, June 1961.
6. A. H. Spano, Experimental and Analytical Reactivity Studies of Clean Critical Stainless Steel Cores, USAEC Report IDO-16691, Phillips Petroleum Co., June 16, 1961.
7. P. W. Davison et al., Microscopic Lattice Parameters in Single- and Multi-Region Cores: A Comparison of Theory and Experiment, USAEC Report WCAP-1434, Westinghouse Electric Corp., Atomic Power Dept., June 1961.
8. W. J. Eich and W. P. Kovacik, Reactivity and Neutron Flux Distribution Studies in Multi-Region Loaded Reactor Cores, USAEC Report WCAP-1433, Westinghouse Electric Corp., Atomic Power Dept., June 1961.
9. W. E. Graves, R-3/Adam Lattice Buckling Measurements in the Process Development Pile, USAEC Report DP-598, Savannah River Laboratory, July 1961.
10. O. R. Hillig, Hallam Exponential Experiments Using U-Mo Fuel, USAEC Report NAA-SR-6118, Atomics International, Sept. 15, 1961.
11. R. A. Bennett and R. E. Heineman, Neutron Rethermalization Cross Section Measurements in Graphite, *Nuclear Sci. and Eng.*, 8(4): 294 (October 1960).
12. R. A. Bennett, Neutron Rethermalization in Graphite and Water, Part I, in Physics Research

Quarterly Report, October, November, December, 1960, USAEC Report HW-68389, pp. 28–49, Hanford Atomic Products Operation, Jan. 20, 1961.

13. F. G. Dawson, Evaluation of Beryllium and Uranium Cross Sections for Neutron Diffusion Theory Calculations, USAEC Report APEX-633, General Electric Co., Aircraft Nuclear Propulsion Dept., October 1958 (published August 1961).
14. E. Fein and L. C. Noderer, An Evaluation of Effective Plutonium Cross Sections in Reactivity Calculations, USAEC Report CEND-146, Combustion Engineering, Inc., Sept. 30, 1961.
15. C. H. Westcott, Effective Cross-Section Values for Well-Moderated Thermal Reactor Spectra, Canadian Report CRRP-787 (AECL-670), Aug. 1, 1958.
16. C. H. Westcott, Effective Cross-Section Values for Well-Moderated Thermal Reactor Spectra (3rd Edition Corrected), Canadian Report AECL-1101, Nov. 1, 1960.
17. J. E. C. Mills and D. L. Reed, A Critical Study of Effective Fission Cross-Sections for Pu^{239}, U^{235}, and U^{233}, British Report AEEW-M-132, May 1961.
18. O. D. Simpson and N. H. Marshall, Doppler Broadening of the Low Energy Total Neutron Cross Section of Pu^{241}, USAEC Report IDO-16679, Phillips Petroleum Co., Aug. 4, 1961.
19. A. J. Goodjohn and N. F. Wikner, Maritime Gas-Cooled Reactor Program: Suggested Values for the Partial Cross Sections of U^{235} for Use in the Neutronic Analysis of Thermal and Intermediate Reactors, USAEC Report GA-2151, General Atomic and Electric Boat Divs., General Dynamics Corp., July 17, 1961.
20. N. F. Wikner and S. Jaye, Energy-Dependent and Spectrum-Averaged Thermal Cross Sections for the Heavy Elements and Fission Products for Various Temperatures and C : U^{235} Atom Ratios, USAEC Report GA-2113, General Atomic and Electric Boat Divs., General Dynamics Corp., June 16, 1961.
21. J. J. Devaney et al., Thorium Cross Sections and Their Temperature Dependence, USAEC Report LA-2525, Los Alamos Scientific Laboratory, July 13, 1961.
22. J. J. Devaney and L. Bordwell, Plutonium-240 Cross Sections and Their Temperature Dependence, USAEC Report LAMS-2574, Los Alamos Scientific Laboratory, Aug. 21, 1961.
23. J. R. Terrall and A. H. Barnett, Calculation of Thermal Average Cross Sections, USAEC Report APEX-626, General Electric Co., Aircraft Nuclear Propulsion Dept., August 1961.

Section

II

Power Reactor Technology

Heat Transfer and Fluid Flow

Conduction

The thermal conductivity of reactor materials, particularly of fuels, continues to be of interest to the design engineer. Reference 1 is a discussion of the thermal conductivity of metallic, nonmetallic, and heterogeneous materials. A discussion of radiant heat transfer is included, which is of particular interest in view of the recent information on the postulated improvement of the thermal conductivity of UO_2 at high temperatures due to radiant heat transfer.[2] At the time of the writing of reference 2, measurements of the thermal conductivity of UO_2 had been reported only to temperatures of about 2000°F, where radiant heat transfer is small. Recently, however, these measurements have been extended to over 3800°F, and, at these temperatures, radiant heat transfer becomes significant. Figure II-1 is a plot of the curve of Bates,[2] plus data of Deem and Lucks[3] and Reiswig.[4] Although the experimental data shown are not in good agreement, they indicate that the minimum value of thermal conductivity has not been reached. This minimum value occurs at the point where the dominant mode of heat transfer changes from conduction to radiant heat transfer and generally occurs[1] at about 2700°F for polycrystalline, nonmetallic materials. Although the Battelle Memorial Institute data[3] lie at temperatures just below this temperature, they still fall close to a $1/T$ variation; both sets of experimental data do, in fact, appear to be measuring only the lattice conduction contribution. Whether this is due to the experimental methods used, to the absence of important radiant heat transfer in the range measured, or to some other cause is a question of some importance to the designer. A good discussion of the mechanisms of high-temperature transport of heat is in reference 5, which also discusses in considerable detail some methods for measuring thermal conductivity.

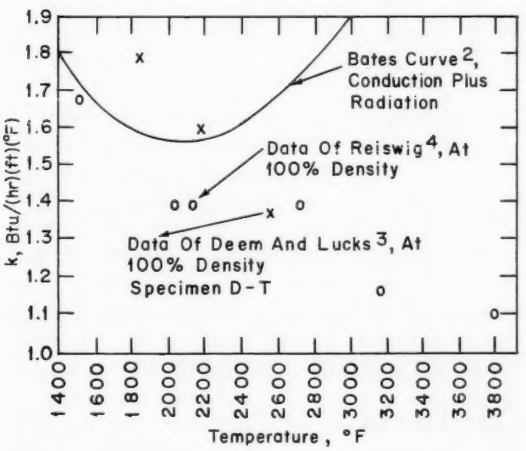

Fig. II-1 Thermal conductivity of UO_2 vs. temperature.

References 1, 3, and 5 discuss the effect of irradiation on thermal conductivity, and reference 3 presents some interesting data on the experimentally observed thermal conductivity of irradiated UO_2. Since the data are tentative and subject to rechecking, they will not be reproduced here, but they show the annealing-out of radiation damage as a function of temperature. Additional data on the conductivity of irradiated UO_2 have recently been reported.[6] The basic purpose of the experiments reported in reference 6 was that of improving the thermal conductivity of UO_2 by the addition of small amounts of other oxides, such as CaO, Y_2O_3, and Nb_2O_5; it was found, however, that these additives decreased, rather than increased, the thermal conductivity. During the course of the studies, undoped UO_2 was used as a "control" and was irradiated in the hydraulic rabbit fa-

Table II-1 CAPSULE DESCRIPTIONS[6]

Identity	Composition	Density, g/cm³	Diam., in.	Enrichment, % U^{235} in U†	Sheath*		Clearance	
					Thickness, in.	Inside diam., in.	Diametral, in.	Axial, in.
SE	UO_2	10.71	0.660	4.9	0.025	0.6684	0.008	0.054
SF	UO_2	10.71	0.660	4.9	0.025	0.6684	0.008	0.054

* Stainless steel.

† Determined by analysis.

Table II-2 AVERAGE THERMAL CONDUCTIVITY[6]

Capsule identity	Melting diam., in.	$\int_{T_s}^{T_m} k\,d\theta$,* watts/cm	Av. k to melting,† Btu/(hr)(ft)(°F)	Grain-growth diam., in.	$\int_{T_s}^{T_g} k\,d\theta$,‡ watts/cm	Av. k to grain-growth temp., Btu/(hr)(ft)(°F)
SE	0	80	2.0	0.3	65§	3.0
SF	0.13	76.5	1.9	0.3	65§	3.0

* Determined from Eq. 18 of Canadian Report CRFD-835; evaluation of Bessel-function term from a graph of this function vs. r/a for an inverse diffusion length κ of 1.54.

† Estimated fuel-surface temperature = 662°F; measured UO_2 melting point = 4892°F; and measured solidus temperature of 3.85 mole % Y_2O_3 solid solution = 4953°F.

‡ Assuming a grain-growth temperature in each case of 2912°F and a surface temperature of 662°F.

§ This number was given as 0.65 in reference 6 and has been changed to be consistent with other data in the reference.—*The Editor*

cilities at Chalk River. The capsule descriptions are given in Table II-1. The existence of melting and grain growth, and the corresponding temperatures, were determined from post-irradiation metallurgical examination of the sectioned capsules. Table II-2 illustrates the results.

Reference 7 describes a transient method for the determination of the thermal diffusivity of metals up to over 3200° F, and data are presented for Armco iron, molybdenum, and titanium.

Reference 8 is another publication in the continuing attack on a difficult conduction problem—that of determining the temperature of a noninfinite solid which is pierced by coolant channels. The geometry studied is shown in Fig. II-2. Both regions A and B are allowed to generate heat; the illustration is for six off-center coolant channels at a temperature T_1 and surrounding a central channel at temperature T_0. An adiabatic boundary condition at a_0 is assumed, and convection boundary conditions in the coolant channels are allowed. The problem is not tractable without a computer, and information on a program for the IBM-7090 computer is included. The temperature field in an infinitely long, eccentrically hollow cylinder with uniform heat generation has been treated also.[9]

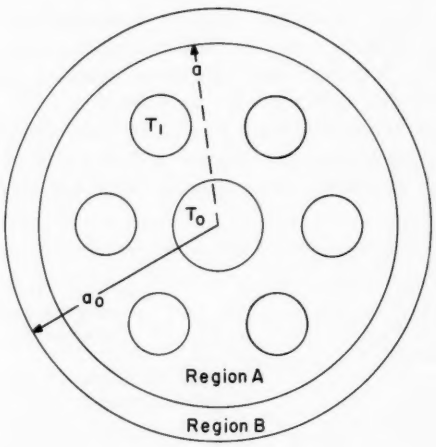

Fig. II-2 Normal cross section.[9]

Water and Gaseous Coolants

Roughened surfaces have been shown to increase burnout heat flux (see *Power Reactor Technology*, Vol. 3, No. 2, page 35); reference 10 presents a friction-factor correlation for

water flowing in an annulus with the inner wall roughened by medium-diamond knurls:

$$\frac{1}{\sqrt{f}} = (\mathrm{Re})^{0.14} \ln \sqrt{\frac{D_e}{\epsilon}} + \frac{29}{(\mathrm{Re})^{0.20}} \qquad (1)$$

The symbols have their conventional meanings, with ϵ being the depth of the roughness. The data lie within 10 per cent of the correlation, and the experimental limits are given in Table II-3. The extension of Eq. 1 to cover cases in which up to 60 per cent of the wetted perimeter is roughened is given by an approximate formula.

Table II-3 EXPERIMENTAL LIMITS[10] OF EQUATION 1

Type of roughness	Medium-diamond knurl
Depth of roughness	0.007 to 0.016 in.
Equivalent diameter	0.29 to 0.51 in.
Reynolds number	100,000 to 250,000
% of wetted perimeter roughened	33 to 39

Additional pressure-loss data are given in reference 11 for any incompressible gas. Complex flow circuits are considered for both series and parallel flow. The report contains an appendix that lists loss coefficients for 23 different duct fittings and connections; this section should serve as a ready source of information that otherwise appears to be scattered over a considerable volume of literature.

Pressure-volume-temperature data for water are contained in reference 12 for pressures up to about 10^7 psi and for temperatures up to 18,000°F.

Reference 13 reports on pool-boiling studies performed for pressures from 1.5 to 4000 psia and for fluid temperatures up to 800°F. Figure II-3 illustrates some of the data obtained and shows that the region wherein transitional boiling occurs is absent at the critical pressure (3208 psia) and above. The nucleate-boiling heat-transfer coefficient increases with pressure up to about 2800 psia and then decreases. Existing correlations of nucleate-boiling peak heat flux with heat-transfer coefficient are compared with the experimental data, and a new correlation is suggested. Heat-transfer coefficients in film boiling are evaluated and compare favorably with several existing correlations. The test section incorporated a sapphire viewing window that allowed observation of the test section at all experimental pressures, but few data are given in the report.

Reference 14 is concerned with local-boiling heat-transfer tests. Data were taken which utilized a tubular, heated test section having an inside diameter of 0.416 in. and a length of 30 in. The test section was appropriately instrumented to measure pertinent temperatures, pressures, flow rates, etc. Test conditions are given in Table II-4. Analysis of the data provided confirmation of the Jens and Lottes local-boiling heat-transfer correlation, although scale formation during the runs makes this conclusion subject to some uncertainties. The corrosion problem presumably was aggravated by the fact that continuous water purification was not provided in the test-equipment setup,

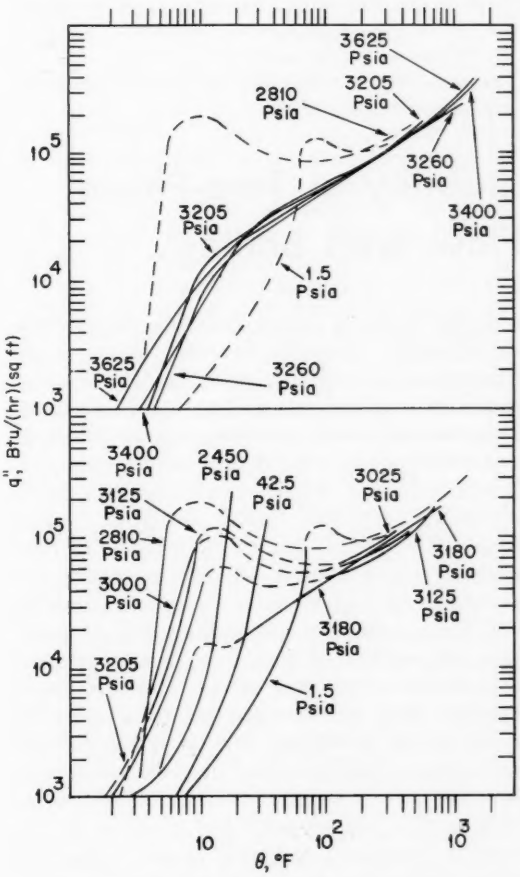

Fig. II-3 Heat flux vs. difference between wall and bulk fluid temperatures, ⅛-in. vertical-plate test section.[13]

Table II-4 LOCAL-BOILING STUDIES—TEST PARAMETERS

Pressure, psia	1100, 1200, and 1300
Inlet temperature, °F	425 and 445
Heat flux, Btu/(hr)(sq ft)	1.20 to 5.55 × 10^5
Mass velocity,* lb/(hr)(sq ft)	3.5 to 10 × 10^5

* Editor's Note: Calculated from data given in reference 14.

except for makeup water. Local-boiling pressure-drop data were correlated by use of an equation of the following form:

$$f/f_{iso} = a + b(\mathrm{St})(\mathrm{Pr})^{2/3} + c(\mathrm{Re}) \qquad (2)$$

where f/f_{iso} = ratio of local boiling to isothermal friction factor
a,b,c = correlation constants
St, Pr, Re = Stanton, Prandtl, and Reynolds numbers

Values of a, b, and c are given for the three pressures studied.

Stability of Two-Phase Flow with Boiling

In the design of boiling reactors, the question of hydraulic stability becomes of increased importance as attempts are made to attain high heat flux and high exit quality. Theoretical and experimental work continues on the problem, and references 15 to 21 represent recent publications on the subject, employing both analog and digital solutions to flow equations, coupled with experimental studies. Reference 15 presents solutions to the nonlinear one-dimensional equations of motion for a two-phase mixture, and these solutions are coupled with the equations of motion of the fluid in the external circuits to obtain the behavior of the entire system. Both forced- and natural-circulation systems can be studied. The two-phase mixture is assumed homogeneous; i.e., the assumption is made that its density, velocity, and pressure distributions can be described in terms of continuous functions, and slip is not allowed. A finite difference method is employed to solve the resulting equations, and a computer code is given. The channel power is assumed to be a chopped cosine. Provision is made for varying the power sinusoidally and for employing a time-independent power.

As an illustration of its use, the program was employed to study the experiments done by Levy and Beckjord. These experiments were reported in reference 22, which was reviewed in *Power Reactor Technology*, Vol. 4, No. 2.* Experimental runs were studied analytically, and it was substantiated that oscillations become more severe as subcooling, power, and channel-flow area are increased. An example is given in Fig. II-4. The particular parameter illustrated is subcooling; as subcooling increases, the loop oscillations become less damped and finally diverge in the case of 45 Btu/lb subcooling. The data illustrated are for natural-circulation runs, although a "boosting" pump was incorporated into the equations to ensure that the fluid was flowing in the proper direction when the power was switched on. This pump was then switched off after about a second to permit natural circulation. The major advantage of such a study, however, is the insight it gives into the detailed instability mechanism. The results given in reference 15 suggest that the inertial effect of the mixture in the chimney plays an important part. "Sharp" instabilities are defined as those for which the acceleration of the fluid at the heated channel inlet approaches infinity, and it is shown that the acceleration of the fluid at the outlet of the chimney is also large and of the opposite sign. The pressure must therefore be a maximum at the boiling boundary, and the reference illustrates that the pressure surge may be resolved as a shock. The damping effects of friction are discussed and are shown to be beneficial to stability. As the power is increased, the void fraction increases and the change in the pressure drop across the chimney, for a given change in inlet velocity to the test section, is relatively larger. This increased pressure drop

* Editor's Note: *Power Reactor Technology*, Vol. 4, No. 2, page 18, states that natural-circulation studies done at Bettis[23] appear to contradict the Levy-Beckjord data with respect to the effect of subcooling. Although the conclusion of reference 23 is that "these flow fluctuations increase at lower inlet subcooling...," Fig. 16 of reference 23 suggests that the flow fluctuations increase at lower inlet temperature. Therefore the Bettis and Levy-Beckjord papers appear to be in agreement on the effect of inlet subcooling.

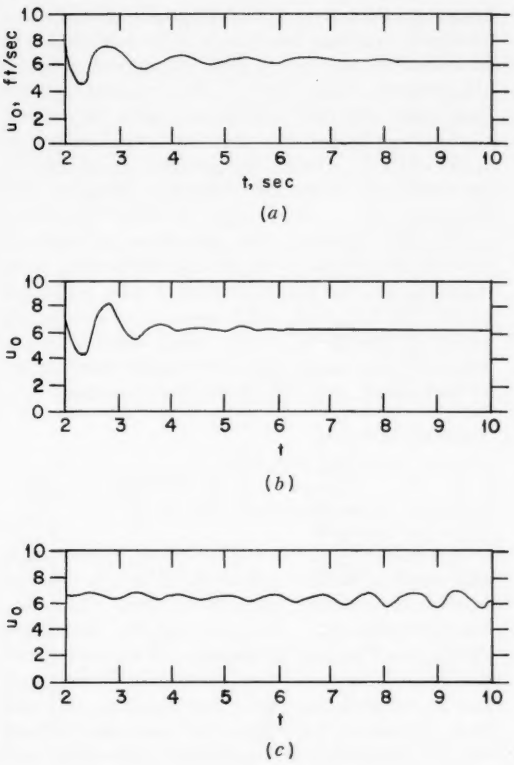

Fig. II-4 Velocity of the coolant at the channel inlet vs. time.[15] (*a*), subcooling = 35 Btu/lb. (*b*), subcooling = 40 Btu/lb. (*c*), subcooling = 45 Btu/lb.

is manifested in larger amplitudes of the other variables, with a resulting decrease in stability.

Reference 16 is another analytical study of the transient operation of two-phase natural-circulation loops. The flow equations were solved on both analog and digital computers, and the limitations and advantages of both systems are discussed. An important difference between references 15 and 16 is that the latter uses a separated-flow model wherein slip is allowed. The results of the digital treatment are compared with experimental data taken in the University of Minnesota two-phase heat-transfer loop at atmospheric pressure; digital runs for a pressure of 300 psia were also performed. In general, good agreement between analytical and experimental results was achieved. The following quotation from reference 16 will serve to summarize the results:

1. The power density (power per unit heater volume) at which oscillations occur has increased by nearly two orders of magnitude in going from one atmosphere to 300 psia.... The trend of increasing stability with pressure has been observed with all experimental test loops.

2. The specification of power density alone, or of any other single variable, is not sufficient for determining the unstable region. The instability is a complex function of power input, system geometry, inlet subcooling, and perhaps other variables. This feature is illustrated by the computed results which show that a region supporting sustained oscillations may be reached by varying either the subcooling or the power input. A similar conclusion, based on experimental results, has been made by Levy and Beckjord.

3. The region of instability appears to be a closed region, outside of which stable operation is possible. At both one atmosphere and at 300 psia, oscillatory behavior occurred at an intermediate range of operating conditions with steady behavior at extremes. There are, however, limitations imposed on the model used in the computer studies that may invalidate any practical application. An example of such a limitation is the possibility of burnout at high power inputs, or at lower inputs if oscillations alter the mechanism of heat transfer. In the model, an arbitrary heat source was assumed to exist without regard to any mechanism.

4. The frequency of oscillations at high pressure is approximately 30 times higher than that of the low-pressure oscillations, in agreement with experimental results. The absolute agreement of predicted and experimental frequencies is difficult to determine and not of vital concern, since no attempt was made to simulate exactly an existing physical apparatus. However, one may observe that at high pressure the frequency is approximately the natural frequency of the system, and the oscillations themselves are approximately harmonic. The natural frequency may be obtained by deriving equations in a LaGrangian system of coordinates, i.e., coordinates which move with the mean velocity of the fluid, and considering natural oscillations about this mean. Hence, the geometry, the mass of fluid within the loop, and the gradient of driving force and resisting force all play important roles in determining the frequency. At low pressure, the oscillations are not harmonic, but resemble relaxation oscillations. Here, again, the oscillatory period will depend on parameters of the system, but the actual and natural frequencies may be completely different. The actual frequencies are strong functions of the transport times within the loop.

5. The mechanism of two-phase vapor-liquid fluid flow and its transient behavior must be known accurately in order to predict the conditions under which instabilities occur, especially at high pressure. From the computed results one can see that solutions are very sensitive to the specification of slip ratio. Although the modification of the problem

to incorporate a variation of slip ratio with superficial velocity seems reasonable in the light of experimental results, it has not been established that the relations valid for steady flow are also valid for continuously time-varying flow.

6. The mechanism by which oscillations are initiated and sustained at high pressure appears to be essentially the same as that at low pressure despite the fact that in one case the oscillations appear to be relaxation oscillations and in the other case nearly harmonic. Differences do exist in the conditions surrounding the oscillatory states, but in each case the cause appears identical.

The reports of General Electric Company's Atomic Power Equipment Department (GE-APED) on the stability of marine-propulsion boiling-water reactors have been published.[17–19] Flow equations are presented which allow for separated flow,[17] but the manner of treating the interactions between the phases and the channel walls is different from that used in reference 16, being based on the momentum exchange model (*Power Reactor Technology*, Vol. 3, No. 4, page 28). The equations are solved by linearizing the equations about the steady state and by investigating the effects of small disturbances. This was done with an analog computer, and the results were compared to experiments done in the GE-APED heat-transfer loop. The comparison of transient responses to a 7 per cent step increase in heating rate is shown in Table II-5. The application of the analog program to the marine boiling-water reactor is illustrated in the reference but will not be discussed here. Reference 17 concludes as follows:

Table II-5 COMPARISON OF EXPERIMENTAL AND ANALYTICAL RESULTS[17]

Parameter	Observed	Computed
Inlet velocity transient, %	−32	−30.5
Oscillation period, sec	3.0	2.4
Damping factor	0.066	0.1

> The parameters governing two-phase flow loop dynamics are revealed by studying the loop equations. First we consider fluid transit time of the two-phase section. Because the loop driving force is weight difference of the columns, and because changes in the average void fraction are transported across the riser at the average two-phase fluid velocity, it is clear that the loop dynamics in the time domain will be dominated by the transit time. Another way of stating this fact is that a change in steaming conditions at the inlet builds up an effect on the driving head during one complete transit time of the riser.... Experimentally it has been noted that loop oscillations, when they occur, do so at cyclic periods a bit longer than the transit time. Analysis predicts the period of an oscillatory system $\frac{4}{3}$ to 2 times the two-phase section transit time.
>
> The second point is the dependence of steaming rate on inlet water velocity and subcooling. This dependence is the primary cause of flow pulsations in the A.P.E.D. loop, and it is of concern in the range of interest to boiling water reactor design. Paradoxically this cause is thermodynamic and not hydrodynamic. Consider the energy equation:
>
> Steaming heat rate
> = total heat rate
> − (subcooling per unit mass)
> × (mass flow rate) (area)
>
> If we suppose inlet velocity increases in a loop that has been in a steady state of operation, the equation states that steaming rate will decrease. The riser steam fraction will then decrease, and with it the driving head during the passage of a transit time. The loop velocity will decelerate as a consequence, and as velocity decreases, the steaming rate will rise. If certain conditions are met, the process will be oscillatory and undamped. The main conditions are that steaming be strongly dependent on inlet velocity, and that the natural circulation driving head be substantial. The conditions can be met with high subcooling and high heating rate. They can also be met at low heating rates with low inlet velocities, but the latter conditions are of less practical interest.

References 18 and 19 give additional information on the analog program plus initial experimental results on a "rocking" (movable) heat-transfer test section.

Reference 20 presents a stability criterion as follows:

$$\left(\frac{dp}{df}\right)_s - \left(\frac{dp}{df}\right)_d \ll 0 \qquad (3)$$

where dp/df is the slope of the coolant flow vs. pressure curve at the intersection of the supply and demand curves. The "demand" curve shows the pressure required to force a given amount of flow through the active portion of the test loop, whereas the "supply" curve illustrates the pressure drop made available to the test section as a function of flow rate.

The subscripts in Eq. 3 refer to the derivatives of the supply and demand curves, re-

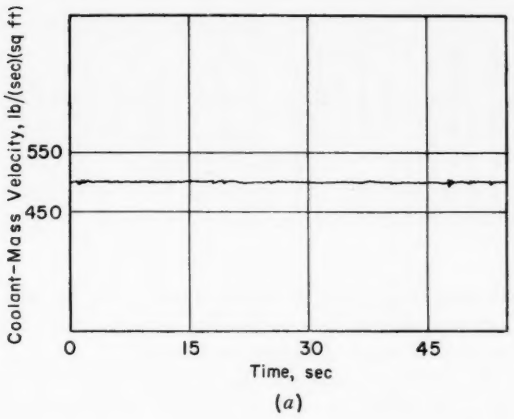

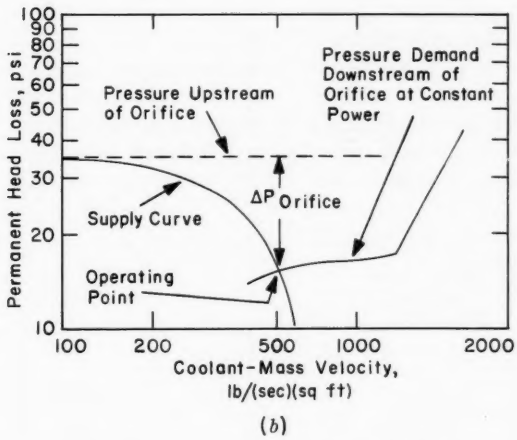

Fig. II-5 Effect of 20-psi inlet orificing on the stability of boiling-water flow.[20] (*a*) Flow trace, coolant-mass velocity vs. time. (*b*) Head loss vs. coolant-mass velocity. Test conditions: pressure = 795 psia, upflow in 18-ft-long tube, mass velocity = 500 lb/(sec)(sq ft), inlet subcooling = 52°C, power = 135 Mw/sq ft of coolant-flow area, exit quality = 23 per cent, heat flux = 288,000 Btu/(hr)(sq ft), tube diameter = 0.49 in.

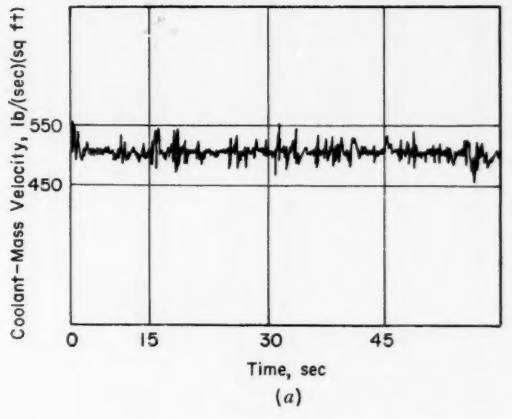

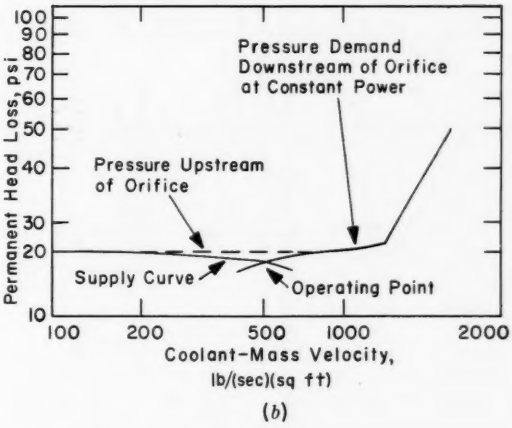

Fig. II-6 Effect of 1.2-psi inlet orificing on the stability of boiling-water flow.[20] (*a*) Flow trace, coolant-mass velocity vs. time. (*b*) Head loss vs. coolant-mass velocity. Test conditions: pressure = 795 psia, upflow in 18-ft-long tube, mass velocity = 500 lb/(sec)(sq ft), inlet subcooling = 52°C, power = 135 Mw/sq ft of coolant-flow area, exit quality = 23 per cent, heat flux = 288,000 Btu/(hr)(sq ft), tube diameter = 0.49 in.

spectively. The effect of inlet orificing can be seen in Figs. II-5 and II-6, which present data on the effect of inlet orificing on coolant-mass-velocity fluctuations. Reference 21 provides additional data on this stability criterion and reports on heat-transfer results employing an electrically heated 19-rod test section.

Boiling Burnout

The subject of boiling burnout continues to receive attention. References 24 and 25 are Pressurized-Water-Reactor (PWR) progress reports that contain a new departure from nucleate boiling (DNB) correlation, as follows:

$$\phi_{DNB}/10^6 = k\left(\frac{H' - H}{H' - H_0}\right)^{1/2} \qquad (4)$$

where $k = 0.84\left[1 + \left(\frac{2000 - P}{800}\right)^2\right]$

$$H_0 = 655 - 0.004\,(2000 - P)^{1.63}$$

Table II-6 DETAILS OF EXPERIMENTAL INVESTIGATIONS OF BURNOUT IN INTERNALLY HEATED VERTICAL ANNULI[26]

Source	Test-section geometry					Range of experimental variables			Comments
	Heater element outside diam., in.	Flow tube inside diam., in.	Test-section length, in.	Annular gap, in.	L/D_e of test section	Pressure, psia	Mass velocity, lb/(hr)(sq ft)	Steam quality at burnout, wt.%	
Engineering Research Laboratories, Columbia University (1960)	1.380	1.902	42	0.261	80.4	1000	$0.31-1.04 \times 10^6$	4.5–25.1	Forced-circulation subcooled water at test-section inlet; resistance-bridge burnout detector used; d-c heating
General Electric Co., U.S.A. (1957)	0.375	0.875	110	0.250	220	1000	$\sim 1.2 \times 10^6$	4.5–73	Forced-circulation subcooled water at test-section inlet; resistance-bridge burnout detector used; a-c heating
	0.540	0.875	110	0.167	328	1000	$0.4-1.8 \times 10^6$		
AERE studies (1961)	0.375	0.546	29	0.085	170	1000	$0.5-3.3 \times 10^6$	5.1–63.7	Forced-circulation steam-water mixture at test-section inlet; resistance-bridge burnout detector used; a-c heating

$$H' = H_g - 0.275\, H_{f_g} - 0.725\, H_{f_g} \left(\frac{300}{H_{f_g}}\right)^{10^6/G}$$

ϕ_{DNB} = limiting DNB heat flux, Btu/(hr)(sq ft)
H = local enthalpy, Btu/lb
P = system pressure
G = local mass velocity, lb/(hr)(sq ft)
H_g, H_{f_g} = water properties evaluated at system pressure

Since the references are progress reports, little additional information is given; however, a topical report presumably will be issued. The correlations do suggest, however, that there is a local enthalpy at which ϕ_{DNB} approaches zero, namely when $H' = H$.

The Atomic Energy Research Establishment (AERE) has been studying burnout in high-pressure boiling-water systems, and data have recently become available.[26] Table II-6 shows the test-section parameters used in the AERE tests and compares them with other similar experiments.* The AERE loop differs in one important respect from the loops of the other investigators shown in Table II-6 in that separate steam and water flows were utilized to feed the test section. The water was about 10°F (subcooled) at the test-section inlet, and the steam was about 10°F (superheated). Usually two or more runs were made at a given set of conditions to verify the burnout data. Preliminary results are shown in Fig. II-7; no correlation is presented in the reference. The method of burnout detection employed was to measure the electrical resistance of approximately the last 20 per cent of the heated length and to shut off the electric power when the surface temperature and resistance of the test section increased to some predetermined

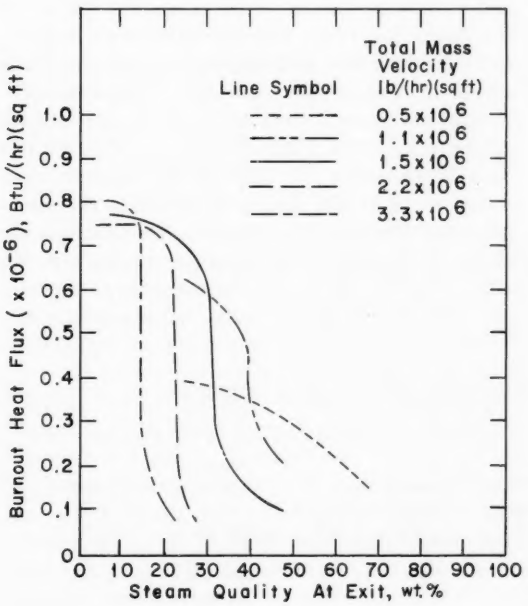

Fig. II-7 The effects of variation of mass velocity and quality on the burnout heat flux for an internally heated annulus at 1000 psia.[26]

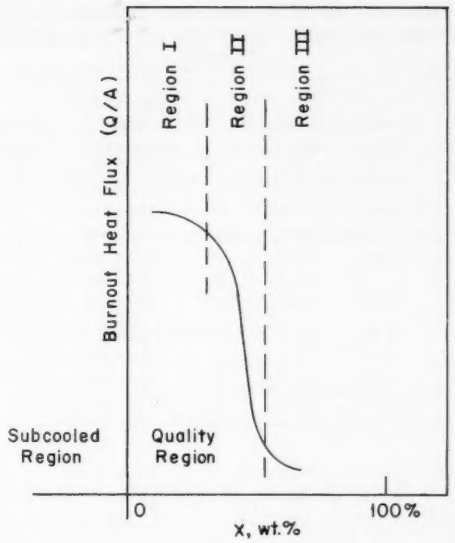

Fig. II-8 Regions of operation of burnout detector circuit.[26]

Table II-7 CRITICAL LINEAR STEAM VELOCITIES IN TEST SECTION AT 1000 PSIA[26]

Mass velocity (G), lb/(hr)(sq ft)	Critical steam quality, wt. fraction	Steam-mass velocity, lb/(hr)(sq ft)	Critical linear steam velocity, ft/sec
0.5×10^6			
1.1×10^6	0.385	0.423×10^6	52.4
1.5×10^6	0.307	0.460×10^6	56.9
2.2×10^6	0.225	0.495×10^6	61.3
3.3×10^6	0.140	0.462×10^6	57.2

*Tables II-6 and II-7 and Figures II-7 and II-8 are reprinted here by permission from the United Kingdom Atomic Energy Authority.[26]

Table II-8 PHYSICAL DIMENSIONS AND RANGE OF BURNOUT FLOW CONDITIONS TESTED IN ROUND TUBES[27]

Element No.	Inside diam., cm	Heated length, cm	*L/D*	Specific mass flow rate, g/(cm²)(sec)	Burnout quality (*X*), %
54	0.52	41.1	79	110–383	20–75
58	0.52	79.8	154	110–388	25–77
52	0.50	21.1	42	114–437	20–71
51	0.52	10.0	19	107–387	17–91
68	0.62	80.0	127	105–395	30–91
38	0.32	80.1	250	115–427	29–86
48	0.40	80.1	200	115–465	27–94
88	0.82	80.3	98	108–400	25–78
06	1.01	60.2	60	110–318	20–80

value. Three regions of burnout are discussed which refer to the behavior of this burnout detector. These regions are shown in Fig. II-8. In region I no indication of the proximity of burnout was given by the detector prior to its operation. In region II random fluctuations were observed whose amplitude increased as power was increased to the point where a trip occurred. Operation in region III resulted in large random fluctuations, and the tests that were carried out were discarded as meaningless. Severe bowing of the element was observed after operation in region III, and temperature oscillations of "tens of degrees" are reported. It is suggested[26] that the boundary between regions I and II is DNB and that the disruption of a thin liquid film on the walls is responsible for the transition into region III. Table II-7 gives steam-mass and linear velocities at a so-called "critical point," which is defined as that exit quality where the burnout heat flux falls from a fairly high value to a much lower value. According to reference 26, the critical linear velocity of 50 to 60 ft/sec compares favorably with other published data.

Reference 27 is a report on the study of wet steam as a reactor coolant and covers work done (1) at the Centro Informazioni Studi Esperienze (CISE) in Italy, (2) at Ansaldo S. A. in Italy, and (3) at the United Nuclear Corporation in this country. Although the wet steam-cooled reactor is not a boiling reactor in the conventional sense, the report is included in this review for the sake of completeness. The reader may wish to consult Vol. 4, No. 1, of this journal to review the steam- or spray-cooled concept. The report[27] contains considerable information relating to corrosion of Zircaloy and stainless steel in dynamic, two-phase tests, mixing of the two phases at coolant-channel inlets, etc., but only the burnout material is considered here. Approximately 1700 burnout measurements were made, both in round tubes and in heated annuli, with either the inner or the outer, or both, annulus walls being heated. Data on the round and annular test sections are given in Tables II-8 and II-9. These experiments were performed by CISE at the Emilia power plant in a 1-Mw test loop. Most of the data were taken at 1000 psia, although runs were made at 600, 800, and 1200 psia for comparative purposes. In general, the shape of the plots of burnout heat flux vs. quality are as shown in Fig. II-8, and the same three regions are noted (except they are numbered in the

Table II-9 PHYSICAL DIMENSIONS AND RANGE OF BURNOUT FLOW CONDITIONS TESTED IN ANNULAR TUBES[27]

Element No.	Surface heated	Channel outside diam., cm	Channel inside diam., cm	Hydraulic diam., cm	Heated length, cm	*L/D*	Mass velocity (*G*), g/(cm²)(sec)	Burnout quality (*X*), %
05	External	1.00	0.50	0.50	58.8	117	116–349	18–85
03	External	1.00	0.30	0.70	58.8	84	111–457	13–78
85	External	0.825	0.50	0.325	51.5	158	100–380	18–93
85	Internal	0.825	0.50	0.325	51.5	158	100–293	25–79
85	Bilateral:							
	Burnout at internal surface	0.825	0.50	0.325	51.5	158	100–293	21–86
	Burnout at external surface	0.825	0.50	0.325	51.5	158	99–380	19–87

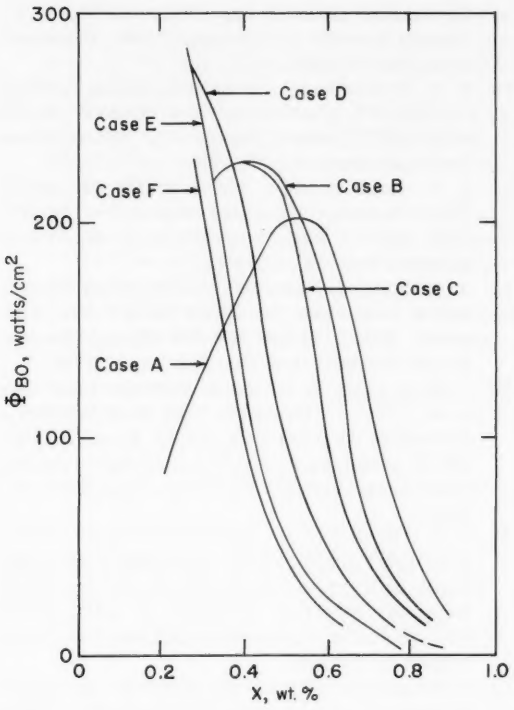

Fig. II-9 Typical burnout-heat-flux data, 1000 psi.[27] Case A: $G/10^6 = 0.81$ lb/(hr)(sq ft). Case B: $G/10^6 = 1.07$ lb/(hr)(sq ft). Case C: $G/10^6 = 1.10$ lb/(hr)(sq ft). Case D: $G/10^6 = 1.63$ lb/(hr)(sq ft). Case E: $G/10^6 = 2.19$ lb/(hr)(sq ft). Case F: $G/10^6 = 2.82$ lb/(hr)(sq ft).

reverse order). Typical data are shown in Fig. II-9; it can be noted that, at several values of the mass velocity, the ϕ_{BO} curves go through a maximum in heat flux. It is stated[27] that this maximum is believed to coincide with a change-over in flow regime from fog flow to a different flow pattern at the test-section *inlet*. The magnitude of the maximum depends on mass velocity, pressure, and L/D and is higher for smaller values of L/D. At high qualities the effect of increased pressure appeared to be a decrease in ϕ_{BO}, other variables being held constant. Annular tubes that were heated externally gave results comparable to the correlation for round tubes (when the hydraulic diameter was used); heating from the inner tube of the annulus resulted in the lower burnout heat fluxes. Reference 27 suggests that an important consideration in design is not only the burnout heat flux but ensuring that the quality never gets into the region corresponding approximately to region II in Fig. II-8.

Additional burnout test data on a seven-rod test section are given in reference 28. The program was reviewed in *Power Reactor Technology*, Vol. 5, No. 1. The recently published data are from a test section using ceramic tubing as spacers between the rods and are compared with data taken when spiral wires were used as spacers. In general, the burnout heat flux was lower when the ceramic spacers were used.

Short Notes

The subject of two-phase pressure drop has been treated in references 29 to 31. Reference 29 suggests that the well-known Martinelli-Nelson pressure-drop correlation corresponds to friction multipliers for mass velocities of approximately 0.6×10^6 lb/(hr)(sq ft), although the reference concludes that mass-velocity correction parameters cannot be recommended until more data are available. A previous reference[32] assumes that the Martinelli-Nelson curves represent the true two-phase friction-factor multiplier for a mass velocity of 1×10^6 lb/(hr)(sq ft). Reference 30 presents data on pressure drop and liquid holdup for air-water mixtures in annular flow in a $1\frac{1}{4}$-in. pipe and compares the data to appropriate correlations. Reference 31 reports pressure-drop data for a 25-rod fuel bundle that employs helical spring spacers deployed between the rods. References 33 and 34 are concerned with steam-void-fraction measurement — reference 33 deals with a test loop, whereas reference 34 discusses the use of activation of cobalt wires in measuring void fractions in the Experimental Boiling-Water Reactor (EBWR). References 35 to 39 are primarily mathematical treatments of diverse reactor heat-transfer problems.

References

1. A. E. Powers, Fundamentals of Thermal Conductivity at High Temperatures, USAEC Report KAPL-2143, Knolls Atomic Power Laboratory, Apr. 7, 1961.
2. J. L. Bates, Thermal Conductivity of UO_2 Improves at High Temperatures, *Nucleonics*, 19(6): 83 (June 1961).
3. H. W. Deem and C. F. Lucks, Thermal Conductivity and Electrical Conductivity of UO_2, in Progress Relating to Civilian Applications During

May 1961, USAEC Report BMI-1518(Del.), Battelle Memorial Institute, June 1, 1961.

4. H. D. Reiswig, Thermal Conductivity of UO_2 to 2100°C, *J. Am. Ceram. Soc.*, 44: 48–49 (January 1961).
5. M. Cutler et al., Thermal Conductivity of Reactor Materials, USAEC Report GA-1939, General Atomic Div., General Dynamics Corp., Jan. 30, 1961.
6. Richard M. Powers et al., The Effect of Solid Solution Additions on the Thermal Conductivity of UO_2, USAEC Report SCNC-317, Sylvania-Corning Nuclear Corp., November 1960.
7. R. L. Rudkin et al., Thermal Diffusivity Measurements on Metals at High Temperatures, Report USNRDL-TR-518, Naval Radiological Defense Laboratory, June 27, 1961.
8. J. F. Heyda and R. G. Herrmann, Temperature Distribution in a Cylindrical Solid with Symmetrically-Placed Longitudinal Coolant Channels, USAEC Report APEX-640, General Electric Co., Aircraft Nuclear Propulsion Dept., April 1961.
9. M. R. El-Saden, Heat Conduction in an Eccentrically Hollow, Infinitely Long Cylinder with Internal Heat Generation, *J. Heat Transfer*, 83(4): 510 (November 1961).
10. W. S. Durant, Friction Factors for Flow of Water in an Annulus with One Roughened Wall, USAEC Report DP-583, Savannah River Laboratory, June 1961.
11. J. L. Hobbs, Pressure Loss Computations in Incompressible Fluid Flow, USAEC Report APEX-754, General Electric Co., Aircraft Nuclear Propulsion Dept., July 25, 1961.
12. J. C. Howard, Thermodynamic Data for Water, USAEC Report UCRL-6455-T, University of California, Lawrence Radiation Laboratory, Apr. 18, 1961.
13. V. E. Holt, An Experimental Investigation of High-Flux Free Convection Heat Transfer to Water Up to Near-Critical Conditions, USAEC Report ANL-6400, Argonne National Laboratory, August 1961.
14. S. Frank et al., PM-1 Task 5, Subtask 5.8, Local Boiling Heat Transfer Tests. Single Tube Heat Transfer and Pressure Drop Tests, USAEC Report MND-M-1857, Martin Co., Nuclear Div., May 1961.
15. J. Randles, Kinetics of Boiling Hydraulic Loops, British Report AEEW-R-87, August 1961.
16. K. Garlid et al., A Theoretical Study of the Transient Operation and Stability of Two-Phase Natural Circulation Loops, USAEC Report ANL-6381, Argonne National Laboratory, June 1961.
17. E. S. Beckjord, The Stability of Two-Phase Flow Loops and Response to Ship's Motion, USAEC Report GEAP-3493(Rev. 1), General Electric Co., Atomic Power Equipment Dept., Sept. 26, 1960.
18. E. P. Quinn and J. M. Case, Natural Circulation Loop Performance at 1000 Psia Under Periodic Accelerations, USAEC Report GEAP-3397(Rev. 1), General Electric Co., Atomic Power Equipment Dept., May 6, 1960.
19. B. R. Bullard and R. M. Kendall, Analog Systems for the T7 Flux Trap Core, USAEC Report GEAP-3575, General Electric Co., Atomic Power Equipment Dept., July 7, 1960.
20. R. R. Hood (Comp.), Heavy Water Moderated Power Reactors Progress Report for January 1961, USAEC Report DP-585, E. I. du Pont de Nemours & Co., March 1961.
21. G. M. Hesson, Report on Heat Transfer Experiments Concerning the PRTR Mark I Fuel Elements, USAEC Report HW-63678(Rev.), Hanford Atomic Products Operation, November 1960.
22. S. Lavy and E. S. Beckjord, Hydraulic Instability in A Natural Circulation Loop with Net Steam Generation at 1000 Psia, ASME Paper No. 60-HT-27 presented at ASME-AIChE Heat Transfer Conference, Buffalo, New York, August 15–17, 1960.
23. O. J. Mendler et al., Natural-Circulation Tests with Water at 800 to 2000 Psia Under Nonboiling, Local Boiling and Bulk Boiling Conditions, ASME Paper No. 60-HT-36 presented at ASME-AIChE Heat Transfer Conference, Buffalo, New York, August 15–17, 1960.
24. Westinghouse Electric Corp., Bettis Atomic Power Laboratory, Pressurized Water Reactor (PWR) Project Technical Progress Report, April 24, 1961 to June 23, 1961, USAEC Report WAPD-MRP-92, 1961.
25. Westinghouse Electric Corp., Bettis Atomic Power Laboratory, Pressurized Water Reactor (PWR) Project Technical Progress Report, June 24, 1961 to August 23, 1961, USAEC Report WAPD-MRP-93.
26. A. W. Bennett et al., Heat Transfer to Mixtures of High Pressure Steam and Water in an Annulus. Part II. The Effect of Steam Quality and Mass Velocity on the "Burnout" Heat Flux for an Internally Heated Unit at 1000 Psia, British Report AERE-R-3804, August 1961.
27. Centro Informazioni Studi Esperienze and United Nuclear Corporation, A Study of Wet Steam as a Reactor Coolant, Joint Summary Report Covering the Period October 1, 1959–May 31, 1961, USAEC Report NDA-2132-6 (CISE Report R-44), Sept. 10, 1961.
28. R. R. Hood (Comp.), Heavy Water Moderated Power Reactors Progress Report for May 1961, USAEC Report DP-625, E. I. du Pont de Nemours & Co., July 1961.
29. B. M. Hoglund et al., Two-Phase Pressure Drop in a Natural-Circulation Boiling Channel, USAEC Report ANL-5760, Argonne National Laboratory, August 1961.
30. G. F. Hewitt et al., Holdup and Pressure Drop Measurements in the Two-Phase Annular Flow of Air-Water Mixtures, British Report AERE-R-3764, June 1961.

31. E. P. Quinn, Pressure Drop of Multi-Rod Elements with Helical Spring Spacers, USAEC Report GEAP-3749, General Electric Co., Atomic Power Equipment Dept., June 1961.
32. P. A. Lottes et al., Lecture Notes on Heat Extraction from Boiling Water Power Reactors, USAEC Report ANL-6063, Argonne National Laboratory, October 1959.
33. A. T. Eurola, On the Measurement of the Dynamic Properties of the Steam Void Fraction in Boiling Water Channels, USAEC Report ANL-6369, Argonne National Laboratory, June 1961.
34. J. A. Thie et al., Void Measurement in a Boiling Reactor, *Nuclear Sci. and Eng.*, 11(1): 1 (September 1961).
35. W. Ciechanowicz, Transient Temperature Distribution of the Cylindrical Fuel Element in the Case of Boundary Conditions Being Time Dependent, *Nukleonika*, 6(5): 317 (1961) (in Polish).
36. R. P. Stein, Studies Related to Predicting Coolant Behavior for Fast Reactor Safety, USAEC Report NDA-2147-8, United Nuclear Corp., Aug. 31, 1961.
37. J. C. Jensen, IBM 650 Routine VII Pressure Drop in Channels with Boiling, USAEC Report DP-597, Savannah River Laboratory, June 1961.
38. W. C. Reynolds et al., HECTIC, an IBM 704 Computer Program for Heat Transfer Analysis of Gas-Cooled Reactors, USAEC Report AGN-TM-381, Aerojet-General Nucleonics, May 1961.
39. N. Clark et al., Heated Annuli Computer Program, USAEC Report APEX-627, General Electric Co., Nuclear Materials and Propulsion Operation, Flight Propulsion Laboratory Dept., August 1961.

Section

III

Power Reactor Technology

Reactor Dynamics and Safety

Transients in a UO_2-H_2O Reactor

Until recently the experimental investigations of self-limiting reactivity excursions in the Special Power Excursion Reactor Test (SPERT) program have been confined to water-moderated reactors that employ highly enriched fuel elements. Although these studies have exposed the general characteristics of reactor self-shutdown and have given results that are rather directly applicable to research reactors and to some other types of highly enriched reactors, exploration of the field of self-limiting transients in low-enrichment, oxide-fueled reactors (of particular interest for the power-reactor designer) has begun only recently. The SPERT Quarterly Technical Report[1] for April, May, and June 1961 gives the results of the first tests on an oxide-fueled core in the SPERT-I reactor. Later results were reported at the 1961 winter meeting of the American Nuclear Society.*[2]

The reactor core used for the tests was made up of rod type fuel elements that had previously been used for the N.S. *Savannah* critical experiment program. The elements were approximately 6 ft long and consisted of stainless-steel tubes with a 0.5-in. outside diameter and a 0.028-in. wall thickness; each tube contained 1600 g of 4 per cent enriched UO_2 powder that was compressed to an effective density of 9.45 g/cm^3. The UO_2 was not sintered after compaction in the fuel tubes. The core contained 592 fuel rods which were arranged in a square lattice with a center-to-center spacing of 0.663 in. This yielded a core with a 19-in. equivalent diameter and a length-to-diameter ratio of 3.7. The uniform void coefficient of reactivity, determined experimentally, was -0.024 cent/cm^3 of void, or -0.39 cent per per cent decrease in moderator density. The temperature coefficient of reactivity, for uniform heating of the moderator, varied from approximately -0.25 cent to -2.4 cents/°C over the temperature range from 18 to 85°C.

The effects of both step and ramp inputs of reactivity were investigated* in the unpressurized reactor at an initial temperature of approximately 20°C. As in the case of previously tested reactors, the results of the step- and ramp-induced excursions were nearly the same when compared at equal values of the minimum exponential period reached during the excursion. For minimum periods longer than about 100 msec, the power excursion consisted of a single burst, but, as tests were made at shorter periods, a secondary peak (and in some cases two or more secondary peaks) was observed. The time interval between peaks was roughly constant. This multiple excursion behavior was traced to bowing and subsequent vibration of the long fuel rods, which in the initial tests were supported only at the ends. The bowing was observed photographically[2] and was later elimi-

*Editor's Note: Two other recent reports that cover the oxide core investigation are F. Schroeder (Ed.), Quarterly Technical Report Spert Project, July, August, and September 1961, Report IDO-16726, Phillips Petroleum Company, Dec. 15, 1961, and A. H. Spano et al., Self-Limiting Power Excursion Tests of a Water-Moderated Low Enrichment UO_2 Core in Spert-I, Report IDO-16751, Phillips Petroleum Company.

*A review of other recent SPERT results was given in the December 1961 issue of *Power Reactor Technology*, Vol. 5, No. 1. It treats the general features of typical test results in some detail and may be helpful as an introduction to the present review.

nated by the installation of supports at intermediate points on the fuel rods. This modification eliminated the secondary power peaks.

The maximum power reached during the step transients is presented in Fig. III-1 as a function of the reciprocal period of the transient. Points are shown for both the initial (unconstrained) core and for the core after the intermediate supports had been installed. The figure shows that the bowing of the fuel rods not only caused multiple power peaks but increased the maximum power reached in excursions in the intermediate range of reciprocal periods. In the long-period range (small values of reciprocal period), the termination of the power rise is attributed to the decrease of moderator density; whereas, in the short-period range, it is attributed primarily to Doppler broadening of the U^{238} resonances as the fuel elements heat up.[2]

The shortest period test, in which the minimum exponential period was about 3.2 msec, was discussed by Spano and Stephan.[2] In this excursion the maximum power reached was 8400 Mw, and the total nuclear energy production was 114 Mw-sec. This excursion, which

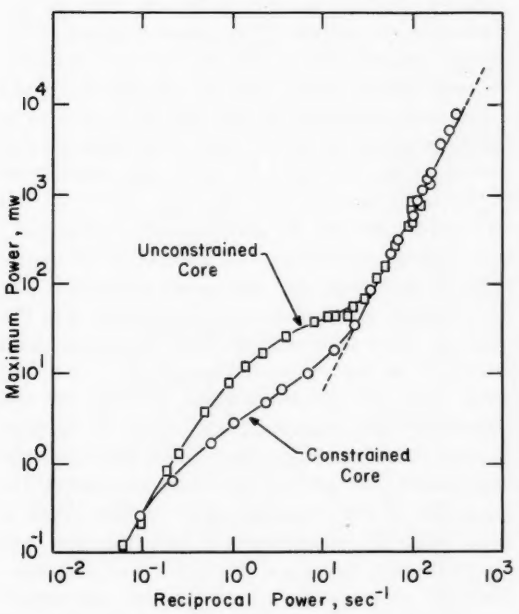

Fig. III-1 Maximum power vs. reciprocal period for self-limiting power excursions in a UO_2 core in the SPERT-I reactor.

in magnitude of period and total energy release was quite comparable to the final, destructive, Boiling Reactor Experiment No. 1 (BORAX-I) excursion, produced no apparent damage in the oxide core. No sintering of the oxide powder was observed upon examination of the fuel elements. It was estimated that the maximum temperature attained by the UO_2 was perhaps 2000°C.

It is shown in reference 1 that the short-period results for the oxide core fall between two previously obtained curves for aluminum-plate cores: (1) that for the B-12/64 core and (2) that for the P-18/19 core.* The shutdown mechanism is, however, quite different for the oxide core; it is important to recognize that the "self-protection" of the oxide core depends upon the availability of a relatively large Doppler coefficient and a substantial fuel temperature margin. The characteristics of the core that was tested appear to be such as to make the Doppler shutdown mechanism quite effective. On the one hand, the relatively low moderator-to-fuel ratio used† probably gives a rather low resonance escape probability, assuring that k_{eff} will be reasonably sensitive to the Doppler broadening of U^{238} resonances; whereas, on the other hand, the rather high enrichment of the fuel gives a relatively short effective neutron lifetime (l/β = 3.7 msec) so that the amount of excess reactivity represented by the 3.2-msec period is not extremely high, amounting to about 1 dollar and 16 cents above prompt critical. The poor conductivity of the UO_2, which is a liability if shutdown must be effected by heating or boiling of the moderator, becomes an asset if Doppler broadening can be counted on for shutdown because it limits the rate at which the nuclear energy released can be transferred to the fuel-element jacket and to the water; thus it tends to avoid jacket melting and the violent production of steam. The removal of excess reactivity by the Doppler effect depends, of course, upon the ability of the fuel elements to stand a large increase in temperature. If the elements are already very hot, as they might be if the reactor were operating at high power at the time of the reactivity increase, then a safe

*The characteristics of these reactors are given in reference 3.

†The lattice spacing is equivalent to an H_2O-to-UO_2 volume ratio of 1.73 for UO_2 of density 10.4 g/cm^3.

extra margin of temperature increase might not be available even with the oxide fuel.

Laboratory Studies

Reference 4 is the 1960 annual summary report of the work on kinetics of heterogeneous water reactors by Space Technology Laboratories, Inc. This work treats the dynamic behavior of reactors of the SPERT type by laboratory investigation of the thermal and hydrodynamic behavior of single coolant channels. Attention has been directed toward the SPERT-IA core, a parallel-plate core that has fuel plates of high thermal conductivity. Both transient and steady-state mockups have been made of single coolant channels with suitable associated coolant systems. The walls of the coolant channels are electrically heated, and provision is made for evaluation of the change in effective density of the water in the channel (by X-ray attenuation in the steady-state case and by a volume transducer in the transient case). The density change may be fed back, via an electronic reactor-kinetics simulator, to control the electric power input to the coolant channel. The reactor is thus simulated by the thermal-hydrodynamic behavior of a single coolant channel plus electronic simulation of the neutron kinetics. The reactivity feedback can, of course, be eliminated at will to permit investigation of the dynamics of the coolant channel alone under various conditions of power input.

The transient investigations that have been reported have reproduced some of the characteristics observed in the SPERT-IA reactor (although most of the tests were made with a coolant channel that was known to be deficient) in that thermal expansion of the channel walls produced an increase, rather than a decrease, in the amount of water in the channel. The steady-state investigation treated mostly the power-flow and power-void transfer functions of the coolant channel, the effects of wall surfaces on bubble nucleation and stability, and the distribution of steam voids within the channel. The work is not at a stage to be of direct use to the reactor designer but it illuminates some of the aspects of the dynamic behavior of water-moderated reactors and will have considerable interest for those concerned with the fundamentals of that subject.

Dynamics of EBR-I

The dynamic behavior of the Experimental Breeder Reactor No. 1 (EBR-I), the first nuclear reactor to produce electric power (1951), has been under investigation for a number of years. Early observations of the reactor operating characteristics disclosed a "prompt" positive component of the power coefficient of reactivity, although the net long-term power coefficient was negative because of a larger and delayed negative component. Later tests showed that operation of the reactor at reduced coolant flow and reduced power, with a large temperature rise across the core, could lead to power oscillations of approximately 30-sec periods if the control system were not manipulated to counteract them. At a still later date (1955), measurements of the reactor transfer function showed a power resonance at a frequency in the range 0.03 to 0.1 cps, the frequency increasing with increasing coolant flow rate. These peculiarities gave no troubles during normal operation, and the reactor was operated in a routine way until 1955. During this period the original (Mark I) core was replaced by a second core (Mark II) which differed slightly in that stiffening ribs on the fuel-element jackets were omitted. Most of the more precise observations on the dynamic behavior were made with the second core, and the general impression was that the undesirable features of the behavior were somewhat accentuated in the second core, although there were no strictly comparable dynamic tests on the two cores. During an investigation of the positive power coefficient of reactivity, with the coolant flow shut off, the power excursion was accidentally allowed to proceed too far, and the Mark II core was melted. This mishap focused attention on the dynamic characteristics of the core, and, at the same time, it removed the possibility of subjecting the core to further experimental investigation. Since that time investigation has proceeded along two paths: (1) analysis of the existing data on the Mark II core and (2) experimental investigation and analysis of a new core (Mark III) that was specifically designed to eliminate the characteristics that were thought to have caused the undesirable features of the Mark II behavior. References 6 and 7 summarize the conclusions drawn from this work. It is worth while to re-

view these conclusions in some detail; they show, on the one hand, that the behavior of the reactor is understandable in principle, and they illustrate, on the other hand, the extremely detailed mechanical and thermal considerations that must be taken into account to predict the dynamic behavior of small, highly leaky fast reactors.

The reactor structure and the coolant-flow path associated with the Mark II core are shown schematically in Fig. III-2. The reactor proper consists of a hexagonal core region that contains a lattice of fuel rods surrounded by a blanket region containing a lattice of larger, natural-uranium blanket rods. Both fuel and blanket rods consist of uranium metal rods that are jacketed with stainless steel, with a thermal bond of NaK between the uranium and the jacket. The uranium in a fuel rod has a diameter of 0.384 in.; the highly enriched segment is $8\frac{1}{2}$ in. long and is between natural-uranium upper and lower blanket sections that are $7\frac{1}{2}$ and $4\frac{1}{4}$ in. long, respectively. Both fuel and blanket rods have long upper extensions of stainless steel which serve as handles for installing and removing the rods. The rods are positioned at the bottom of the reactor by a grid plate and at the top by a series of plates (Fig. III-2), each of which has the characteristics of a

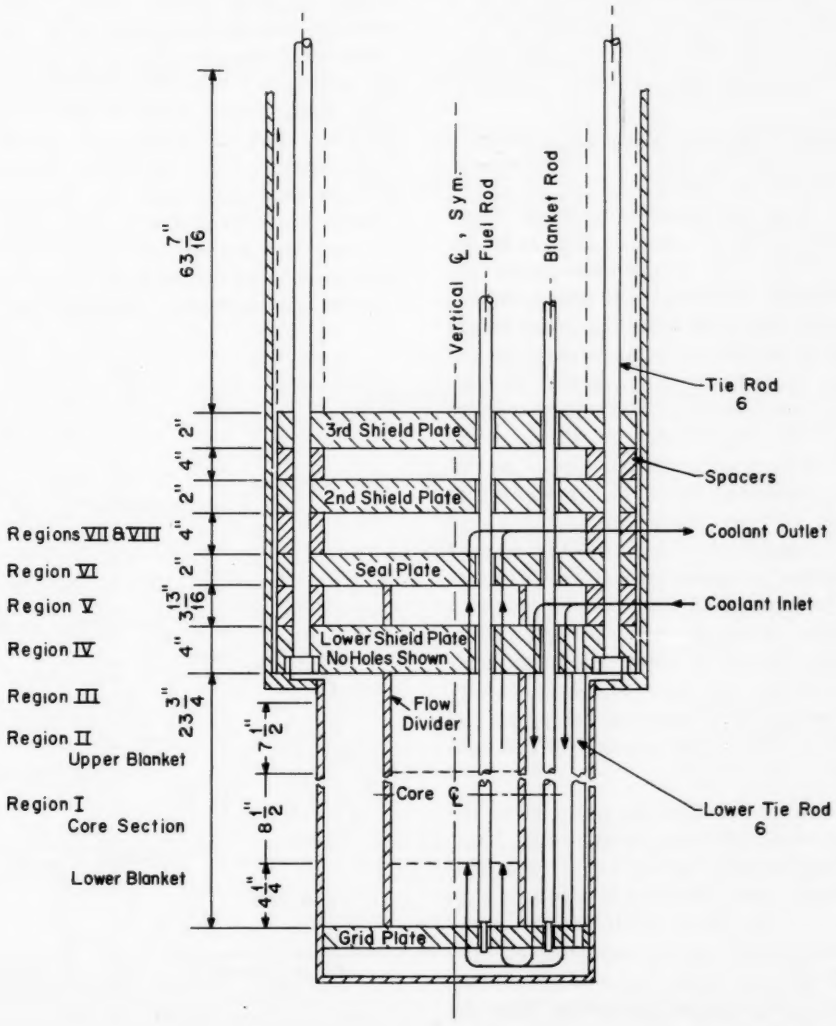

Fig. III-2 Schematic view of EBR-I structure.[6]

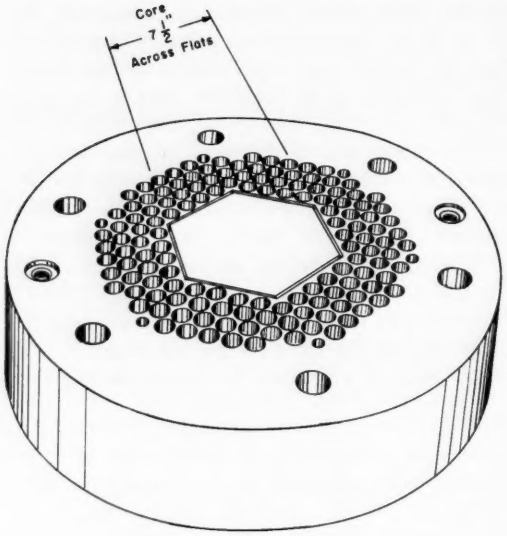

Fig. III-3 EBR-I lower shield plate.[6]

grid plate. The bottommost of these upper plates (called the lower shield plate) is shown in Fig. III-3. The extension handles on the fuel rods are roughly triangular in cross section over the length that penetrates the lower shield plate so as to allow room for passage of the NaK coolant (Fig. III-4). As indicated in Fig. III-2, the coolant makes a double pass through the reactor, flowing downward through the blanket and upward through the core. The two passes are separated by a flow divider that extends from the seal plate to the bottom grid plate. The temperature rise across the reactor during operation is approximately 100°C. The central (core) portion of the lower shield plate will, therefore, under steady power conditions, be approximately 100°C hotter than the outer portion, and there will be a temperature difference of some 100°C between the upper and lower faces of the outer portion of the seal plate.

A typical cross section through one of the holes in the shield plate is shown in Fig. III-4; the clearances between a fuel rod and the several grid plates are indicated in part *a* of Fig. III-5. Part *a* of Fig. III-5 illustrates the situation in which the fuel rod is assumed to be centered in all the grid-plate holes at room temperature and with no power production. When the temperature of the coolant is raised, say to the operating level of 150°C, the grid plates expand but the fuel rods do not necessarily move until the expansion has become great enough to close the clearance on one side of the rod. The situation after such a temperature increase, with no power production, might be as in part *b* of Fig. III-5. At the time the reactor begins to produce power, the temperature of each fuel rod (except the center one) will be slightly higher on the side facing the center of the core than on the side facing the periphery of the core; this is caused by the radial dropoff of the neutron flux. This causes a bowing of the fuel rod, convex toward the reactor center line, which could conceivably cause the effective position of the rod (insofar as it affects reactivity) to move either toward or away from the reactor center, depending upon the restraints imposed by the several grid plates. The analysis of reference 6 has indicated that a typical fuel-rod configuration would be that shown in part *c* of Fig. III-5, in which the bowing has been sufficient to close the outer clearance on the bottom grid plate and the uppermost (third) shield plate. Once these clearances have been closed, any further bowing of the rod moves fuel toward the center of the reactor and causes a reactivity increase. This mechanism can ac-

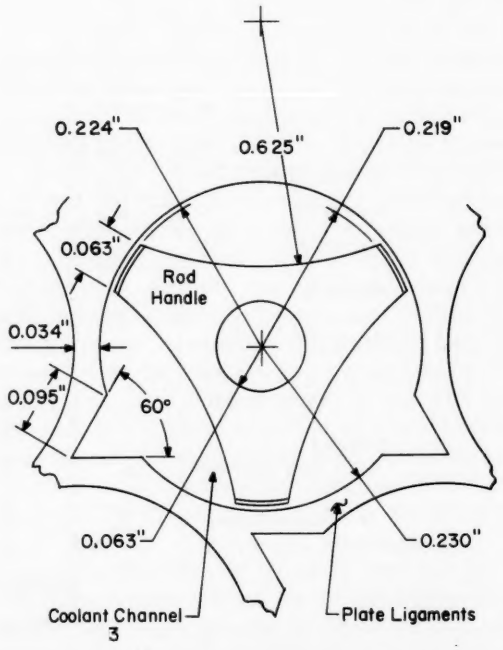

Fig. III-4 Horizontal cross section through lower shield plate and rod handle,[6] EBR-I.

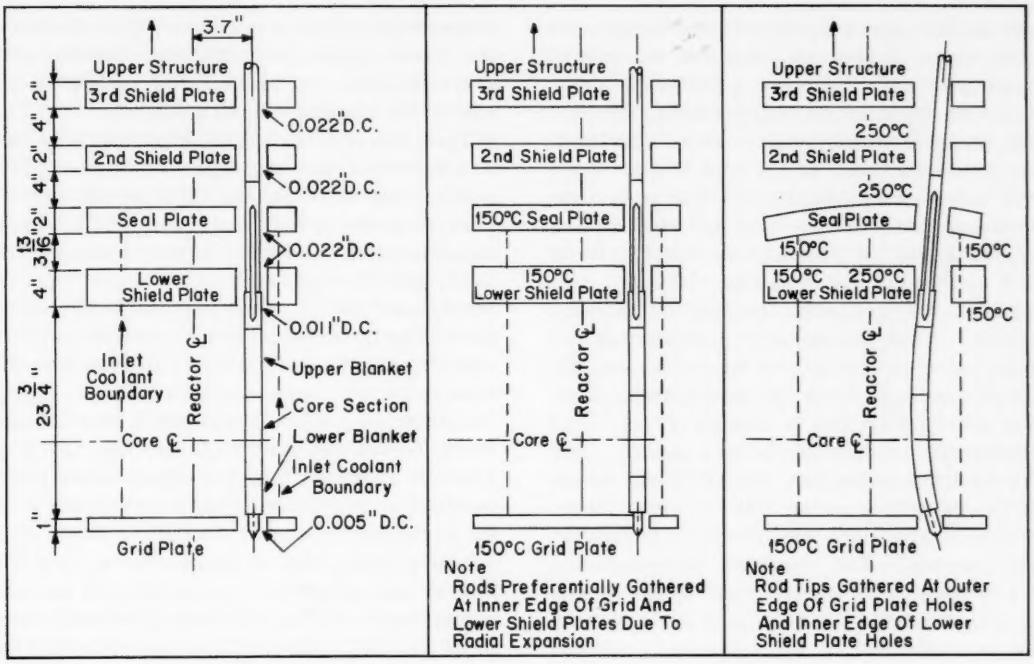

(a) (b) (c)

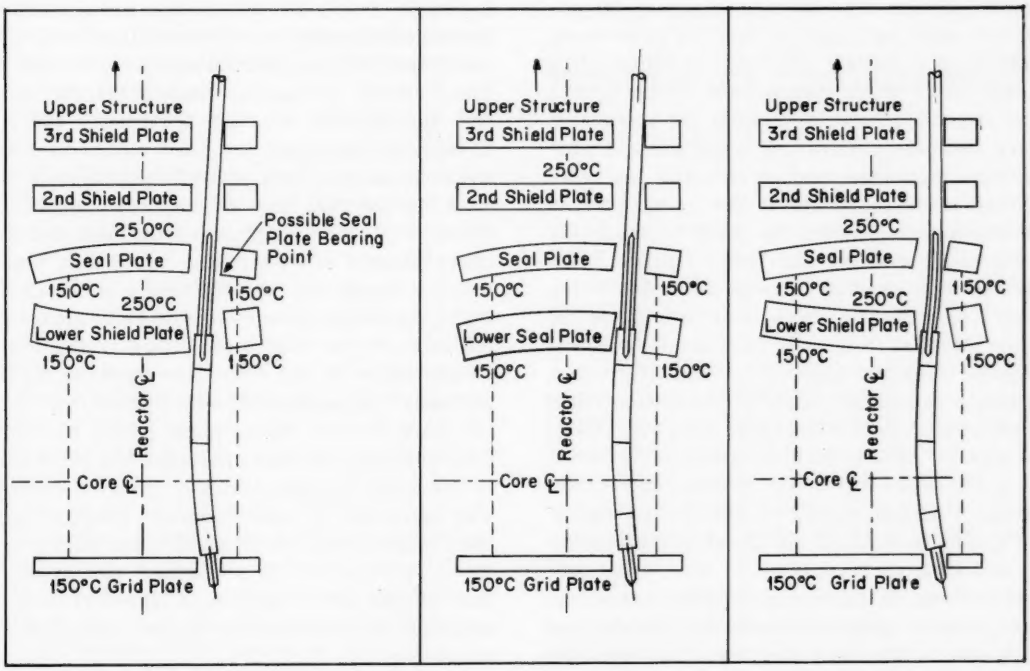

(d) (e) (f)

Fig. III-5 Typical bearing points of EBR-I fuel rods under various conditions of temperature and power.[6] (Clearances and curvatures are greatly exaggerated.)

count for the observed positive power coefficient of reactivity. It is to be noted that, because of the temperature differential between the upper and lower faces of its outer region, the seal plate buckles slightly under power operation. Since the temperature of the core section of the lower shield plate has increased as power has increased, there will be a radial expansion of its central grid (i.e., the core section, Fig. III-3) which will tend to move the tops of the fuel rods away from the core center line and thus decrease reactivity. This will result in a negative power coefficient of reactivity, but the coefficient will be a delayed one since the temperature of the lower shield plate can be raised only by heat transferred to it from the flowing coolant. This is in contrast to the positive coefficient, which results directly from the fuel-rod temperature distribution and which may therefore be considered "prompt." The magnitude of the shield-plate expansion is, of course, affected by the fact that the heated, central grid portion of the plate is restrained by the massive peripheral ring, which remains in contact with the cold inlet coolant. Measurements on a duplicate of the actual lower shield plate indicate that the central portion expands approximately 75 per cent as much as though it were not restrained.

There is a further effect due to the buckling of the lower shield plate itself which occurs when reactor power is changed. At the time a power increase occurs, the outlet coolant temperature increases, and, eventually, the temperature of the lower shield plate must increase correspondingly. Since the plate is relatively massive, the coolant will lose a fraction of its extra heat in passing through the holes in the plate. Consequently, for a short time after the power increase, the lower face of the plate will be hotter than the upper face, and differential expansion will cause the plate to assume a dished shape, convex downward (part *d* of Fig. III-5). Conversely, if the reactor power is reduced, the plate will, for a short time thereafter, assume a dished shape, convex upward (part *e* of Fig. III-5). Thus, if the power of the reactor is oscillated, there will be an inward and outward rocking of the tops of the fuel rods as the lower shield plate assumes alternately one configuration and then the other. The resulting reactivity coefficient will be related to the rate of change in reactor power rather than to the power level and will be negative in sign—that is to say, a positive rate of change of power will cause a reduction of reactivity. This dishing of the lower shield plate has been demonstrated experimentally by preferential heating of one side of the plate in the laboratory.

This mechanical analysis of the core has demonstrated the existence of three power coefficients of reactivity: (1) a prompt positive coefficient due to fuel-rod bowing, (2) a delayed negative coefficient due to radial expansion of the lower shield plate, and (3) a delayed negative coefficient due to flexing of the lower shield plate. The first two of these are related to easily observable characteristics of the reactor. The first must be of such a magnitude as to explain the observed positive power coefficient of reactivity. The second must be larger than the first since it is known that the steady-state power coefficient of reactivity was negative and since the second component is the only negative component that has been recognized as being effective at steady power. A more detailed analysis is required to relate all three of the coefficients to the dynamic behavior of the reactor. This has been attempted in reference 6. The measured transfer function of the reactor with the Mark II core has been analyzed in terms of three basic feedback processes which have been assigned individual transfer functions and time constants consistent with the mechanisms described above. The feedback processes resulting directly from fuel temperature changes (primarily the rod bowing, but also the axial and radial fuel expansion and the expulsion of coolant from the core by thermal expansions) are lumped together as "core" feedback processes and are characterized by a core time constant, τ_f, which is very nearly the thermal time constant of the fuel rods. Three time constants enter the transfer function for radial expansion of the lower shield plate: (1) the core time constant, (2) the transport lag associated with coolant flow from the core to the shield plate $[\tau(w)]$, and (3) a time constant, τ_r, that characterizes the heating of the plate by heat transfer from the coolant. The same set of time constants characterizes the flexing of the lower shield plate except that τ_r is replaced by τ_p, a "flexing" time constant that is different in magnitude (shorter) than τ_r although it is determined by the same types of processes.

A model of the type described above is consistent with the observed transfer functions of the reactor, and the time constants deduced from first principles appear also to be con-

sistent with the observed behavior, inasmuch as it was possible to reproduce the observed transfer function of the reactor reasonably well provided that assumed values were used for the coefficients of the three feedback terms. The reference[6] tests the validity of the model by comparing the values of these assumed coefficients (which may be regarded as having been deduced from the reactor transfer function) with those which would be calculated from first principles. The conclusion is that the deduced positive coefficient is reasonably consistent with the mechanical analysis but that the deduced negative coefficients are about three times as large as one would expect from the mechanical analysis. Oddly enough, if the mechanical analysis is modified by the assumption that the fuel-rod bowing is more pronounced, higher negative coefficients result; the handle extensions of the fuel rods are then forced into contact with the holes in the seal plate and those in the second and third upper shield plates. This in turn causes the expansion of the lower shield plate to work against a short lever arm and thereby amplifies the effect of its expansion on the movement of the fuel rod (part *f* of Fig. III-5). The reference concludes that sufficient amplification of this kind can be visualized to bring the mechanical analysis into agreement with the transfer function of the reactor.

These explanations of the behavior of the reactor with the Mark II core gain considerable support from the observed fact that the positive coefficient of reactivity and the tendency to oscillation were eliminated when the Mark III core was installed. Reference 7 describes the experimental and theoretical investigation of the Mark III core. This core[8] is quite different from the Mark II in that the fuel rods are not supported by grid plates but are assembled into hexagonal subassemblies of 36 rods each, contained within hexagonal stainless-steel tubes. Triangular adapters on the ends of the fuel rods fit into locating holes in a rod sheet at the bottom of the subassembly structure. Longitudinal external ribs on the rods act as spacers, and a tightening mechanism at the center of the subassembly forces the rods against each other and against the hexagonal subassembly wall. The mechanism can be tightened after the subassemblies are installed in the reactor, and it can be loosened for the removal of individual rods. The subassemblies, in turn, are held in a firmly packed array by core clamps around the periphery of a form-fitting retainer ring. Two important effects of this construction are as follows: it restrains both the fuel rods and the subassemblies against bowing, and it causes the core to behave, under radial thermal expansion, more or less as a unit rather than as a collection of rods whose positions are determined by interactions between the expansions of grid plate and fuel-rod–grid-hole clearances.

It appears probable that reference 6 has carried the analysis of the Mark II core about as far as it can go without recourse to experiments that would be possible only if the core were still in existence. Although it has not been possible to derive, quantitatively, a transfer function that reproduces the amplitude characteristics of the observed transfer function, the time constants involved do appear to be understandable, and possible reasons for amplitude discrepancies, although they are not removable, are certainly recognizable. The study has apparently accomplished its purpose by demonstrating that the behavior of the reactor did not involve any phenomena that are not understandable and that the principles of predicting the power coefficients for fast reactors are well understood.

Melting of Fast-Reactor Fuel Elements

The initial experiments on the transient heating of fast-reactor fuel elements in the Transient Reactor Test Facility (TREAT) are reported in reference 9. TREAT is a special transient reactor that was built at the National Reactor Testing Station for experiments of this general type. The TREAT core consists of a nearly homogeneous mixture of graphite and enriched uranium oxide which has high heat capacity. This reactor can be pulsed safely to produce high rates of transient heat generation in sample fuel elements installed in its test holes. The reactor and its characteristics are described in references 10 to 16.

Although TREAT may be used for the transient irradiation of various types of fuel elements and other samples, its major use, and the one for which it was particularly designed, is the investigation of fuel elements for fast-neutron reactors. The mode of failure of fuel elements in fast reactors and the phenomena associated with

failure are particularly important because of the conceivable possibility that an extensive meltdown of a fast-reactor core could result in the redistribution of fuel to form a supercritical mass. The experiments described in the reference are directed basically at determining the mode of failure of two typical but markedly different types of fuel elements: (1) those of the Experimental Breeder Reactor No. 2 (EBR-II) and (2) those of the Enrico Fermi Fast Breeder Reactor (EFFBR). The experiments that were reported treated the failure of the elements when no coolant was present. The tests involved pulsing the elements to various known power levels, most of which were sufficiently high to cause failure of the element. The observations included the shape and magnitude of the power pulse, as inferred from the reactor power-measuring instruments; surface temperatures and, in some cases, internal temperatures of the fuel elements; and postirradiation examination of the elements or their remains. A paper presented at the winter meeting of the American Nuclear Society[17] has also described some tests in which the behavior of the element was observed by a motion-picture camera through a transparent window in the test capsule.

The EBR-II fuel element consists of a uranium alloy pin that is 0.144 in. in diameter by 14.22 in. long, canned in a type 304 stainless-steel tube with a 0.009-in. wall, with a sodium bond between the fuel pin and the can. The bonding sodium normally fills the tube to a level approximately 0.6 in. above the top of the fuel pin, and a void space, approximately 1 in. long, is left above the sodium level. The EBR-II and its fuel element have been described in *Power Reactor Technology*, Vol. 1, No. 3, June 1958, and Vol. 4, No. 4, September 1961, and in references 18 and 19.

The EFFBR fuel element consists of a 0.158-in.-diameter uranium-molybdenum alloy fuel pin, clad with 0.005-in.-thick zirconium. The pin and cladding are metallurgically bonded. The EFFBR and its fuel elements are described in reference 20.

The EBR-II fuel elements are approximately 18 in. long; full-length fuel elements were used for the tests. The EFFBR fuel elements, which are approximately 32 in. long, were represented by half-length fuel elements in the TREAT tests.

Several different typical characteristics of the EBR-II fuel-element behavior were observed, depending upon the maximum temperature reached by the jacket during the test. These tests were, of course, excursion tests of short duration (the TREAT reactor can give power bursts of variable duration from about 0.2 to 30 sec), and the observed behavior of the test elements must be considered as typical of such conditions. In general the EBR-II fuel element did not suffer any damage if the outer cladding temperature did not exceed approximately 960°C. In this temperature range* the sodium bond did, however, boil locally, and some of the sodium was expelled from its normal position upward into the void space near the top of the element, leaving unbonded regions which might have caused harmful overheating of the fuel pin if the element had subsequently been used in an operating reactor.

The temperature region above 960°C, and up to 1000°C, was characterized by the formation of areas of stainless steel–uranium alloy. The alloy formation was accentuated at pressure contact points, particularly when contact was increased by warping of the fuel element. Penetration of the jacket would sometimes occur and sometimes it would not, depending upon the presence of sufficient pressure contact points between the uranium and cladding surfaces.

Failure of the element always occurred at jacket temperatures between 1000 and 1015°C. The stainless steel–uranium alloy would penetrate the cladding and then be forced out (but not violently) by the pressure of vaporizing sodium. Under the effect of gravity and the sodium vapor pressure, the alloy tended to flow downward; this increased the contact time between uranium and cladding and led to extensive dissolution of the cladding.

Above 1015°C, failure of the fuel element was violent. The rapidly vaporizing sodium developed a high pressure which forced the uranium out of the element and ejected it laterally and, occasionally, upward. At considerably higher temperature (1250 to 1400°C), jacket penetrations occurred at a number of places along the length of the element. When the element was vented at the top, to prevent a pressure buildup, the uranium was sometimes driven upward by the force of vaporizing sodium trapped at the base of the element. The venting tended to reduce the

*The melting point of uranium is 1133°C; the boiling point of sodium, at atmospheric pressure, is 881°C.

violence of the failure by preventing the buildup of high pressures. When the sodium bond was purposely omitted from the experimental elements, a quiet meltdown characteristic resulted. The fuel melted and flowed downward inside the jacket and ultimately dissolved large portions of the cladding near the base of the element.

When the refractory metals tantalum and niobium were substituted for the stainless steel in the EBR-II fuel-element jackets, the maximum temperature attainable before failure increased from about 960 to about 1400°C. When failure did occur, the uranium was ejected from a very localized penetration and, in general, all of it left the confines of the jacket during the excursion. The jacket was not extensively dissolved.

In the case of the EFFBR fuel elements, considerable fine surface cracking and warping of the fuel element occurred, without failure, at temperatures below about 1300°C. In one such case some of the fuel alloy dribbled out through one of the cracks in the cladding. At higher temperatures failure occurred by what seemed to be a simple solution of the cladding. The fuel dissolved large portions of the cladding, escaped, and flowed downward to the bottom of the test capsule without evidence of violence.

Reference 20 states that the typical high-temperature failure of the sodium-bonded elements, in which all the fuel is expelled rapidly through a penetration near the hottest point in the fuel pin, suggests a mechanism by which a supercritical assembly might conceivably be formed in the course of a fast-reactor accident. It also states that extensive theoretical work is under way to see whether such a phenomenon could lead to a dangerous rate of reactivity insertion in EBR-II.

References

1. F. Schroeder (Ed.), Quarterly Technical Report, SPERT Project, April, May, June 1961, USAEC Report IDO-16716, Phillips Petroleum Co., Sept. 15, 1961.
2. A. H. Spano and L. A. Stephan, Experimental Investigation of the Kinetic Behavior of a 4%-Enriched UO_2 Reactor in SPERT-I, *Trans. Am. Nuclear Soc.*, 4(2): 312 (November 1961).
3. S. G. Forbes et al., Analysis of Self-Shutdown Behavior in the SPERT-I Reactor, USAEC Report IDO-16528, Phillips Petroleum Co., July 23, 1959.
4. Space Technology Laboratories, Inc., Kinetic Studies of Heterogeneous Water Reactors Annual Summary Report, 1960, USAEC Report RWD-RL-190, Dec. 30, 1960.
5. R. O. Brittan, Some Problems in the Safety of Fast Reactors, USAEC Report ANL-5577, Argonne National Laboratory, May 1956.
6. R. R. Smith et al., A Mechanism Explaining the Instability of EBR-I, Mark II, USAEC Report ANL-6354, Argonne National Laboratory, September 1961.
7. R. R. Smith et al., Instability Studies with EBR-I, Mark III, USAEC Report ANL-6266, Argonne National Laboratory, December 1960.
8. R. E. Rice et al., EBR-I, Mark III—Design Report, USAEC Report ANL-5836, Argonne National Laboratory, March 1958.
9. C. E. Dickerman et al., Studies of Fast Reactor Fuel Element Behavior Under Transient Heating to Failure. I. Initial Experiments on Metallic Samples in the Absence of Coolant, USAEC Report ANL-6334, Argonne National Laboratory, August 1961.
10. G. A. Freund et al., TREAT, a Pulsed Graphite-Moderated Reactor for Kinetics Experiments, *Proceedings of the Second United Nations International Conference on the Peaceful Uses of Atomic Energy, Geneva, 1958*, Vol. 10, p. 461, United Nations, New York, 1958.
11. D. R. MacFarlane et al., Hazards Summary Report on the Transient Reactor Test Facility (TREAT), USAEC Report ANL-5923, Argonne National Laboratory, October 1958.
12. G. A. Freund et al., Design Summary Report on the Transient Reactor Test Facility (TREAT), USAEC Report ANL-6034, Argonne National Laboratory, February 1960.
13. H. P. Iskenderian, Physics Analyses of the TREAT Reactor Design, USAEC Report ANL-6025, Argonne National Laboratory, August 1959.
14. H. P. Iskenderian, Post Criticality Studies on the TREAT Reactor, USAEC Report ANL-6115, Argonne National Laboratory, February 1960.
15. F. Kirn et al., Reactor Physics Measurements in TREAT, USAEC Report ANL-6173, Argonne National Laboratory, October 1960.
16. D. Okrent et al., The Reactor Kinetics of the Transient Reactor Test Facility (TREAT), USAEC Report ANL-6174, Argonne National Laboratory, September 1960.
17. C. W. Dickerman et al., Photographic Studies of In-Pile Fast Reactor Fuel Sample Meltdown, *Trans. Am. Nuclear Soc.*, 4(2): 314 (November 1961).
18. L. J. Koch et al., Construction Design of EBR-II: An Integrated Unmoderated Nuclear Power Plant, *Proceedings of the Second United Nations Inter-*

national Conference on the Peaceful Uses of Atomic Energy, Geneva, 1958, Vol. 9, p. 323, United Nations, New York, 1958.

19. L. J. Koch et al., Experimental Breeder Reactor II (EBR-II): Hazard Summary Report, USAEC Report ANL-5719, Argonne National Laboratory, May 1957.
20. A. Amorosi and J. G. Yevick, An Appraisal of the Enrico Fermi Reactor, *Proceedings of the Second United Nations International Conference on the Peaceful Uses of Atomic Energy, Geneva, 1958*, Vol. 9, p. 358, United Nations, New York, 1958.

Section

IV

Power Reactor Technology

Design Practice

The Elk River Reactor

This summary of the Elk River reactor design is the third in a series of power-reactor design summaries (see *Power Reactor Technology*, Vol. 4, No. 3, for the Yankee Nuclear Power Station, and Vol. 4, No. 4, for the Dresden Nuclear Power Station). The Elk River reactor is being constructed under a contract between the Rural Cooperative Power Association (RCPA) and the AEC. The data given here are from the Final Hazards Report[1] (including its additions and corrections) and from Vol. II of the Operations Manual.[2] Additional information can be found in reference 3.

The Elk River reactor is designed to operate initially as a natural-circulation, light-water-boiling, indirect-cycle system; the secondary steam is fed to a coal-fired superheater and then to the turbine-generator unit. Permanent features of the plant have been designed for a future doubling of the reactor output from 58.2 to 116.4 Mw(t).

As a partial consequence of this allowance for a future power increase, much latitude has been incorporated into the plant design. For example, the reactor pressure vessel has four 16-in. nozzles which will be capped during initial operation but which can be used in future operations for forced-circulation inlet and outlet connections (i.e., two loops are provided). Also, considerable flexibility has been incorporated in the core design. The space in the core plate and core shroud structure accommodates 164 fuel assemblies, but only 148 fuel assemblies will be used during initial operation.

The following three features give added latitude within each fuel assembly: (1) the stainless-steel cladding contains 602 ppm natural boron, (2) the center fuel-rod position of each fuel assembly can be filled with either a fuel rod or a boron rod, and (3) besides the 148 regular fuel assemblies that are enriched 4.3 per cent in U^{235} (see definition of enrichment below), 22 fuel assemblies are available which are enriched to 5.23 per cent ("spiked" assemblies). These spiked assemblies are on standby if needed to meet reactivity design requirements at any time between initial startup and the attainment of a selected fuel burnup (about 10,000 Mwd/ton).

The reactor will probably be the first indirect-cycle boiling reactor to go into operation and the first boiling reactor to use ThO_2-UO_2 fuel on a long-term basis (the BORAX-IV core used ThO_2-UO_2, but long life was not an objective).

Fuel Rods

The basic fuel used in the fuel assemblies is a mixture of thoria (ThO_2) and urania (UO_2) enriched to 93.5 wt.% in the U^{235} isotope. There are 148 regular fuel assemblies and 22 spiked fuel assemblies; the enrichment for the regular fuel is 4.3 per cent and for the spiked fuel is 5.23 per cent, where the enrichment of the thoria-urania mixture is defined as the following weight ratio:

$$\frac{(U^{235}) \text{ as metal}}{(Th + U^{235} + U^{238}) \text{ as metal}}$$

If the spiked assemblies are not required at initial startup, all 148 fuel-assembly positions will contain the 4.3 wt.% fuel. The thoria-urania mixture is in the form of a solid solution. Pellets that are 95 per cent of the theoretical density are obtained by pressing a mixture of ThO_2 and UO_2 powder, combined with a binder, which is then sintered in air at 1700°C. The mixture has a melting point of about 5900°F. The pellets are cylindrical, having a nominal

outside diameter of 0.407 in. and a length of 0.500 in. A type 304 stainless-steel tubular jacket that contains 602 ppm natural boron is used to encase 120 of these cylindrical pellets to form a fuel rod (fuel pin) with an over-all length of approximately 62 in.

Total number of fuel rods in core	3700*
Total fuel-rod length	62 in.
Length of thoria-urania in each fuel rod	60 in.
Outside diameter of fuel jacket	0.450 in.
Pellet dimensions	0.407 in. in diameter × 0.500 in. long
Number of pellets per fuel rod	120
Total number of pellets in core	About 4.4×10^5
Pellet density	94% of the theoretical density
Jacket material and thickness	Type 304 stainless steel containing 602 ppm natural boron; 0.020-in. wall thickness
Jacket thickness-to-diameter (OD) ratio	0.0444
Pellet-jacket clearance (nominal)	0.0015 in. on radius
Additional gas space	Approximately 1 in. at the top of each fuel rod
Filling gas	Helium

Fuel-Element Assemblies

A fuel-element assembly (Fig. IV-1) is composed of 25 fuel rods that are arranged in a 5 × 5 array. The spacing between the rows of fuel rods in each individual assembly is maintained by two spacers, each located about 20 in. from either end of the fuel rods. These spacers, shown in outline in section B-B, Fig. IV-1, are fabricated by spot welding with type 304 stainless steel. End fittings for each fuel-rod jacket are designed to protrude through upper and lower support plates (grids). The upper support plate is welded into a top alignment box, and the lower support plate is welded into a bottom nozzle. A shoulder-and-nut arrangement on the protruding fuel-rod end fittings allows the fuel rods to move in an axial direction, sliding freely in the fuel-assembly support plates, thus allowing for variations in axial thermal expansion of the individual fuel rods within each assembly. The top alignment box is free to move vertically in the fuel-assembly-alignment grid structure, allowing freedom of movement for the fuel rods relative to the distance between the upper and lower fuel-rod support plates. Flat springs, made by cutting and bending the top box of each fuel assembly, maintain the radial alignment of the upper ends of the fuel assemblies. Flow loop tests on prototype elements with lead replacing fuel were done to investigate the stability of the tubes and their tendency to vibrate under boiling conditions; no visible vibration was discernible. The center rod of each fuel assembly is interchangeable with a borated stainless-steel rod, which is used for control of initial reactivity and flattening. In the fuel-enrichment calculations, it was assumed that 40 per cent of the fuel assemblies contained the borated rods. Individual fuel assemblies are not sheathed. There are 164 fuel-assembly positions in the core; 16 of these positions will be occupied by dummy fuel assemblies to prevent coolant bypass of the operating assemblies. The 16 extra positions are available for operating assemblies if they are needed to meet future design requirements.

Total number of fuel assemblies	148
Number of fuel assemblies in core with regular fuel	Between 126 and 148*
Number of fuel assemblies in core with spiked fuel	Between 0 and 22*
Number of fuel rods per assembly	25
Center-to-center distance between fuel rods	0.75 in.
Fuel-element lattice	Square
Pattern in core formed by all 148 assemblies	Approximately a 60-in.-diameter circle
Over-all length of fuel assembly	$81\frac{5}{8}$ in.

* There are 148 fuel assemblies; the middle fuel rod of each assembly is interchangeable with a borated stainless-steel rod that may be used for initial control flexibility.

* Spiked assemblies may not be needed at initial startup but may be needed at a later point in core life to permit a longer core lifetime.

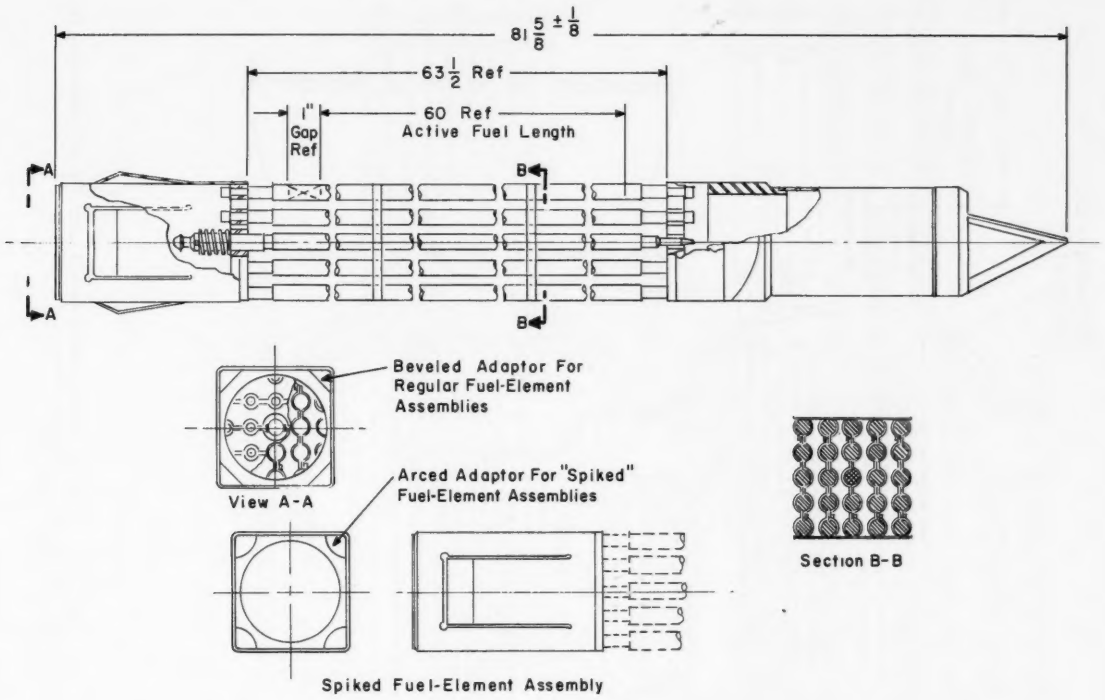

Fig. IV-1 Fuel-element assembly for the Elk River reactor.[1]

Method of holding fuel rods	Two intermediate wire spacer grids, an upper support plate, and a lower support plate

Control Rods

Thirteen boron–stainless steel cruciform control rods are mounted on the bottom of the reactor vessel. Their withdrawn position is above the core; therefore reactivity is decreased by their downward movement and increased by their upward movement. During normal operation, one peripheral rod is used as a regulating rod and the remaining 12 are used as shim rods.

Number	13
Material	2.0 wt.% natural boron in stainless steel
Dimensions	Cruciform, $14\frac{7}{8}$-in. span
Active length	58 in.
Spacing to adjacent control rods	Except for peripheral assemblies, each four-assembly fuel cluster is surrounded by control-rod blades on all four sides
Followers	45-in.-long, Zircaloy cruciform
Method of control-rod removal	Bayonet coupling
Upward motion of rod	Increases reactivity
Control rods driven from	Below

Core Structure

The core structure (Figs. IV-2 and IV-3) is a 5-ft right-circular cylinder that can accommodate 164 fuel assemblies. The core is supported by a 6-in.-thick core plate, which in turn is supported and held in place by a cylindrical barrel that is fastened to the bottom head of the pressure vessel. There is an alignment hole in the core plate for the lower end of each fuel assembly; upper alignment is provided by a Zircaloy shroud structure that separates the entire length of the core into cells, each accommodating four fuel assemblies. The cruciform control rods are guided into the spaces between the individual cells of this Zircaloy shroud structure. The control-rod guide and

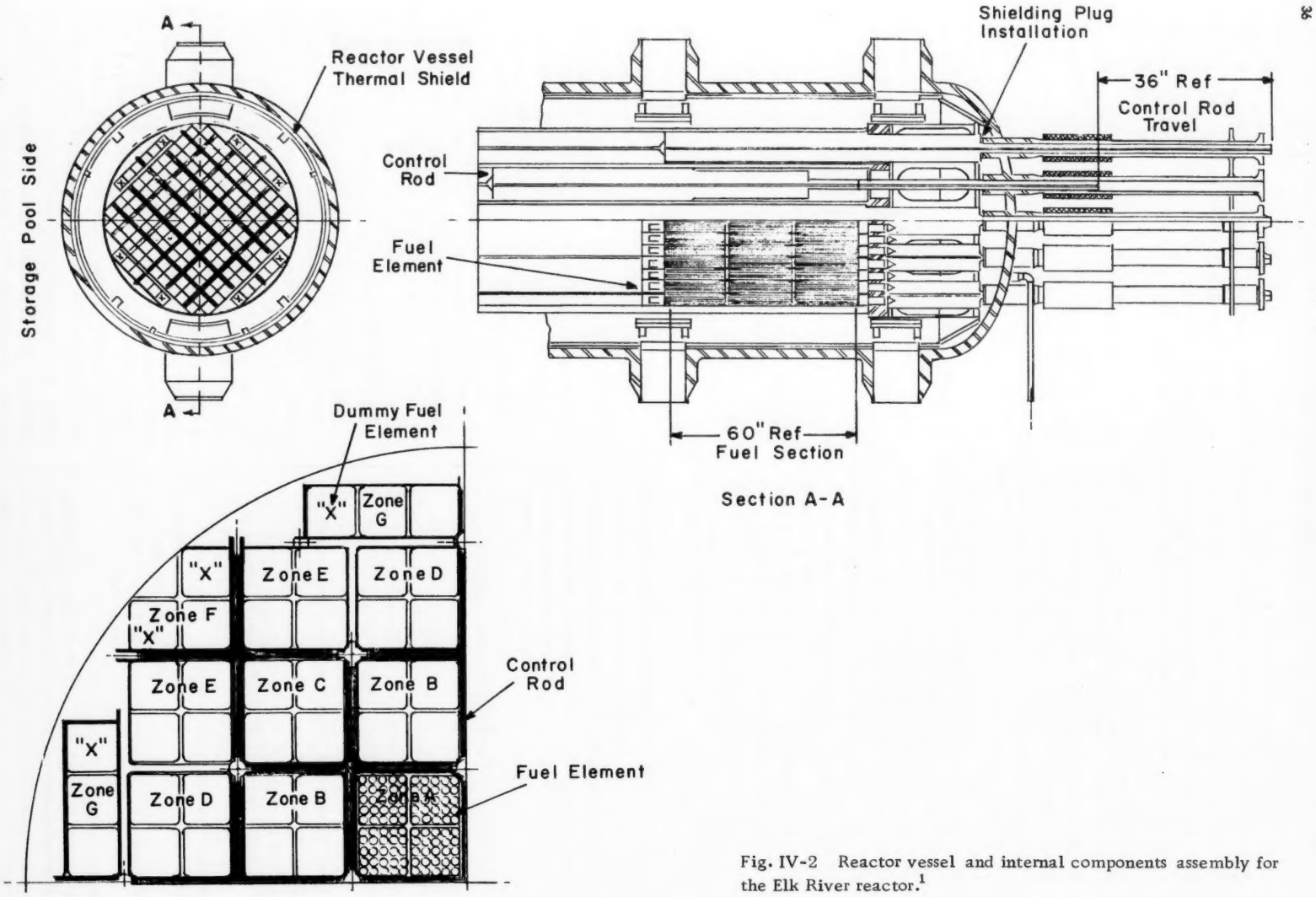

Fig. IV-2 Reactor vessel and internal components assembly for the Elk River reactor.[1]

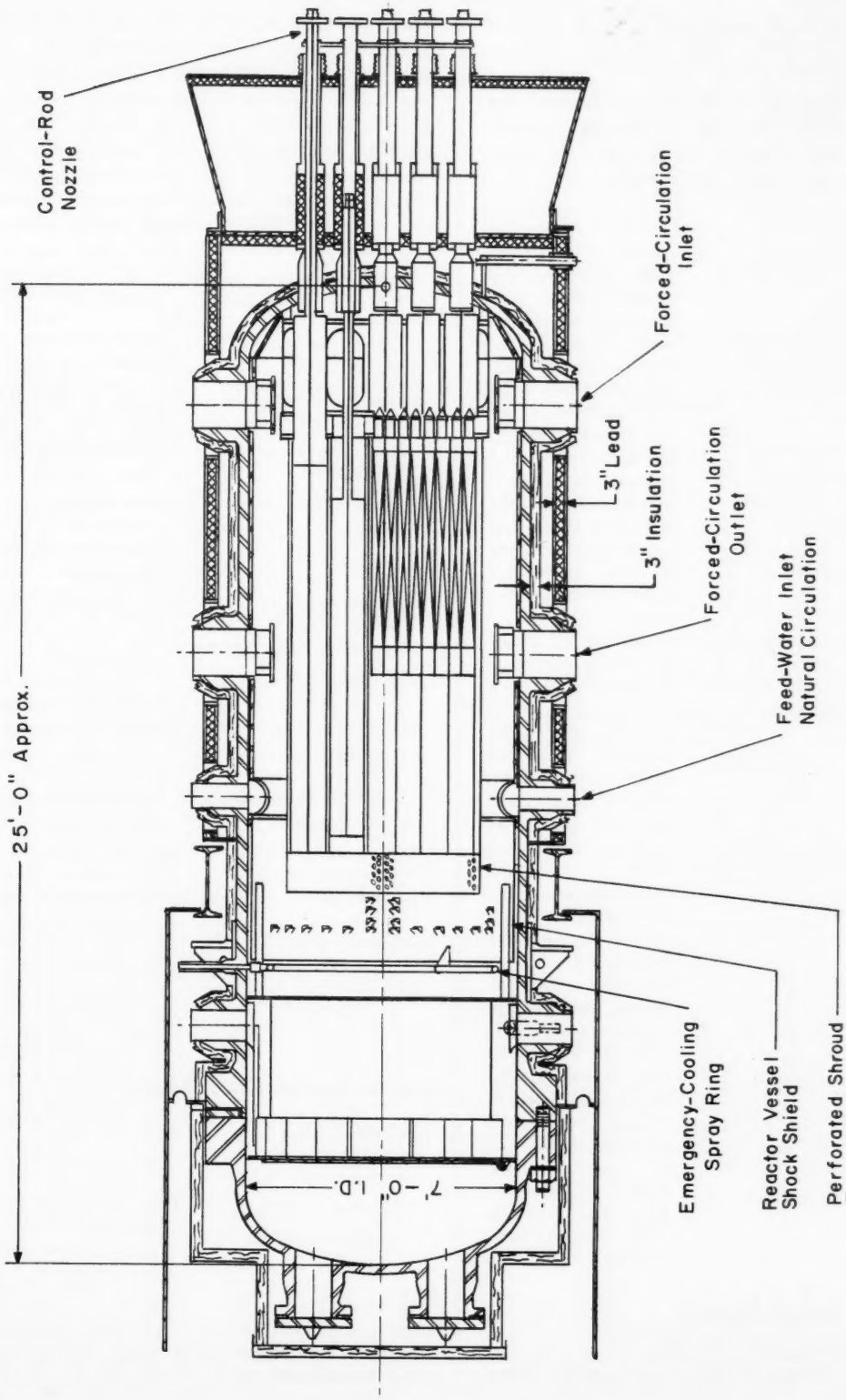

Fig. IV-3 Pressure vessel showing vertical section through the Elk River reactor.[1]

shroud assembly is shown in Fig. IV-3. A 5-ft-high stainless-steel riser structure, plus a 12-in. perforated riser extension, is located above and fastened to the Zircaloy shroud; the entire assembly is fixed to the bottom core plate. The 5-ft riser is divided into the same number of cells as the core shroud.

Dimensions	14 ft 7¼ in. from the bottom of the core-plate support barrel to the top of the perforated riser extension
Method of supporting fuel assemblies	Bottom support plate and cell type (four fuel assemblies per cell) Zircaloy shroud structure
Fuel assembly hold-down	Friction of flat springs, which are part of the top boxes of the fuel assemblies, bearing on upper part of Zircaloy shroud structure
Control rods guided by	Zircaloy shroud structure in core and riser structure above core
Coolant-flow guides	Recirculating water is directed down the annular space between the reactor pressure vessel and the outer surfaces of the riser and the core shroud structure; the flow down the annulus turns 180° at the bottom of the pressure vessel, flows through the lower fuel-assembly fittings, and upward past the fuel elements where the flow is divided, for clusters of four assemblies each, by the Zircaloy shroud; the flow is then guided upward by the riser structure to the steam-water separation point

Fuel and Control Program

Approximately 40 per cent of the fuel assemblies will have a boron rod in place of the center fuel rod at initial startup. It is planned to operate about 4750 Mwd/metric ton* (320 days) with these boron rods in place. After this time the boron rods will be replaced by 4.3 per cent enriched fuel rods. The reactor will then operate another 4750 Mwd/metric ton. The spiked fuel assemblies (if not required at initial startup) will then be used to extend the core lifetime beyond 9500 Mwd/metric ton.

Boron rods (each of 60 fuel assemblies contains a boron rod in center position) replaced after	320 days (4750 Mwd/metric ton)
Spiked fuel assemblies installed after	640 days (9500 Mwd/metric ton)
Average fuel lifetime exposure	9500 Mwd/metric ton
Maximum fuel lifetime exposure	>9500 Mwd/metric ton (dependent upon effectiveness of spiked fuel program)
Average fuel exposure between fuel-assembly replacement	9500 Mwd/metric ton
Burnable poison	600 ppm natural boron in the fuel cladding
Positions of control rods in fresh operating core (equilibrium xenon and samarium)	A peripheral control rod is used as a regulating rod, whereas the remaining 12 are utilized as shims
Program of rod withdrawal as burnup proceeds	When the regulating rod has reached the end of its travel in compensating for fuel burnup, the shim rods will be positioned to keep the regulating rod in its proper operating range

Spatial Distribution of Power

Maximum-to-average power ratio	3.45
Flattening method	Boron rods are interchangeable with the center fuel rod of each fuel assembly

* Megawatt days per metric ton of thorium metal plus uranium metal.

Heat Removal

Average core inlet water velocity	5.3 ft/sec
Central assembly inlet velocity	5.8 ft/sec
Total coolant flow rate through core	27,000 gal/min or 1.02×10^7 lb/hr
Primary steam flow	258,000 lb/hr
Secondary steam flow	225,000 lb/hr
Average steam quality at core exit	0.028 (wt. fraction)
Subcooling of flow to core	2.4°F
Temperature of feed water to reactor	450°F (subcooler exit)
Reactor (boiling) water temperature	536.5°F (936.5 psia)
Primary outlet steam temperature	536.5°F
Fraction of heat removed by temperature rise	0.14
Fraction of heat removed by boiling	0.86
Number of passes	1
Maximum heat flux	313,000 Btu/(hr)(sq ft)
Maximum fuel centerline temperature	2819°F
Average heat flux	90,700 Btu/(hr)(sq ft)
Average power density in core	25.6 kw/liter
Specific power	14.6 Mw/metric ton of thorium + uranium
Equivalent fuel-to-cladding thermal conductance	907 Btu/(hr)(sq ft)(°F)

Pressure Vessel (Fig. IV-3)

Materials	A-302 grade B carbon steel with type 304 stainless-steel internal cladding
Dimensions:	
Inside diameter	7 ft
Over-all inside height	25 ft
Shell thickness	3 in.
Cladding	0.109 in.
Weight (all internals including core)	200,020 lb
Operating pressure	936.5 psia (initially); 1168 psig (future)
Design pressure	1250 psig
Test pressure	1875 psig
Material between core and vessel	1-in.-thick stainless-steel cylindrical thermal shield with outer surface located $\frac{1}{2}$ in. from pressure-vessel wall, extending from below core to near the top of the riser. A louvered $\frac{1}{8}$-in. thermal-shock shield extends from the top of the thermal shield to an elevation above the emergency-cooling-water spray rig
Maximum temperature used in design of pressure vessel	650°F
Maximum thermal stress expected on inner surface of vessel (due to gamma heating)	9060 psi
Thermal-shock design limit	35°F over a 15-sec period
Maximum vessel wall heating and cooling rate (except for emergencies)	150°F per hour

Nozzle schedule:

Title	Nominal size, in.	Quantity	Location
Head nozzles	12	4	Top head
Steam outlet	10	2	18 ft $10\frac{1}{4}$ in. above vessel bottom
Feed-water inlet	8	2	13 ft 0 in. above vessel bottom
Forced-circulation outlet*	16	2	9 ft 4 in. above vessel bottom
Forced-circulation inlet*	16	2	3 ft 0 in. above vessel bottom
Control-rod nozzles	4	13	Bottom head
Liquid-level connections	$1\frac{1}{2}$	3	$7\frac{1}{8}$ in. below bottom of vessel; 18 ft $10\frac{1}{4}$ in. above bottom of vessel;

*Initially capped off. To be used in the future if forced circulation becomes necessary for operation at 116.4 Mw(t).

Nozzle schedule (Continued):

Title	Nominal size, in.	Quantity	Location
			3rd nozzle 14 ft 1 in. above bottom of vessel
Emergency cooling nozzle	$1\frac{1}{2}$	1	17 ft $4\frac{1}{4}$ in. above vessel bottom
Dome vent connection	1	1	Top head
Liquid poison inlet	$2\frac{1}{2}$	1	Lower plenum below core
Type of heads			Elliptical
Method of holding head on			Bolted flange

Reactor Instrumentation and Control

Failed fuel-element detection: For gross detection, a fission-product monitoring system is located in the off-gas system from the H_2-O_2 recombiner

Nuclear operating instruments and locations:

Two startup channels: Two BF_3 proportional counters with scalers and logarithmic count-rate meters. These instruments also supply signals to interlocks which prohibit rod withdrawal when reactor period is less than 7 sec. Range: one set for 10^2-10^6 neutrons/(cm^2)(sec) and one set for 10^4-10^8 neutrons/(cm^2)(sec)

Two log n channels: Two compensated ionization chambers, logarithmic amplifiers. These instruments also supply signals to interlocks which prohibit rod withdrawal when the reactor period is less than 15 sec. Range: 10^6-10^{13} (full power) neutrons/(cm^2)(sec)

Two linear power channels: Two compensated ionization chambers, electrometer instrument. These instruments also supply signals to an alarm set at 140% of any set range (will also be used as an aid during startup due to their low range). Range: 10^6-10^{13} neutrons/(cm^2)(sec)

Three high-flux safety channels: Three uncompensated ion chambers to scram reactor when flux exceeds a selected normal level. Alarm sounds at 10% above full power; provides scram signal at 125% of full power. Two out of three required for scram during power operation; one required during startup. Scram level can be adjusted to lower level for startup. Range: 10^7-10^{14} neutrons/(cm^2)(sec)

These nine flux detectors are located in four holes which penetrate the biological shield. One hole is located approximately at the core horizontal center line, tangent to the outside of the reactor pressure vessel, and extending completely through the biological shield. Four channels (one log n, one linear power, and two safety) are located in this hole. A similar hole parallel to this one, but on the opposite side of the reactor vessel, contains one log n channel, one linear power channel, one safety channel, and one spare position. Two radial holes, terminating at the pressure-vessel outer wall, each contain one startup BF_3 channel.

Neutron-source strength and location: Antimony rod encased in beryllium. Source strength greater than 10^{10} neutrons/sec. The assembly is $3\frac{1}{4}$ in. in diameter and 24 in. long. It is located in a dummy fuel

	assembly on the core periphery
Control-rod drive	Rack-and-pinion type. Rod-drive motors, located in a room below the reactor, are connected to the control-rod extensions by flexible shafts equipped with magnetic couplings. The 228-lb control rods will be scrammed under gravity when the magnets are de-energized. Accuracy of indicated position is ±0.05 in. Total stroke is 56 in.
Maximum rod withdrawal rate	½ in./sec
Scram time	2.5 sec (maximum)
Liquid poison system	12 cu ft of boric acid under a 32-cu ft air cushion. An air compressor keeps the tank under 2000-psia pressure. If any control rod does not hit bottom within 2.5 sec after scram signal, an alarm sounds and an operator must decide whether to use boric acid. 0.145 Δk total worth
Additional reactivity control	Boron rod replacing central fuel rod in 40% of the fuel assemblies. Boron content in cladding is 602 ppm by weight

Excess reactivity:	
Effect	$\Delta k/k$
Cold to hot (68 to 506°F)	0.0113
Doppler broadening due to power change from 0 to 58.2 Mw (0 voids)	0.0026
Voids (0 to 17.6%)	0.0230
Equilibrium xenon	0.0171
Equilibrium samarium	0.0069
Change in boron pin temperature from 68 to 506°F	0.0107
Design excess (to account for uncertainties)	0.0159
Fuel burnup	0.0800
Shutdown safety margin	0.0624
Total control required	0.2299
Worth of control agencies:	
Rods with center rod out	0.1490
Boron rods replacing central rods in 40% of assemblies	0.0234
Boron in cladding	0.0575
Total available control (12 control rods)	0.2299
Total available control (13 control rods)	0.2639

Primary Coolant Circuit (Fig. IV-4)

Steam and water that leave the tops of the fuel assemblies pass upward through the core and riser shroud and separate at the reactor water surface. The water phase recirculates (by gravity) down the annulus between the reactor pressure vessel and the riser and core shroud; the water turns 180° at the bottom of the pressure vessel and is directed back upward through the fuel assemblies. Steam passes into the pressure-vessel steam dome and then out through two 10-in. nozzles. Each 10-in. steam line leads to a separate loop that begins with an 8-in. T fitting with one 8-in. side capped but available for future expansion of the system to a 116.4-Mw(t) plant. The 8-in. line leads to the primary side of a steam generator where the primary steam is condensed by secondary water, thus producing saturated secondary steam to be fed to the separately (coal) fired superheater. The condensate collection level is above the reactor water level; thus primary condensate flows from the steam generator to a subcooler that cools the water to 450°F (86.5°F subcooled). This subcooled water is then introduced back into the annulus portion of the reactor, via a spray ring, where it mixes with and subcools the naturally recirculating water by 2.4°F before it reenters the bottom of the fuel assemblies.

Number of independent loops (primary steam-condensate loops)	2

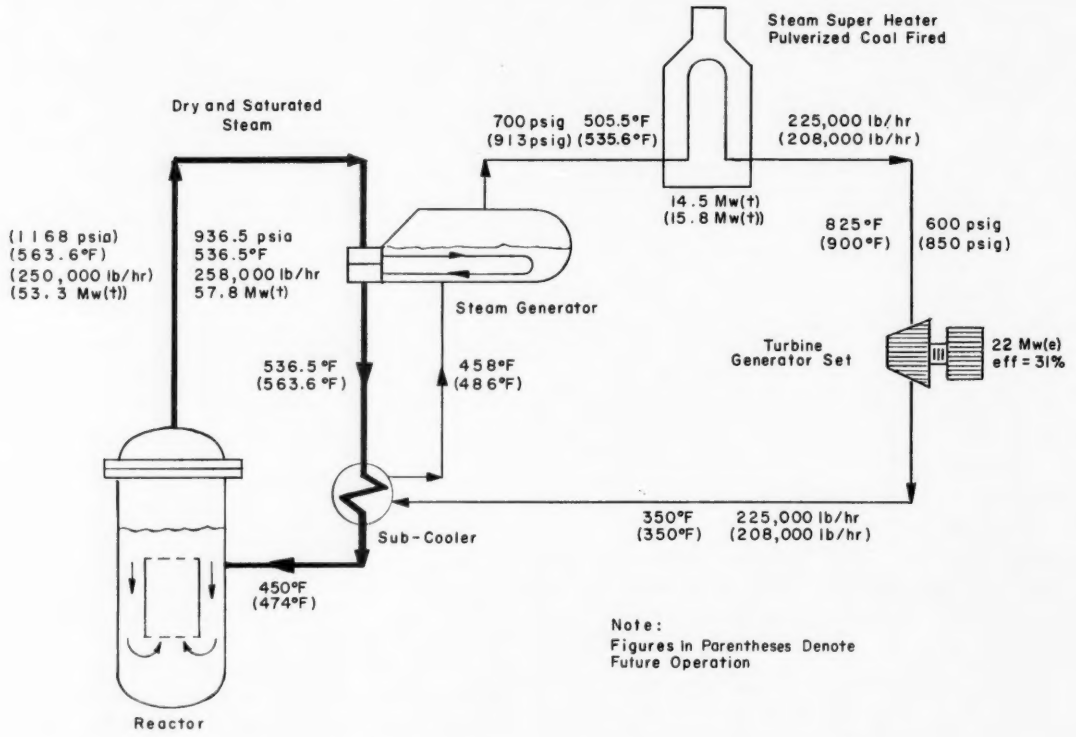

Fig. IV-4 Simplified flow diagram of primary coolant circuit for the Elk River reactor.[1]

Number of steam generators per loop	1
Number of pumps per loop	None
Circulation rate per loop	258,000 lb/hr
Method of pressure limitation	A dump valve to the emergency condenser opens at 1210 psig. There is also one relief valve in each primary steam loop, one set at 1240 psig and the other at 1250 psig
Provisions for shutdown cooling	After shutdown, reactor steam is bled to the emergency condenser until the reactor water temperature reaches 250°F. A decay-heat cooling system is then used to lower water temperature to 120°F
Type of steam generators (called evaporator-condensers in reference 1)	Horizontal U-tube type with gravity drain to a subcooler
Size of steam generators	50-in. shell inside diameter, 23 ft 6 in. long, $1^{11}/_{16}$-in. shell thickness
Construction of steam generator	642 U tubes; $^{15}/_{16}$-in. triangular pitch; $^{3}/_{4}$-in. outside diameter × 16 BWG wall, 8-in. shell inlet; 8-in. shell outlet, 14-in. channel inlet, 8-in. channel outlet
Heat-transfer area of steam generator	4710 sq ft (70 sq ft of disengaging surface)
Design pressure of steam generator	1000-psia shell side; 1250-psia tube side
Test pressure of steam generator	1500-psia shell side; 1875-psia tube side
Operating pressure of steam generator	715-psia shell side; 950-psia tube side
Heat-transfer area of subcooler	369 sq ft (U-tube type)
Design and test pressures of subcooler	Same as steam generator
Materials (ASTM specification and grade):	

Steam generators:	
Shell	A-212 grade B carbon steel
Tubes	Type 304 S.S., A-249 (welded seam)
Tube plate	A-105-Cl-2 steel
Other primary surfaces	Lined with type 304 S.S.
Subcooler:	
Shell	A-106 grade B carbon steel
Tubes	Type 304 S.S., A-249 (welded seam)
Tube plate, headers	A-105-Cl-2 steel
Emergency condenser:	
Shell, water boxes, tube sheets, nozzles	A-285 grade C carbon steel (Monel clad on primary side)
Tubes	70% copper, 30% nickel
Startup heater:	
Water box, tube sheet, tubes, nozzles	Type 304 S.S.
Shell side	Carbon steel
Piping	Primary water and steam type 304 S.S.
Handling of leakage	Primary leakage is not expected to exceed 3 gal/day. This leakage will drain to a collection tank and can be returned to the system as primary makeup. Two 3000-gal retention tanks receive waste water from all potentially contaminated drains

Treatment of Primary System Water

Additives to reduce oxygen content	None; however, the amount of free oxygen is reduced by recombination as described below
Handling of radiolytic gases	Radiolytic (decomposition) gases formed in the reactor are carried over to the steam generators. They are removed at the lower channel section of the steam generator and piped to a recombiner system. About 3 scfm of H_2 and O_2, carried with a small quantity of steam, will be recombined, exit as steam from the recombiner, condense in a heat exchanger, and then be fed back to the primary system. The catalyst bed consists of platinized alumina balls
Purity specifications	Reactor water is maintained at a specific resistance of 1×10^6 ohm-cm, equivalent to 0.5 to 1.0 ppm total solids
Ion exchangers	Two ion exchangers (one in use normally); 12-gal/min purification water flow; effluent specific resistance is 12×10^6 ohm-cm, *p*H 7.0. Resin in cartridge is removed for normal replacement of resin; if highly contaminated, entire exchange unit is removed
Monitoring of water	Radiochemical analysis is performed before waste water is released from retention tanks

Fuel Handling

Expected frequency	Replacement of boron rods (in center of fuel assemblies) at the end of about 320 days. Placement of spiked fuel assemblies about 640 days after initial startup. Added core life following placement of spiked assemblies is unspecified
Method of entrance to vessel	Four 12-in. nozzles in head, as well as removable head for operations that cannot be performed through 12-in. nozzles. Refueling is accomplished with the head removed
Method of handling fuel	Manual, underwater handling, using a

	grappling tool and crane. A minimum of 8 ft of water is present during transfer from the reactor cavity to the fuel canal to the fuel storage well

Steam Plant

Number of turbines	1
Type	Nonreheat, preferred-standard, 3600 rpm, single-case, condensing unit with four extraction points for feed-water heating. Turbine exhausts to a single-pass, divided-water-box surface condenser
Steam conditions	Normal turbine throttle conditions are 850 psig, 900°F, exhausting at 1.5 in. Hg. Secondary steam flow is 225,000 lb/hr, and primary steam flow is 258,000 lb/hr
Feed-water heaters	First two stages: two vertical, closed, low-pressure, shell-and-tube types. Third stage: vertical, direct-contact, deaerating type. Fourth stage: horizontal, closed, high-pressure type
Turbine rating	20,000 kw at 85% power factor; capability of 23,000 kw; designed for 900-psig, 900°F throttle conditions, exhausting at 1.5 in. Hg
Reactor thermal power	58.2 Mw. Reactor vessel, shielding, and containment shell designed for future increase to 116.4 Mw
Superheater thermal power	Approximately 17.1 Mw
Gross electrical output	22,000 kw
Gross efficiency	29.3%
Heat rate	11,600 Btu/kw(e)-hr

Plant Arrangement

The containment building houses the reactor, the steam generators, the switchgear, the motor control centers, and other auxiliary equipment connected with operation of the nuclear plant. A personnel air lock with a 5- by 7-ft door, a 2.5-ft emergency air lock, and an 8- by 10-ft freight door provide access to the containment building. The reactor control room and turbine-generator unit are located in a conventional steam-plant building. The coal-fired superheater is located in a separate building directly behind the steam-plant building.

Containment

The containment building is basically a cylinder with a hemispherical top and ellipsoidal bottom (Fig. IV-5). The internal diameter of the cylinder is 74 ft, and the total height of the building is 115 ft, 18.5 ft of which is below grade. A 30,000-gal water storage tank is attached to the inside upper portion of the hemispherical top. The inside of the containment shell is lined with 24-in.-thick concrete that tapers to about 4 in. thick at the upper part of the hemispherical top.

Diameter	74 ft
Over-all height	115 ft
Wall thickness:	
Ellipsoidal bottom	0.70 in.
Cylindrical sides	0.875 in.
Hemispherical top	0.50 in.
Portion of hemispherical top above water tank	0.70 in.
Free volume	287,000 cu ft
Design pressure	21 psig
Basis for design pressure	Design pressure must equal or exceed pressure produced within the container if the primary system ruptures and flashing of primary water occurs. Conditions at a reactor power of 116.4 Mw(t) were assumed. No credit is taken for shell heat dissipation or heat sink represented by 24-in. concrete liner and internal components
Pneumatic test pressure	26.25 psig

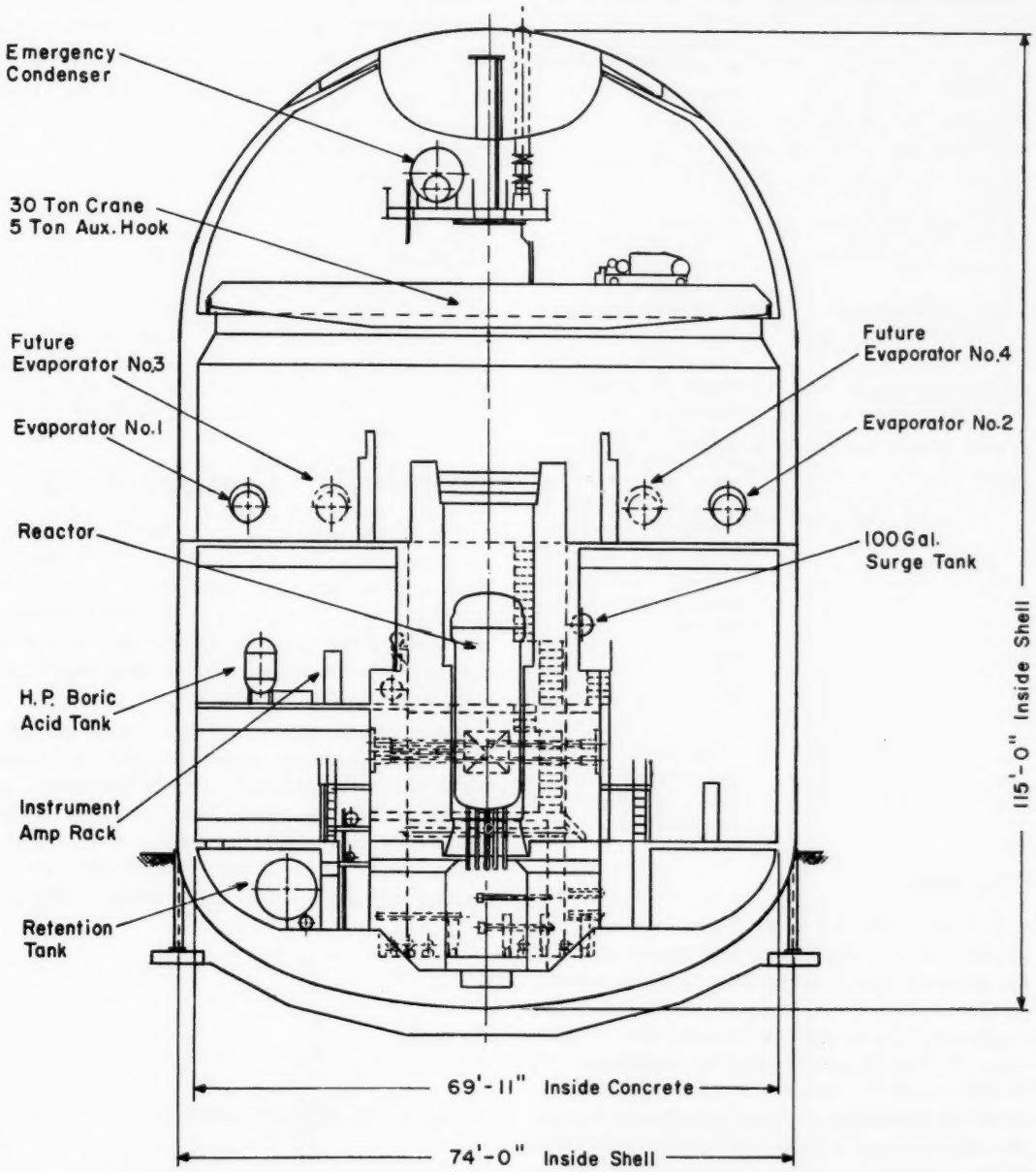

Fig. IV-5 General containment-arrangement cross section for the Elk River reactor.[1]

Maximum leakage rate	0.1% per day at 21 psig
Missile protection	2 ft of concrete lining inside of cylindrical sides and at least 2 ft of concrete at all points in bottom of building; concrete tapers to 4 in. at the 30,000-gal storage tank
Doors and other openable penetrations	5- × 7-ft personnel air lock; 2.5-ft emergency air lock; 8- × 10-ft freight door
Other penetrations	250 cables ranging from $\frac{1}{2}$ to $1\frac{1}{8}$ in. in diameter. Standard conduit fittings, which contain a neoprene bushing compressed around the cable, are used. Holes in the containment vessel are tapped for the fittings. The cables run through a steel box, attached to the vessel, forming a 3-in. space that is filled with epoxy resin. One 20-in. outside air inlet and one 24-in. outlet are closed by dampers for isolation of building. Two vacuum breaker lines are used

Plant Control

Twelve of the 13 control rods are used as shims, and the 13th is used as a regulating rod. All rods are moved manually until the operating power level is reached, at which time the regulating rod is switched to automatic operation. As burnup progresses, the regulating rod is automatically withdrawn. The 12 shims are manually positioned at required intervals to keep the regulating rod within the proper operating range. Primary and secondary steam pressures are the two controlled parameters. One control loop maintains primary steam pressure at a predetermined value, for a given load, through the adjustment of the regulating rod. The second loop holds a uniform steam pressure at the turbine throttle valve by varying the governor-valve position. Coupling between primary and secondary systems is effected by introducing signals into the secondary system whenever the primary pressure set point is changed.

Shielding

The biological shield around the reactor is designed to reduce the dose rate at the outer surface of the shield to 2.5 mrem/hr when the reactor is operating at 116.4 Mw(t). The thickness of ordinary concrete needed to meet this requirement was calculated to be 9.5 ft; however, only 8.5 ft will be installed initially, with foundations designed for the additional foot to be added if needed. Concrete shielding is provided around all possible major sources of radioactivity. These major sources were not enumerated in reference 1; however, the steam generators, purification filters, ion exchangers, and water-retention tanks are examples.

Pathfinder Control Rods

The Pathfinder Atomic Power Plant of the Northern States Power Company will use cruciform control rods, approximately 9 ft long and of 10-in. span, composed of 2 per cent boron–stainless steel of $\frac{1}{4}$-in. thickness. Reference 4 reports the development of welding techniques used to fabricate these rods.

After an investigation of three basic fabrication approaches, the approach selected was to weld two flat plates to a third flat plate, as indicated in Fig. IV-6. The operating conditions of the control rod subject it to flowing steam and water at 500°F and 600 psi, to impact and shock loads, and to wear, which are

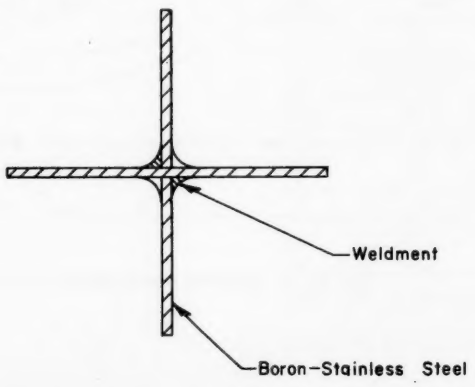

Fig. IV-6 Cross section of Pathfinder control rod (not to scale).

associated with its normal motion and scram operation. The tolerances necessary to ensure free motion in the control-rod guides are relatively close. The investigation indicated that these requirements could best be met by the use of a manual metal arc-welding process, using a coated electrode ($^3/_{32}$-in.-diameter type E308-16), while the pieces were held in a very rigid jig to preserve correct alignment during welding and cooling. Since the operating stresses on the rod are not large, intermittent welds were used. Tests of the welds showed adequate tensile strength; when fracture occurred it was, in all cases but one, in the base metal rather than in the weld. Dimensional inspection analysis showed that the rod assembly was held well within the specified tolerances. Maximum bow and twist in the 9-ft lengths were less than $^1/_{16}$ in. The maximum angularity deviation between blades was held to within $\pm^1/_4°$.

The reference[4] states that control rods that are fabricated in this way are now in use at the Allis-Chalmers Critical Test Facility and are to be specified for the Pathfinder plant.

References

1. W. S. Farmer and D. G. Strawson, Final Hazards Report for the RCPA Elk River Reactor at Elk River, Minnesota, and Additions and Corrections to Final Hazards Report for the Elk River Reactor at Elk River, Minnesota, USAEC Report TID-11734, Allis-Chalmers Mfg. Co., Nuclear Power Dept., July 8, 1960.
2. Allis-Chalmers Mfg. Co., Nuclear Power Dept., Operations Manual, Volume II, Plant Specifications, Dec. 2, 1960.
3. A. W. Kramer, *Boiling Water Reactors*, Addison-Wesley Publishing Co., Reading, Mass., 1958.
4. Joseph F. Potochnik, Pathfinder Atomic Power Plant. Welding of Boron Stainless Steel Control Rods, USAEC Report ACNP-6106, Allis-Chalmers Mfg. Co., Atomic Energy Div., Mar. 1, 1961.

Section

V

Power Reactor Technology

Materials

Beryllium

Interest has been maintained in beryllium metal since the earliest days of nuclear-reactor development. Although the metal has served successfully as a moderator material, its utilization as a fuel-element cladding has been prevented by the following considerations:

1. Unsatisfactory mechanical properties, particularly the lack of ductility at room temperature, which results in elongations of less than 2 per cent.
2. Possible lack of corrosion resistance to conventional reactor coolants
3. Susceptibility to radiation damage
4. High cost and toxicity
5. Lack of satisfactory fabrication methods

However, the potentialities of beryllium are so great, primarily because of its low neutron-absorption cross section, that strenuous efforts are being made toward the solution of the problems presented by the above factors. A general review of the metal was given in the September 1959 issue of *Power Reactor Technology*, Vol. 2, No. 4, page 67.

Probably the most dramatic recent development is the preparation of single-crystal beryllium with room-temperature elongations as great as 92 per cent. These single crystals were prepared (by zone refining) at the Franklin Institute.[1] They show that the ductility of beryllium is controlled by certain impurities and that the metal itself is not inherently brittle. Although single-crystal results cannot necessarily be duplicated readily in commercial polycrystalline material, a practical solution of the ductility problem now seems more probable, and work is continuing at the Franklin Institute and at Nuclear Metals, Inc., on the problem. Although improvements in mechanical properties are certainly desirable, it has not been shown that the better-quality beryllium now available is inadequate for reactor use.

Contributing to the difficulty of the problem of the mechanical properties of beryllium is the highly anisotropic nature of the hexagonal metal. Properties vary more with crystallographic direction in beryllium than they do in such other hexagonal metals as zirconium and magnesium; the major difficulty is that, at room temperature, slip can take place only on the basal plane. The texture of the metal, therefore, has a marked effect on its mechanical properties (particularly on ductility) because of the importance of basal-plane alignment. Since the tube is the most commonly used form for power-reactor applications and since tubes are most readily made by extrusion—a process that usually has a marked effect on texture—studies have been made to determine the degree of basal-plane alignment caused by variations in extrusion techniques. A study reported in reference 2 shows that basal-plane alignment in an extruded finned tube is nearly the same whether the tube is produced by the single extrusion of a hot-pressed billet (randomly oriented) or from a previously hot-extruded (highly oriented) rod. The final tube texture depends only on the amount of reduction during the final extrusion. This result permits a wider choice of starting materials.

Although considerable effort and some progress are apparent in the field of mechanical-properties investigation, there is apparently no information on the corrosion behavior of beryllium in hot water or steam. Corrosion results are limited to those developed by the British for the CO_2-cooled Advanced Gas-Cooled Reactor (AGR) and to work at Oak Ridge National Laboratory (ORNL) on cor-

rosion by the impurities in the helium coolant of the Experimental Gas-Cooled Reactor.

The behavior of beryllium in CO_2 at 600°C and above is not fully understood; it apparently is not presently considered by the British to be satisfactory in view of their decision to employ stainless-steel-clad fuel elements in the AGR and to restrict the use of beryllium to experimental channel loops.[3] In arriving at this decision, progress on fabrication development was considered to be slow but satisfactory, the irradiation resistance of beryllium was considered to be adequate, and the major difficulty was considered to be the lack of corrosion resistance. Recent work[4] at ORNL has shown that high-carbon (1.6 per cent) beryllium goes to "breakaway" behavior in as little as 16 hr at 700°C in helium that contains 100 ppm H_2O. Metallographic examination indicated intergranular attack on the Be_2C sites. The reaction of carbides with moisture, even in quite small quantities, may be one of the mechanisms of attack in hot gases.

Except for the fuel materials, beryllium is probably the only reactor material that forms gas within the metal lattice under irradiation. The volume of helium formed in beryllium by the $(n,2n)$ and other reactions is less than that of the fission gas released in uranium at the same irradiation level, but, under certain conditions, it is sufficient to destroy the structural properties. At low temperatures (500°C or below), helium will form only small bubbles in the metal lattice. As the temperature increases to a 700°C range,[5] larger bubbles will accumulate by diffusion, and swelling will take place up to a 30 vol.% increase at 1000°C. The threshold for damage[6] is around 10^{19} nvt (fast). In addition to swelling, the formation of large bubbles at the grain boundaries might eventually make the metal permeable to gases. Ductility decreases[6] can be expected in heavily irradiated beryllium at higher temperatures (~700°C).

Despite possible difficulties with texture, as discussed above, extrusion is the most attractive method for the fabrication of beryllium tubing for fuel-element cladding. The high thermal conductivity of the metal (42 per cent of that of copper) would indicate that, unlike stainless steel, an extended-surface beryllium fuel element would have marked advantages in heat transfer. A program for the development of fabrication methods, conducted by General Nuclear Engineering Corporation,[7] had as its objective the production of finned beryllium tubing to be used for jacketing oxide fuel elements in a gas-cooled (CO_2) reactor. The tube dimensions were 0.500 in. in inside diameter and 0.035 in. in minimum wall thickness; the 12 rounded triangular fins had a helical twist of about one-half turn in a 24-in. length and were 0.160 in. high. Two methods of producing such tubing were investigated by Nuclear Metals, Inc. The first, the so-called "filled-billet" technique, involves the extrusion of a cylindrical billet through a cylindrical, smooth die. The final, finned shape results from the form of the beryllium in the billet, which is machined to have the same relative shape as the product but which has a magnified cross section. The spaces between the fins of the billet are filled with iron, and the assembly is clad in iron before extrusion. Experiments with this method were quite successful. The second technique was simpler and was found to be superior. It employs a ribbed die, and the billet is simply a clad, thick-walled, beryllium tube. The finned shape is impressed by passage through the ribs of the die. It was found possible to produce the twist on the tubes during the extrusion by giving a slight angle to the ribs in the die. A preliminary production run of 200 ft of tubing of apparently high quality was produced by the method to satisfactory tolerances. Failure stresses that were determined by the tube-burst technique were as high as 95,000 psi.

The extrusions that are described above were carried out at temperatures in the 1700 to 1800°F range. A group of extrusion experiments was also carried out in the "warm" range, below 1000°F, at Brush Beryllium Co. At this temperature, beryllium may be extruded without cladding. However, it was not possible to produce satisfactory extrusions at the lower temperatures because the fins could not be fully formed.

Work at Sylcor on the impact extrusion (Dynapak) of beryllium rods produced some material that had 100,000-psi ultimate strength, 50,000-psi yield, and elongations of 10 per cent at room temperature in the direction of extrusion. The fabrication of finned tubing was not attempted by this method.

To summarize, appreciable progress has been made, and work is continuing on the problems concerned with the mechanical properties of beryllium. Less progress has apparently been made with beryllium–carbon dioxide cor-

rosion investigations, but the extent of the radiation-damage problem has been clarified, and limiting temperatures and exposures are more clearly understood. Work on the fabrication of beryllium tubing for fuel-element cladding has produced promising results.

Zirconium Alloy Pressure Tubes

The pressure-tube concept permits the construction of reactors with high operating pressures without the requirement for large, thick-walled pressure vessels and the size and cost limitations which such pressure vessels entail. Neutron economy dictates, however, that pressure tubes be built from low-cross-section materials. The Plutonium Recycle Test Reactor at Hanford will employ pressure tubes of Zircaloy-2, operating at a pressure of 1050 psig at 542°F. The environment will be hot pressurized water on the inside and an inert gas contaminated with small amounts of water vapor on the outside. The work reported in reference 8 is concerned with the inspection and corrosion testing of 97 of the tubes.

Wall thicknesses of the tubes were determined ultrasonically, and fluorescent-penetrant techniques were used to find areas that required further inspection by immersion ultrasonics or radiography. Descriptions of the tests and their results are given in detail in the reference. All tubes were pickled in HNO_3-HF and were corrosion tested at 750°F and 100 psi for 36 hr. Tubes showing dubious areas were repickled after vapor blasting to remove the oxide. Of 97 tubes, 89 were sound and satisfactory for use after the above corrosion tests and other tests.

The development of pressure-tube reactors fosters the desire for zirconium alloys of higher strength. Such alloys should, of course, retain adequate ductility and corrosion resistance and should have cross sections approaching those of the original zirconium. High-strength alloys, if available, would also be of considerable value for fuel-element cladding. Nuclear Metals[9] has reported the results of efforts to produce such alloys. Heat-treatable molybdenum-aluminum alloys that ranged in composition from 1 per cent molybdenum–5 per cent aluminum to 7 per cent molybdenum–2 per cent aluminum were investigated, and so were two alpha-stabilized alloys that contained 7 per cent tin and 1.5 and 2.5 per cent aluminum. Room-temperature yield strengths as high as 191,000 psi were obtained, but the elongations were low (13 to 2.6 per cent). The corrosion behavior during six-day exposures to 680°F water and to 750°F steam ranged from poor to bad.

References

1. W. Hodge, Review of Recent Developments in the Technology of Beryllium, DMIC-Memo-123, Battelle Memorial Institute, Defense Metals Information Center, Aug. 18, 1961.
2. N. A. Hill, Textures in Beryllium Tubes Produced from Hot Extruded Rod, British Report AERE-R-3701, May 1961.
3. The Advanced Gas-Cooled Reactor, *Nuclear Eng.*, 6(59): 151 (April 1961).
4. Oak Ridge National Laboratory, Gas-Cooled Reactor Program, Quarterly Progress Report for Period Ending June 30, 1961, USAEC Report ORNL-3166, Aug. 28, 1961.
5. R. S. Barnes, The Effect of Neutron Irradiation on Beryllium, *Nuclear Eng.*, 6(59): 149 (April 1961).
6. R. S. Barnes, The Behaviour of Irradiated Beryllium, British Report AERE-R-3769, July 1961.
7. General Nuclear Engineering Corp., Gas-Cooled Reactor Project Terminal Report No. 9, USAEC Report GNEC-176, June 10, 1961.
8. R. L. Knecht, The Physical Integrity and Corrosion Resistance of the Zircaloy-2 Pressure Tubes for the PRTR, USAEC Report HW-67677, Hanford Atomic Products Operation, December 1960.
9. G. A. Henrikson, High-Strength Zirconium-Base Alloys, USAEC Report NMI-1244, Nuclear Metals, Inc., Feb. 22, 1961.

Section

VI

Power Reactor Technology

Containment

One of the generally recognized economic handicaps under which nuclear power plants presently operate is the requirement of a containment building that must meet very rigid specifications for leaktightness and usually must be capable of withstanding substantial internal pressures. Any saving in plant cost which can be made through proper choice of the containment approach and through economy in construction of the containment building is likely to be of significant magnitude. It seems probable that the optimum approach to containment design will vary with the type, power output, and location of the reactor and with the characteristics of the site. Any new approaches that open up the possibility of a wider range of construction materials and techniques could eventually lead to savings for nuclear plants in general. Two recent containment structures, that for the Heavy-Water Components Test Reactor (HWCTR) and that for the Boiling Nuclear Superheater (BONUS) Power Station, are of interest in this respect. Although the two plants differ widely in their basic approaches to the containment problem, they are similar in that both use concrete (suitably coated to ensure imperviousness) as part of the containment barrier.

The HWCTR building, shown in Fig. VI-1, is cylindrical in shape, is about 117 ft high, and is constructed with the lower half below grade. The BONUS station, shown in Fig. VI-2, employs a hemispherically shaped building that is 120 ft high and has only a 37-ft section below grade level. Both plants use concrete as the primary containment material for all subgrade construction. Containment above grade is provided by the usual steel envelope that is joined to the subgrade concrete structure. All items of plant equipment lie within the containment building in each plant; however, the HWCTR is not an electric power producer, and the plant does not contain power-conversion equipment.

HWCTR

More specifically, the HWCTR is housed[1] within a concrete-and-steel containment vessel that is 70 ft in inside diameter and 117 ft 6 in. high. The lower 57 ft 6 in. of the vessel lies below grade and consists of a prestressed concrete cylinder of 1.5-ft wall thickness and a 5-ft-thick foundation slab that is 70 ft in diameter. The upper 65 ft of building height above grade is composed of a 29-ft-long cylindrical steel shell that is topped by a hemispherical dome. The two sections are joined at grade level by bolting the mounting flange of the cylindrical steel shell portion of the vessel to studs embedded in the top surface of the lower-segment concrete wall. The building is designed for a leakage rate of less than 1 per cent of the contained free volume per 24 hr, at an initial pressure of 24 psig.

Originally it was intended[1] to provide the usual sealed all-steel building for the HWCTR. However, a study indicated that the usable volume could be increased and the cost of containment could be decreased significantly if a reinforced-concrete structure were used. Although a concrete structure was not expected to exhibit the same degree of leaktightness as comparable steel construction, the below-grade location of the concrete portion of the structure was expected to compensate somewhat for this lower integrity. Moreover, it was felt that the prestressed concrete would be effective in reducing the size of any postpouring cracks, which could cause excessive leakage, and would also reduce the thickness required to withstand the design pressure.

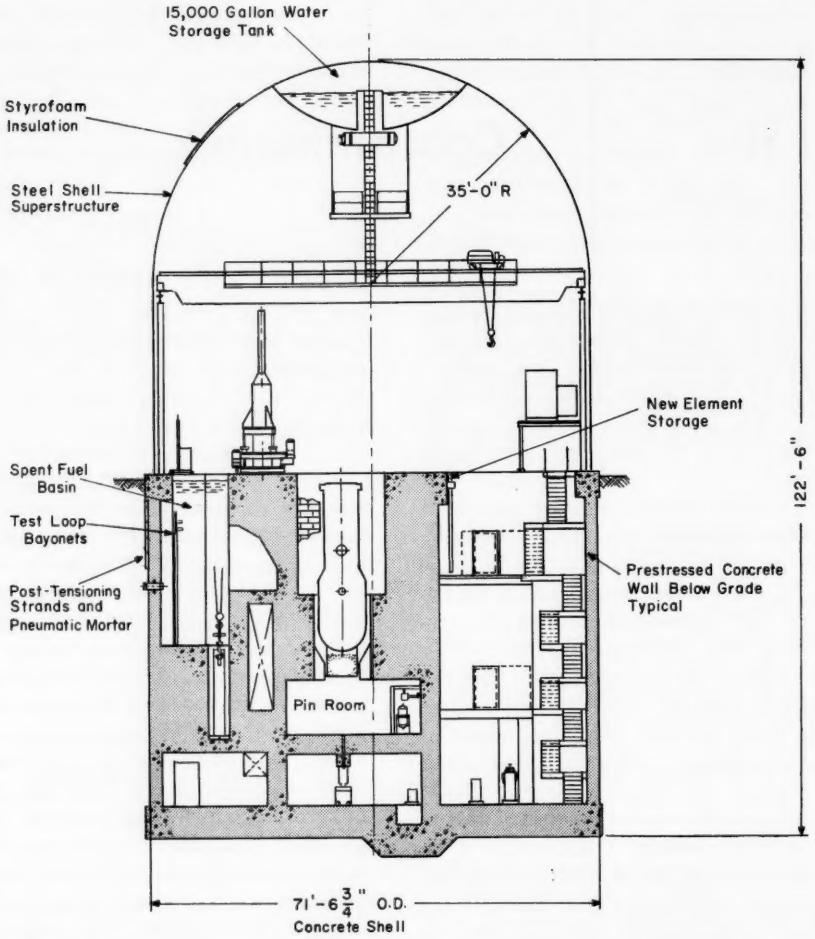

Fig. VI-1 Perspective of HWCTR containment building.[1]

As a prelude to the actual design of the concrete portion of the containment vessel, the following items were investigated:

1. The concrete mix required to accomplish an extensive, monolithic, vertical pour
2. The most suitable method of depositing the necessary depth of concrete within the restricted work space available
3. The permeability of thick-cast concrete sections and methods for the reduction of any excessive gas outleakage encountered
4. The difficulties associated with concrete-building wall penetrations required for piping and instrumentation

As a result of these investigations, a concrete design of medium slump ($3\frac{1}{2}$ to 4 in.) was selected. It was also shown that placement of the concrete could best be accomplished by depositing the mix through vertically oriented 8-in.-diameter rubber chutes, called "elephant trunks," located at 8-ft intervals around the periphery of the building. The concrete permeability tests established that the leakage rate through the 18-in.-thick concrete wall, at the design pressure of 24 psia, was within the specified limits. Furthermore, this leakage could be substantially reduced by the application of a 2-in.-thick layer of pneumatic mortar to the exterior of the wall and a coating of thermal-setting plastic resin (the brand name is Liquid Tile) on the interior surfaces. Consequently these additional precautions were taken in the construction. It was also determined

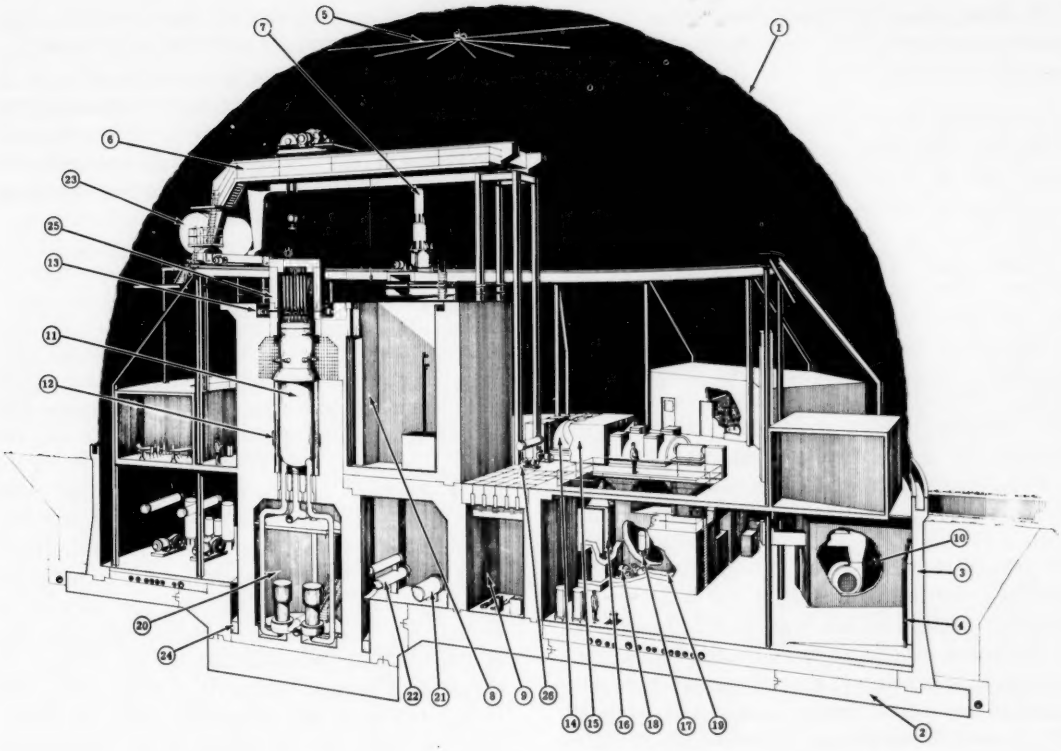

1. Steel Dome
2. Foundation Mat
3. Retainer Wall
4. Freight Door
5. Building Spray
6. Polar Gantry Crane
7. Fuel Unloading Coffin
8. Spent-Fuel Storage Pool
9. Solid-Radioactive-Waste Storage
10. Building Ventilation Intake Fan
11. Reactor Pressure Vessel
12. Neutron-Shield Tank
13. Control-Rod-Drive Motor Trench
14. Turbine-Generator
15. Turbine Shield
16. Condenser
17. Condensate Pumps
18. Evacuator Pump
19. Gland Seal Condenser
20. Reactor Circulating-Water Pump Room
21. Startup Heater
22. Reactor Water-Purification Coolers
23. Emergency Condenser
24. Reactor Pit Water Moat
25. Removable Concrete Shield
26. Fuel Pool Cooling System

Fig. VI-2 Perspective of BONUS containment building.[2]

that the use of impact wrenches to tighten building-penetration pipe flanges resulted in disruption of the seal between the pipe and the concrete.

The following construction sequence was used in the erection of the building:

1. Placement of the 72 ft 2 in.-OD mat type foundation slab

2. Installation of all interior shielding walls, floors, and other concrete structures

3. Placement of the subgrade containment-building exterior walls

4. Prestressing exterior concrete subgrade wall

5. Application of pneumatic mortar and Bitumastic No. 50 damp-proofing to exterior surface of subgrade walls and backfilling

6. Erection of steel portion of building and attachment to subgrade walls

7. Installation of grade-level-finish floor, emergency exits, and steel-shell exterior insulation

Placement of the concrete for the exterior subgrade wall was accomplished in a continuous pour to eliminate all joints except those occurring at the foundation slab and at the steel shell. The concrete was poured in 2-ft lifts at the rate of 4 ft/hr to prevent overloading the forms. The concrete wall was prestressed by the use of 39 bands of $1^{9}/_{16}$-in.-diameter galvanized-steel strand, and each strand was sheathed with galvanized steel. The strands were stretched to a final net stress of 104,500 psi between welded-steel-plate pilasters located at 90° intervals around the wall.

Following prestressing, the exterior surfaces of the subgrade containment wall were coated with a 2-in.-thick layer of pneumatic mortar to prevent damage to the steel strand and to improve the leaktightness of the building. The interior surface of the wall and both surfaces of the grade-level slab were coated with a layer of Liquid Tile primer, a modified high-viscosity primer, and a final coat of Liquid Tile surfacer No. 1 mix. In addition, a layer of 10-oz fiberglass fabric reinforcing was applied to the subgrade containment-building wall following the initial primer coat. As a precaution against joint leakage, a coating return of 3 ft was provided on all abutting concrete walls and floor slabs and a 1-in. coating lap was used on all embedded steel plates.

The building has been completed and has been successfully pressure tested and leak tested. The report[1] states that the cost of the building was only two-thirds that of a comparable all-steel structure. As a consequence of the experience gained in this construction, the report makes the following recommendations:

1. Erect the subgrade containment-building walls and grade slab before the erection of interior walls and floor slabs.

2. Increase the thickness of the subgrade containment-building wall to 2 ft 0 in.

3. Provide piping space between grade-level structural slab and finish slab.

4. Allow ample space between subgrade containment-building wall penetrations to facilitate concrete placement.

5. Install reactor prior to completion of steel shell.

6. Consider the use of "sprayed-on" polyurethane insulation for exterior of steel shell.

7. Use expansion joints at the junction of all interior walls and floor slabs with the subgrade containment-building wall or provide independent support for these items to minimize the danger of cracking of the containment-building wall.

8. Use pregreased, prestressed cables.

BONUS

The BONUS-plant containment building[2] consists of a concrete foundation slab that is 182 ft in diameter and capped by a steel dome that is 166 ft 8 in. in diameter at the base and 109 ft $2^{1}/_{2}$ in. high. The lower 26 ft $4^{1}/_{2}$ in. of the dome length is a cylindrical section that rests upon the foundation slab and extends upward to about 3 ft above grade level. The remaining 82 ft 10 in. of height approximates a hemisphere in shape and is welded to the top edge of the cylindrical section. The below-grade segment of the shell is protected against earth-fill side thrust by a tapered concrete retaining wall that is located upon the foundation slab, at its periphery, and extends about 3 ft above grade level. Except for that area which lies directly beneath the reactor and fuel-storage facilities, the foundation slab is overlaid with a layer of sand, about 18 in. thick, topped by a 6-in.-thick basement floor slab. The sand-filled space is used for the routing of permanent plant piping and electrical conduit. The building is designed for an internal pressure of 5 psig and for a maximum outleakage of 0.2 per cent of the building volume at the maximum expected pressure of 4.3 psig.

The BONUS containment building differs from existing power-reactor containment structures in that (1) it houses the entire power plant, including all auxiliary systems; (2) it is designed for comparatively low pressures; and (3) it is constructed mostly above grade. Item 3 is a consequence of the high water table existing at the plant site. The low design pressure results from the relatively large volume, which is a natural consequence of housing the entire plant within the single building. The decision to enclose the entire plant instead of only the reactor and reactor-related systems was based upon considerations of both safety and economy.

As in the case of the HWCTR building, careful consideration was given to the question of the

permeability of the concrete. This problem is somewhat reduced because of the low maximum internal pressure (~5 psig), which reduces the difficulties of achieving a satisfactory seal and decreases the leakage rate through a given opening. In order to determine the extent of the problem and the possible solutions thereto, a research and development program was carried out to (1) measure the permeability of concrete in this application, (2) find the most suitable concrete mixes, and (3) develop a suitable sealing membrane that could be economically applied to the surface of the extensive and segmented foundation slab. The results of the program are given in reference 3.

The program indicated that, when elasticity and self-healing capabilities were considered, sealing membranes made of coal tar derivatives gave the best over-all systems. The foundation-slab construction-joint seals were made with Jet Careylastic, a rubberized coal tar elastic joint sealer normally used in jet fuel tanks. The foundation-slab membrane, applied over the entire surface of the slab, consisted of three plies of coal tar pitch, each $^{3}/_{16}$ in. thick, interlaced with two plies of asbestos felt. The wall membrane was composed of three coats of Bituplastic 33, a coal tar polymer emulsion. This material was also used as a floor membrane under walls and foundations that imposed medium to light loads. Water glass was used as the membrane under heavy-bearing-load conditions.

The BONUS containment building has been erected and has been successfully pressure tested and leak tested. During construction the surface of the foundation slab was covered with water, and the excellent sealing capabilities of the resultant water membrane were demonstrated. Consequently provisions have been included to permit the sand-filled space between the floor slab and the foundation slab to be flooded with water as a further guarantee against gas outleakage in the event of an accident.

References

1. H. W. Bellas, Heavy Water Components Test Reactor, Savannah River Plant, Composite Concrete-Steel Containment Vessel Engineering Considerations, USAEC Report DP-599, E. I. du Pont de Nemours & Co., June 1961.
2. General Nuclear Engineering Corp., Boiling Nuclear Superheater (BONUS) Power Station Final Hazards Summary Report, December 1961.
3. General Nuclear Engineering Corp., Containment Membrane Development for the BONUS Reactor Building, USAEC Report GNEC-168, May 15, 1961.

Section

VII

Power Reactor Technology

Operating Experience

Dresden

The design characteristics of the Dresden Nuclear Power Station were summarized in the September 1961 issue of *Power Reactor Technology*, Vol. 4, No. 4. Summaries of the operating experience have recently been given by Murray Joslin,[1] Vice President of Commonwealth Edison Company, and by I. L. Wade[2] of Commonwealth Edison and T. Trocki[2] of General Electric Company. Commonwealth Edison owns and operates the plant, which was supplied by General Electric.

The Dresden plant first produced power in April 1960, reached full output of 192,800 kw(e) (gross) in June 1960, and began regular commercial service in October 1960. The reactor was shut down from November 1960 to June 1961 to permit modifications of the control rods and control-rod drives and for inspections. From June through September 1961, the plant was base loaded; the maximum operating power was about 190 Mw(e) on week days and was reduced to 150 Mw(e) in the early morning hours and on week ends. During this four-month run, the plant load factor was about 80 per cent and the reactor availability was 100 per cent.

The plant was shut down on Oct. 2, 1961, for an inspection that was required under its license; references 1 and 2 cover the period up through the completion of this inspection. Although the modifications of the control rods and control-rod drives required a rather long shutdown, they did not represent inherent difficulties but rather were representative of the incidental difficulties that may be found in the early operation of a new and complex equipment installation. The problems were corrected, and the performance of the plant has been quite satisfactory. The October 1961 inspection showed that reactor components were in excellent condition. All in all, the operating results to date appear highly encouraging as an indication of the performance to be expected from the reactor in its future operation and from future boiling-water reactors.

The general nature of the difficulties with the control-rod drives is well known, but a description in some detail appears to be worth while. A diagram of the drive is given in Fig. VII-1.* The early difficulties that occurred in November 1959, during the period of critical testing, involved three cases of failure of the shear pin in the coupling head between the drive and the control rod. Shearing of the pins allowed the rods to remain in the reactor, in the shutdown position, when the drives were withdrawn. An investigation revealed that a loose-fitting coupling connection between the drive and the rod had created a hammer action on the shear pin. The trouble was corrected by decreasing the coupling clearance and by replacing the rolled shear pins with solid pins of greater strength.

The later difficulty was a cracking of the index tube (Fig. VII-1) that is the main driving member used for moving the control rod. Serious cracking was found in five index tubes and five guide roller mounts that were distributed among eight of the 80 drives; cracking of lesser significance was found in nine additional drives. Some of the tubes had cracks that were both longitudinal and circumferential, and these cracks occurred randomly along the entire length of the tube. One of the tubes was completely parted. After careful investigation it was concluded that the failures were characteristic of stress-corrosion cracking and that the 17-4 PH stainless steel of the index tubes, which had been heat-treated to its condition of maximum hard-

*Figures VII-1 and VII-2 are reprinted here by permission from the American Society of Mechanical Engineers.[2]

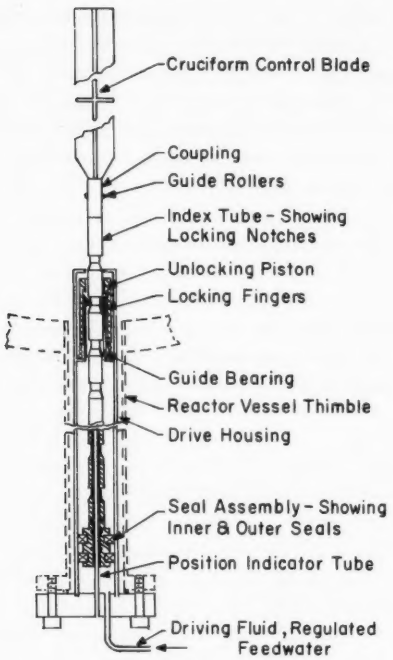

Fig VII-1 Schematic of control-rod drive and control blade of the Dresden reactor.[2]

ness by aging for 1 hr at 900°F, was susceptible to stress-corrosion cracking in high-temperature water at applied stress levels down to one-sixth of the yield strength. It was also found that similar material did not show the susceptibility to stress corrosion, even under stresses up to and slightly above the yield strength, after aging at temperatures in the 1050 to 1100°F range. In cases where 17-4 PH stainless-steel material was required,* the difficulty was corrected by replacing the original 17-4 PH stainless-steel parts with parts of the same material that had been aged for 4 hr at 1100°F. Other parts were replaced by alternate materials. In the case of the 17-4 PH stainless-steel replacement parts, the aging was done after the fabrication steps had been completed; previously some of the parts had contained high residual stresses due to cold straightening after the heat treatment.

*A discussion of the use of 17-4 PH stainless steel for critical reactor components may be found in the September 1961 issue of *Nuclear Safety*, Vol. 3, No. 1, page 39.

During the inspections incidental to the 17-4 PH problem, cracking was found in the boron–stainless steel control rods. The steel contained 18 per cent chromium, 12 per cent nickel, and 2 per cent natural boron. Cracking in the control rods was found in the base material in the vicinity of the welds that joined the plates to form the cruciform shape. It was concluded that the cracking was due to a combination of residual fabrication stresses and a loss of ductility in operation as a result of neutron absorption. The control rods were all replaced with control rods that consisted of boron carbide powder encapsulated in an assembly of $\frac{1}{4}$-in.-diameter type 304 stainless-steel tubes. The tubes are arranged in a cruciform pattern that is sheathed by type 304 stainless steel. The replacement control rod is the same size and the same shape as the boron–stainless steel rod; it weighs 40 per cent less and has a slightly greater reactivity effect.

A further result of the very thorough inspection given the Dresden reactor during its shutdown for the modifications was the observation, by periscope, of several hairline cracks along the edge of the fillet welds in the eggcrate lower support grid. This grid is the vertical core support member. These cracks are very fine, and they appear to have little depth. It was concluded that the cracks could have occurred after "soaking" of the completed structure at 600°F (to establish dimensional stability). It was also concluded that, in their existing condition, the cracks did not significantly affect the functioning of the support structure. They are to be kept under observation when the reactor is opened for servicing or refueling.[2]

The first reinspection of the reactor (in October 1961) showed apparently no change in the cracks in the grid plate, and the earlier opinion is supported that they are only minor fabrication cracks. The inspection also showed that the control rods and control-rod drives were in excellent condition.[1]

The operating experience to date has given valuable and encouraging information on reactor power control, carryover of radioactivity, equipment performance, and operating requirements.

The dual-cycle steam system allows controlled power changes from 55 to 100 per cent of full load without movement of control rods. The control of reactor power has thus been effected by turbine valve regulation of the secondary steam flow rather than by regulation

Table VII-1 POWER-PEAKING FACTORS MEASURED IN THE DRESDEN REACTOR[2]

Factor	Value at Half power	Value at Full power
Axial	1.6	1.5
Radial (includes intercontrol rod)	1.3	1.35
Local (corner rod)	1.39	1.39
Transient and maneuvering	1.25	1.25
Total	3.6	3.5

with control rods. Load pickup above 125 Mw(e) has been carried out at rates up to 8 Mw(e) per minute; the normal rate of pickup is about 5 Mw(e) per minute. Both generator and turbine trip tests have been performed satisfactorily with this plant. Turbine trip tests that were performed at 150 Mw(e) showed a rise in primary pressure of only 20 psia. Trip-off tests of two out of the four water-recirculation pumps, with the reactor at 75 per cent of full load, showed that the core water flow dropped only to 70 per cent of full flow. Circulation was maintained at a substantial level by natural convection in the loops that had inoperative pumps. The power output dropped only 8 per cent from the initial value.

The stability of the reactor has been demonstrated by (1) power oscillation tests, (2) tests at 137 per cent of rated primary steam flow, and (3) tests at very high core steam contents with both natural- and forced-circulation flow.

Measurements indicate that a substantial degree of power flattening is afforded by appropriate programming of the bottom-entering control rods, in conjunction with the permanent radial pattern of void distribution that is determined by a set of fixed orifices in the coolant channels. The power-peaking factors in the reactor at full power and at half power are given in Table VII-1. It is stated that the in-core ion-chamber system is of considerable value in arriving at control-rod programs that minimize power peaking. The system comprises 16 axial strings of miniature ion chambers ($\frac{1}{4} \times 2$ in.); each string contains four chambers.

Measurements and observations to date have indicated negligible carryover of activated solids into the turbine; separation factors for radioactive solids from the reactor to the steam are indicated to be in the order of 10^4 to 10^6. At full power the specific activity of the water at the core outlet is 3×10^6 dis/(cm^3)(sec); owing to the difference in density, the specific activity of the steam is lower by a factor of about 20. This activity, due principally to N^{16}, decays significantly in transit to the turbine because of oversized primary steam lines. Radiation levels around the turbine are shown in Fig. VII-2. Inspectors have entered the low- and intermediate-pressure sections of the turbine casings without contamination; similar experience has been encountered with the condenser and the hotwell. Measurements of activities of corrosion products in the recirculating reactor water have indicated that the longer-lived corrosion prod-

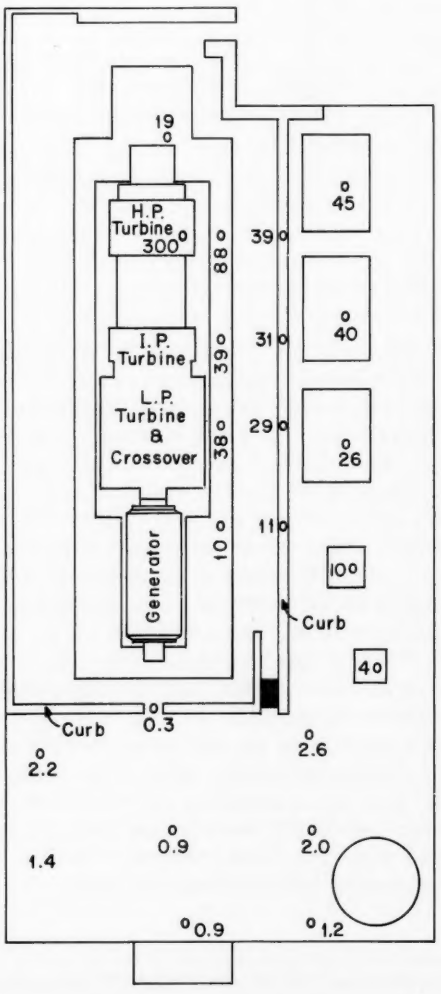

Fig. VII-2 Radiation levels (in mr/hr around Dresden turbine-generator at full-power operation.[2]

Table VII-2 SUMMARY OF WATER CONDITIONS IN THE DRESDEN REACTOR[2]

	Feed water	Reactor water
Conductivity, μmhos	0.10	0.25
Average pH	7.2	6.9
Chloride, ppm	<0.010	<0.014
Total iron, ppm	0.035	0.022
Total copper, ppm	0.017	0.010
Oxygen level, ppm	0.005	~0.25

ucts (Cr^{51}, Fe^{59}, Co^{58}, and Co^{60}) are behaving as in other water-cooled power reactors with respect to general activity levels and growth rates. An additional corrosion product (Cu^{64}) shows up from the copper-nickel alloy tubes in the primary feed-water heaters. Typical conditions of the feed and reactor water, as maintained by the full-flow feed-water demineralizer and the bypass demineralizer on the recirculating water, are given in Table VII-2.

The discharged gaseous activity from the stack has been far below the continuous limit of 0.70 curie/sec. Nitrogen-13 has been the principal activity measured in the off-gas; the activity has been about 500 μc/sec at full reactor power. The levels of fission gases that were measured in the stack have also been low, amounting to approximately 100 μc/sec during early operation. This activity was attributed to uranium contamination on the surfaces of the fuel elements. A small increase in the level, which occurred during later operation, may indicate leakage from fuel elements or from an in-core ion chamber. The fission-gas activity has been noted to respond to the motion of certain control rods; this observation agrees with previous experience in the Experimental Boiling-Water Reactor (EBWR) and indicates that it may be possible to narrow the search for suspected leaking fuel to within a small region of the core.

The plant performance and the experience with plant equipment have generally been good. The station delivers the design gross output of 192,800 kw and a net output of 184,000 kw, some 4000 kw higher than the design value. The plant heat rate is 11,090 Btu/kw-hr (net) at condenser pressure of $1\frac{1}{2}$ in. Hg. The canned-rotor pumps for primary-system water recirculation have performed satisfactorily during all operations. The reactor vessel head has been removed and reinstalled a number of times without difficulty in sealing. Experience with the packed valves in the primary and secondary steam system has been comparable to that in conventional plants; however, maintenance has been complicated due to limited accessibility because of radiation. The in-core ion-chamber system, which is used to take advantage of the power-flattening capability within the large boiling-reactor core, has proved to be extremely useful. Initially, a high rate of failure of the ion-chamber units was experienced; however, improved design and less handling have resulted in fewer failures.

The plant operating staff consists of 94 people; 40 are assigned to plant operation, 14 to mechanical and electrical maintenance, 25 to the technical staff, and 15 are management and service personnel. The central control room, which contains controls for the entire plant, is normally attended by only two operators, both of whom are licensed. Additional manpower required for peak maintenance work is obtained from other generating stations in the area; similarly, some of the Dresden manpower is loaned to other stations as required.

BORAX-IV

An evaluation of the Boiling Reactor Experiment No. 4 (BORAX-IV) fuel elements is given in reference 3. These elements were not intended for an extended period of use; however, they represent a novel design approach that may have some usefulness for other applications. The fuel element consisted of a box of six plates of extruded X-8001 aluminum. The plates were extruded so as to contain eight tubular cavities that were connected by the aluminum plate. Within the tubular cavities the ThO_2-UO_2 pellets were thermally bonded to the cladding with lead.

The elements operated at various times between December 1957 and February 1958, and they achieved a burnup of 1960 Mwd/ton. After a shutdown[3] for core revision, activity was discovered in the water, and it was found that 22 of the original 59 elements had developed defects. The cause of failure appeared to be that the reactor pressure had collapsed the $2\frac{1}{2}$-in. tubular free space provided at the end of the fueled length. This sharp reverse bending initiated cracks that had then corroded through during the shutdown. Except for the cracks, no other difficulty with corrosion was encountered, and other design features of the element, such

as the silicon-bonded end closures, operated satisfactorily.

References

1. M. Joslin, Dresden Up to Now, paper presented at the Annual Conference of the Atomic Industrial Forum, Chicago, Ill., Nov. 6–8, 1961.
2. I. L. Wade and T. Trocki, Performance and Operating Experience of the Dresden Nuclear Power Station, Paper 61-WA-268 presented at the Winter Meeting of the American Society of Mechanical Engineers, Nov. 26–Dec. 1, 1961.
3. C. F. Reinke et al., Metallurgical Evaluation of Failed BORAX-IV Reactor Fuel Elements, USAEC Report ANL-6083, Argonne National Laboratory, May 1961.

Section

VIII

Power Reactor Technology

Nuclear Instrumentation Systems

The December 1961 issue of *Power Reactor Technology*, Vol. 5, No. 1, contained information on the nuclear instrumentation systems for 13 power reactors. The purpose of this section is to present data on 11 additional power reactors. Figures VIII-1 to VIII-11 are block diagrams of the systems, and Table VIII-1 summarizes the salient features of these systems. Most of the information was taken from preliminary and final hazards summary reports. Some changes may have been made in some of the systems after publication of the summary reports, particularly in the cases of the preliminary hazards summary reports, but nevertheless it is felt that the data reflect design practice in the United States.

It is shown in Table VIII-1 that there is a barely discernible trend to a total of approximately seven channels; two cover the source range, two cover the intermediate or period range, and three serve the dual purpose of indicating power level in the full-power range and of providing a high-level trip signal for reactor protection. As in the systems previously surveyed, the BF_3 counter appears to be the most popular source range detector. The compensated ion chamber (CIC) is used without exception for intermediate-range operation, whereas common practice is again about equally divided between the use of compensated and uncompensated ion chambers for the power-range channels.

The same divergence in practice in the use of the low-level period information, which was discussed in the December 1961 issue of *Power Reactor Technology*, Vol. 5, No. 1, is evident in Table VIII-1. Although almost without exception the low-level period is measured, only about half of the designs specify a low-level period trip.

References

1. Carolinas Virginia Nuclear Power Associates and Westinghouse Electric Corp., Nuclear Power Dept., Preliminary Hazards Summary Report, Vol. II, USAEC Report CVNA-27(Pt. B, Vol. II), July 15, 1959.
2. J. G. Gallagher (Ed.), Hazards Summary Report for the SM-1A, USAEC Report APAE-13(Suppl. 2) (Rev. 1), Alco Products, Inc., October 1960.
3. W. Haass and J. Sieg, PM-1 Nuclear Power Plant Addendum to Hazards Summary Evaluation, USAEC Report MND-M-1853(Add. 1), Martin Co., Nuclear Div., 1961.
4. D. L. Fischer et al., The General Electric Vallecitos Boiling Water Reactor. Final Hazards Summary Report, USAEC Report SG-VAL-2 (2nd Ed.), Atomic Power Equipment Dept., General Electric Co., May 8, 1958; additional information supplied by J. B. Violette, Manager, VBWR, private communication.
5. Pacific Gas and Electric Co., Preliminary Hazards Summary Report, Humbolt Bay Power Plant Unit Number 3, USAEC Docket No. 50-133, Apr. 15, 1959.
6. Consumers Power Co., Application to U. S. Atomic Energy Commission for Reactor Construction Permit and Operating License. Part B. Preliminary Hazards Summary, Report NP-8329, 1959.
7. Puerto Rico Water Resources Authority and General Nuclear Engineering Corp., Boiling Nuclear Superheater (BONUS) Power Station Preliminary Design Study and Hazards Summary Report, USAEC Report TID-8524, Dec. 21, 1959.
8. Allis-Chalmers Drawing 43-500-923-04, supplied by K. H. Gruenwald, Nuclear Power Dept., Allis-Chalmers Mfg. Co., private communication.
9. J. Jacobson (Ed.), Final Safeguards Summary Report for the Piqua Nuclear Power Facility, USAEC Report NAA-SR-5608, Atomics International, Aug. 1, 1961.
10. Atomics International, Final Summary Safeguards Report for the Hallam Nuclear Power Facility, USAEC Report NAA-SR-5700, Apr. 15, 1961.
11. L. J. Koch et al., Experimental Breeder Reactor II (EBR-II), Hazards Summary Report, USAEC Report ANL-5719, Argonne National Laboratory, May 1957.

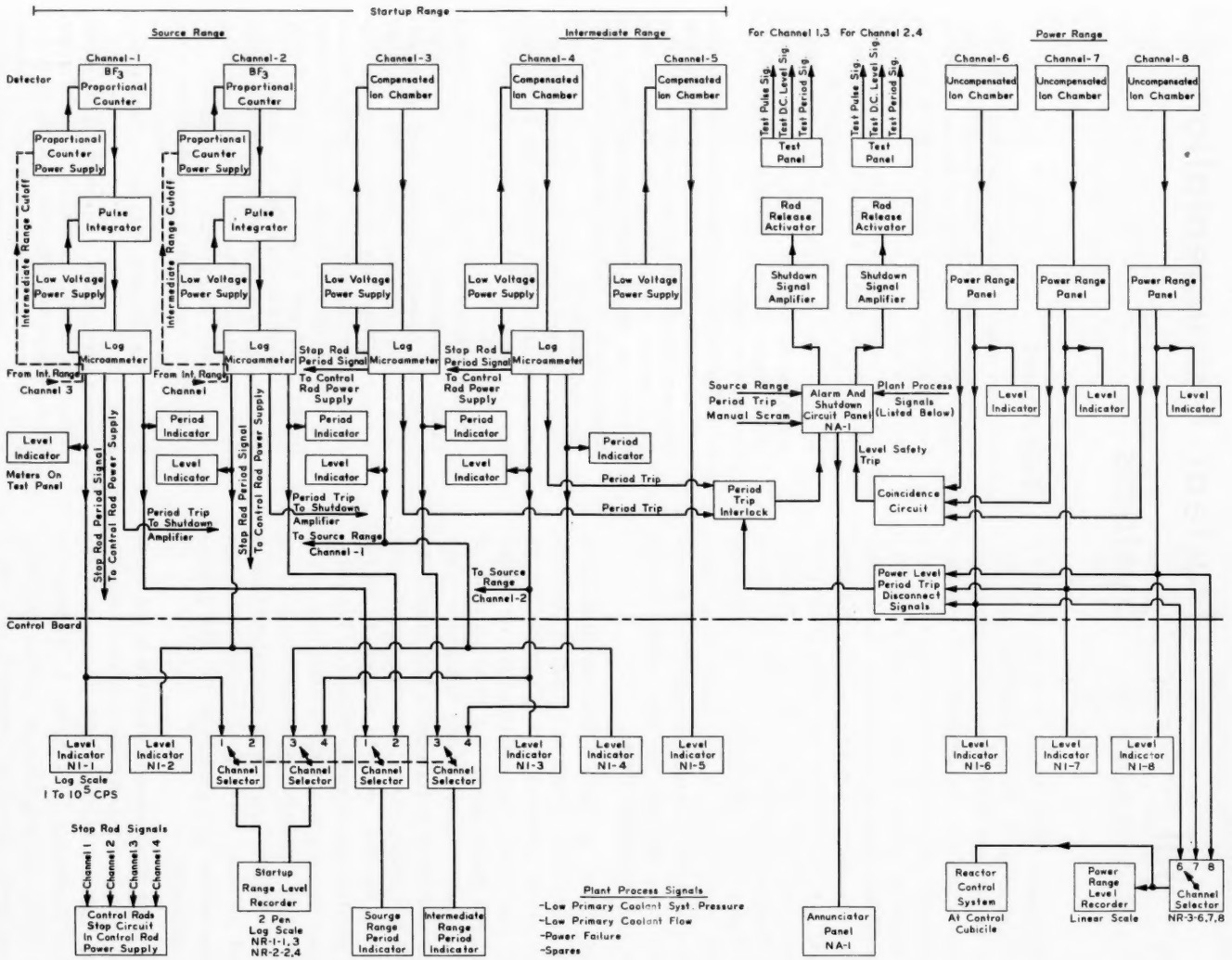

Fig. VIII-1 Block diagram[1] of nuclear instrumentation system, Carolinas-Virginia Tube Reactor (CVTR).

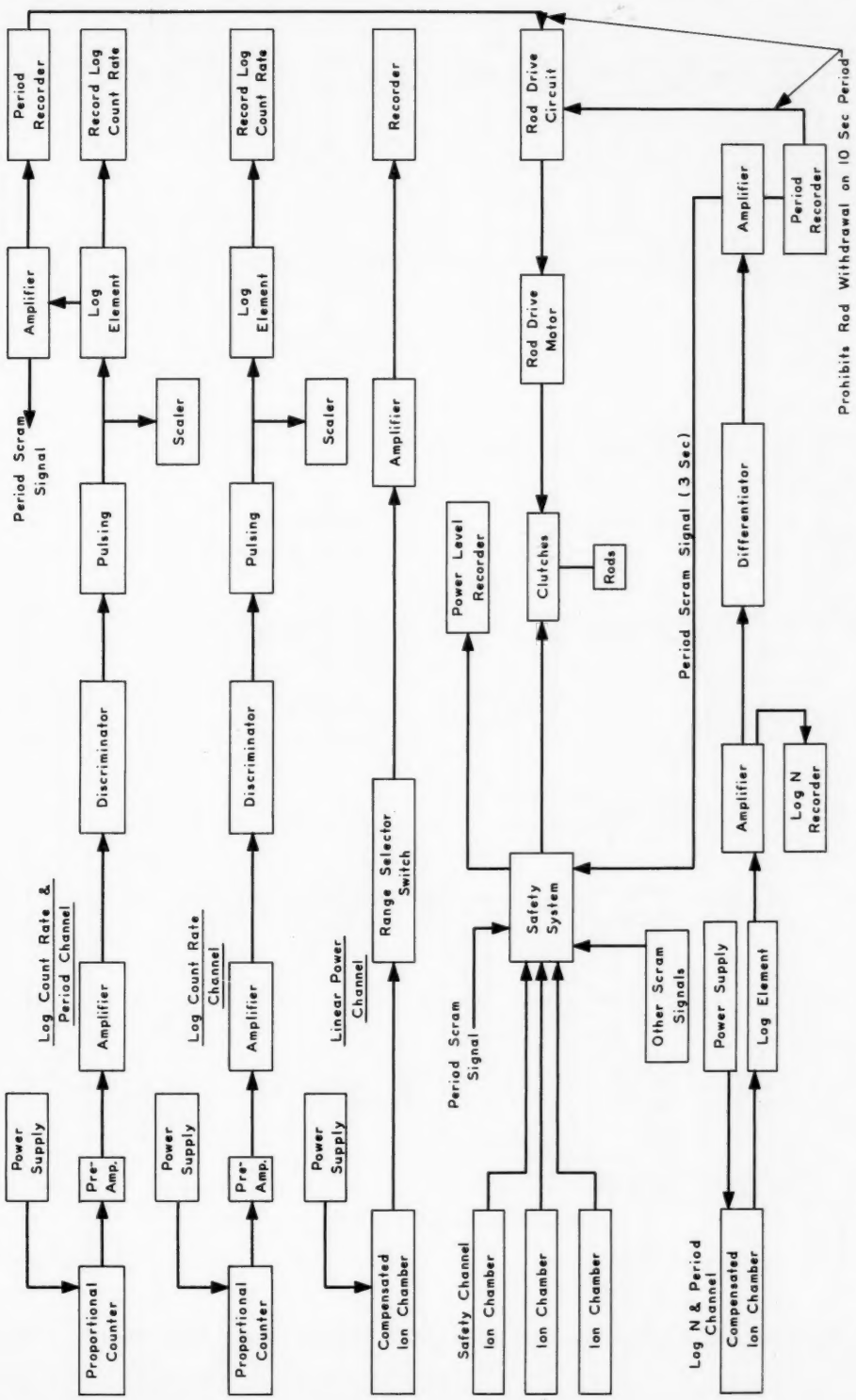

Fig. VIII-2 Block diagram[2] of nuclear instrumentation system, Stationary Medium Power Plant No. 1A (SM-1A).

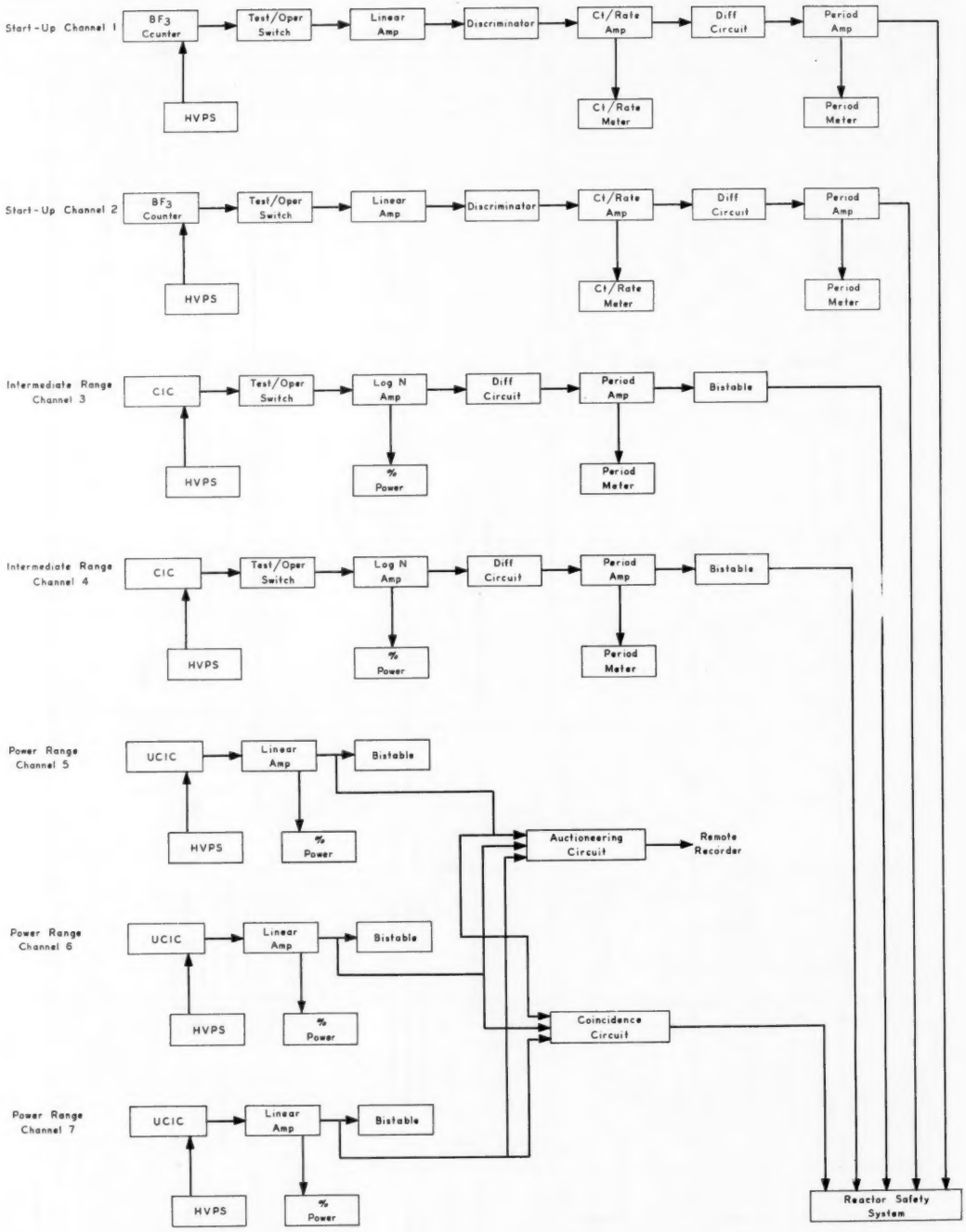

Fig. VIII-3 Block diagram[3] of nuclear instrumentation system, Portable Medium Power Plant No. 1 (PM-1).

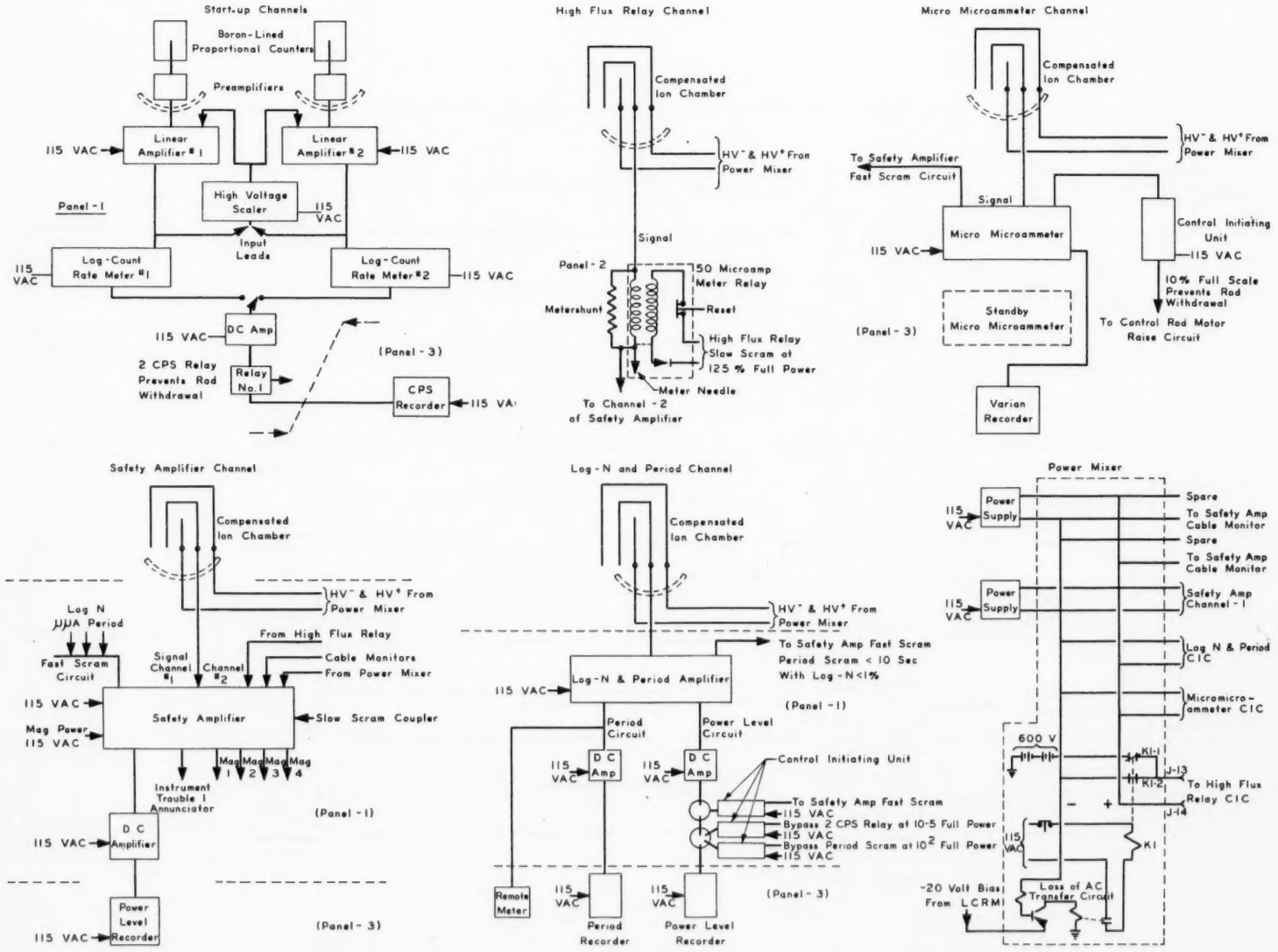

Fig. VIII-4 Block diagram[4] of nuclear instrumentation system, Vallecitos Boiling-Water Reactor (VBWR).

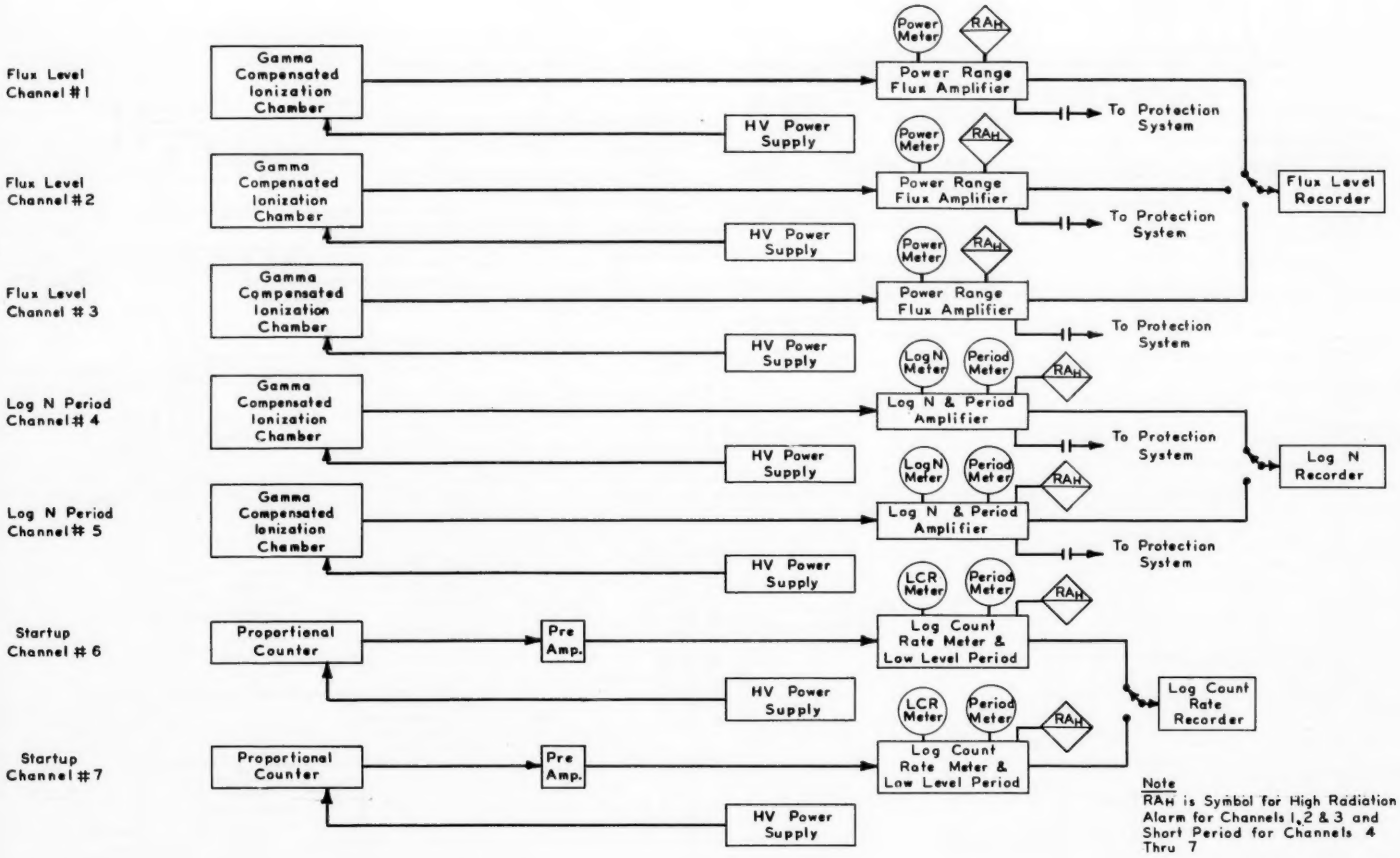

Fig. VIII-5 Block diagram[5] of nuclear instrumentation system, Humboldt Bay Power Plant.

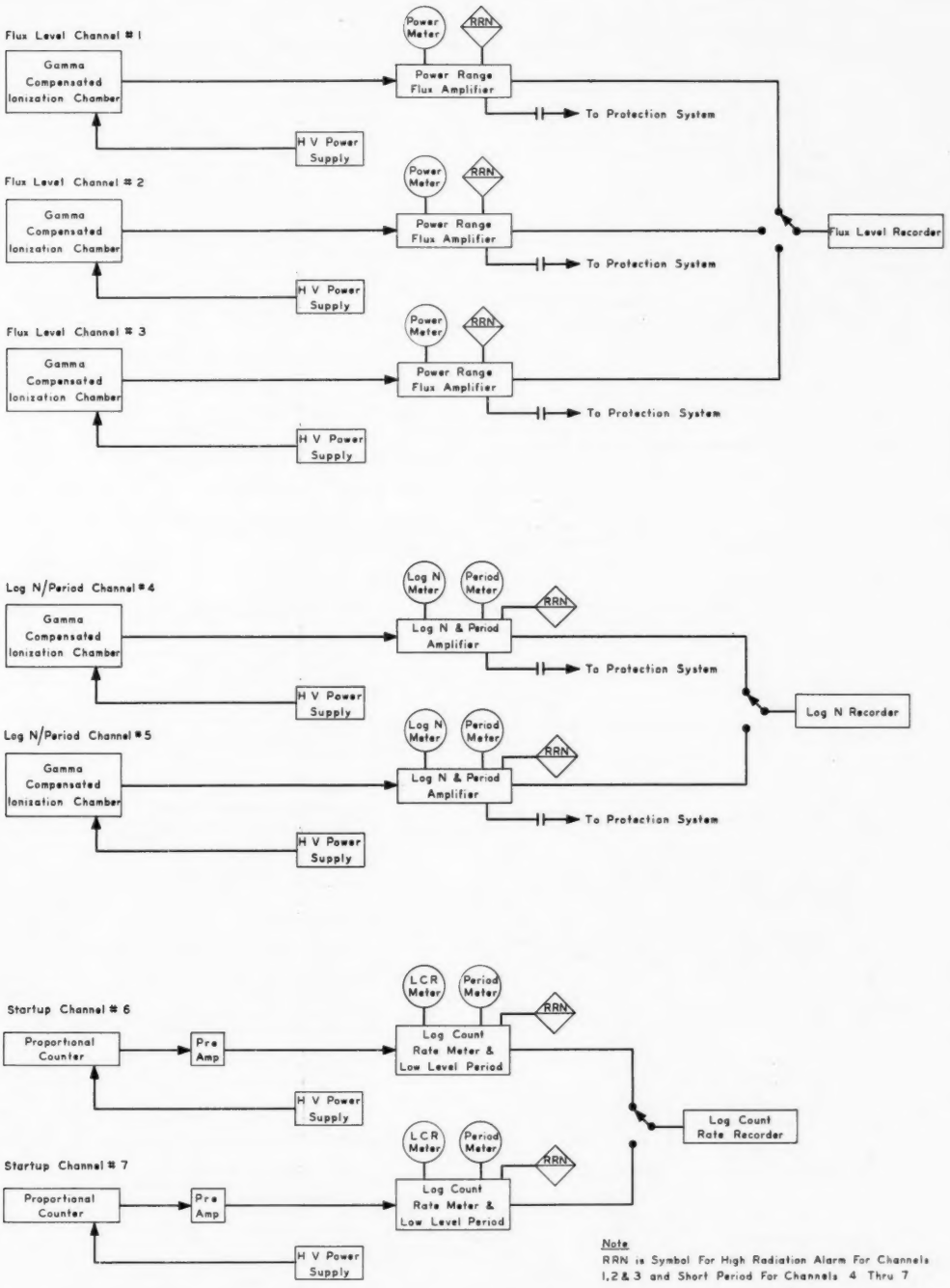

Fig. VIII-6 Block diagram[6] of nuclear instrumentation system, Big Rock Point reactor.

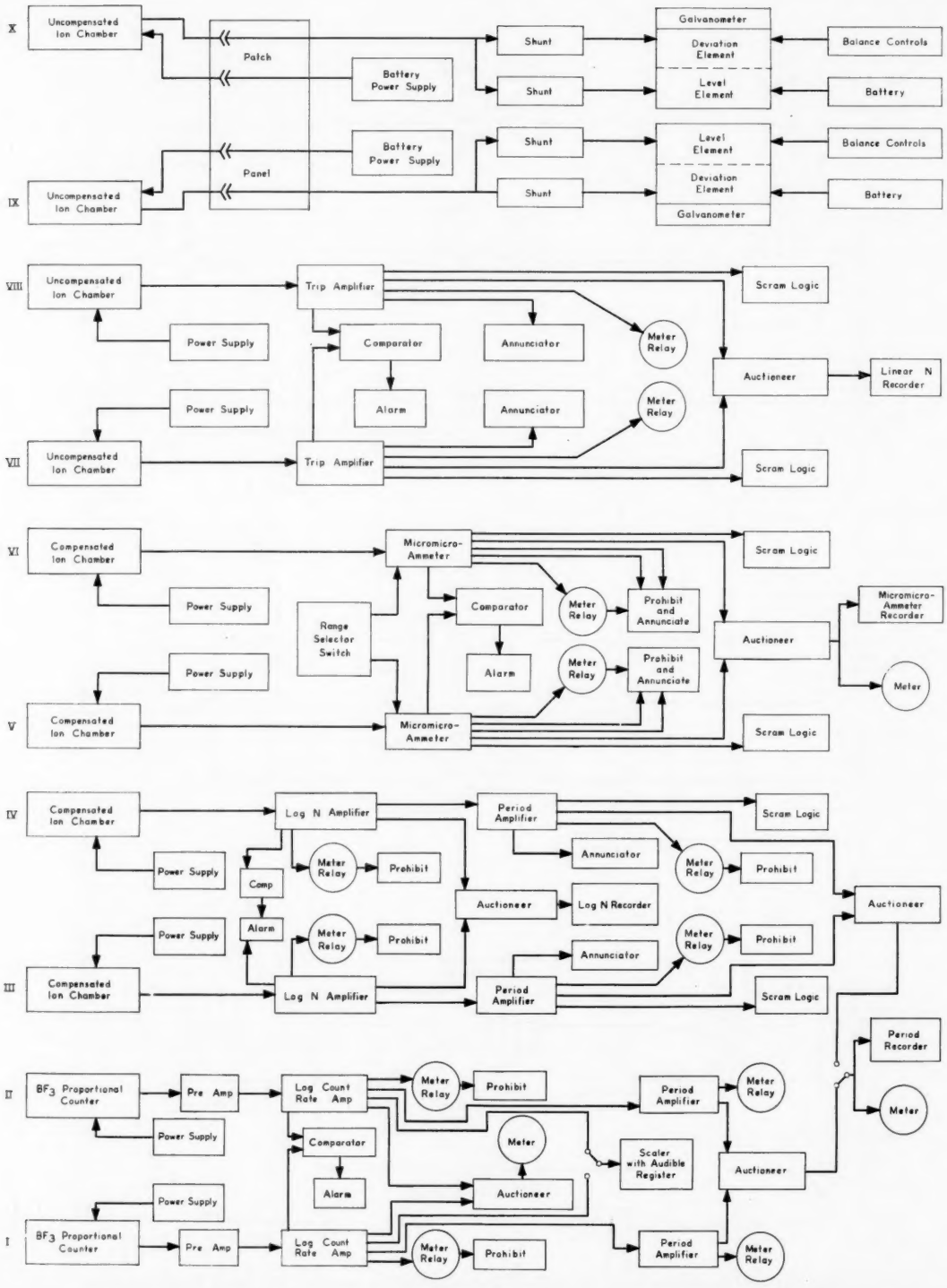

Fig. VIII-7 Block diagram[7] of nuclear instrumentation system, Boiling Nuclear Superheater (BONUS) Power Station.

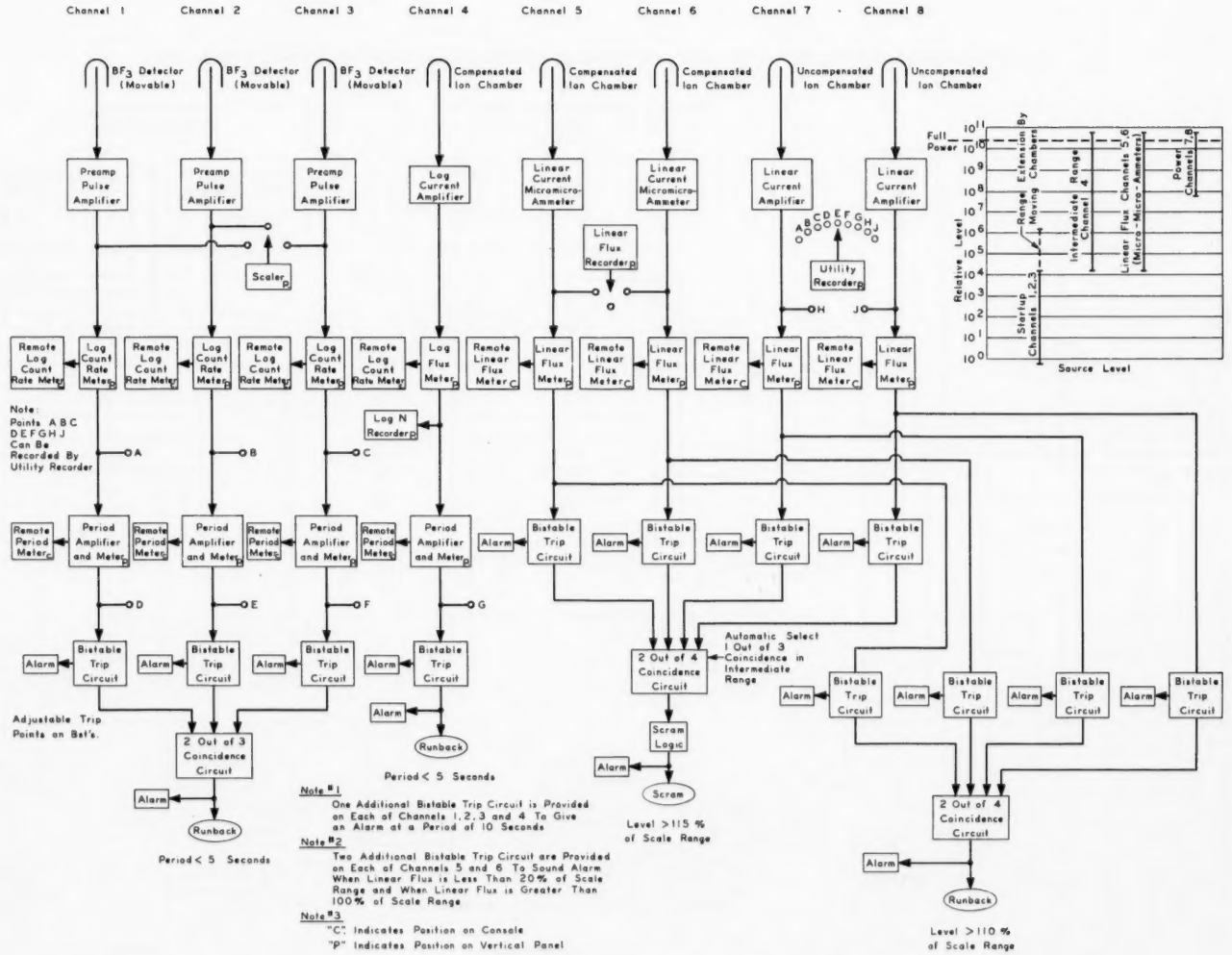

Fig. VIII-8 Block diagram[8] of nuclear instrumentation system, Pathfinder Atomic Power Plant.

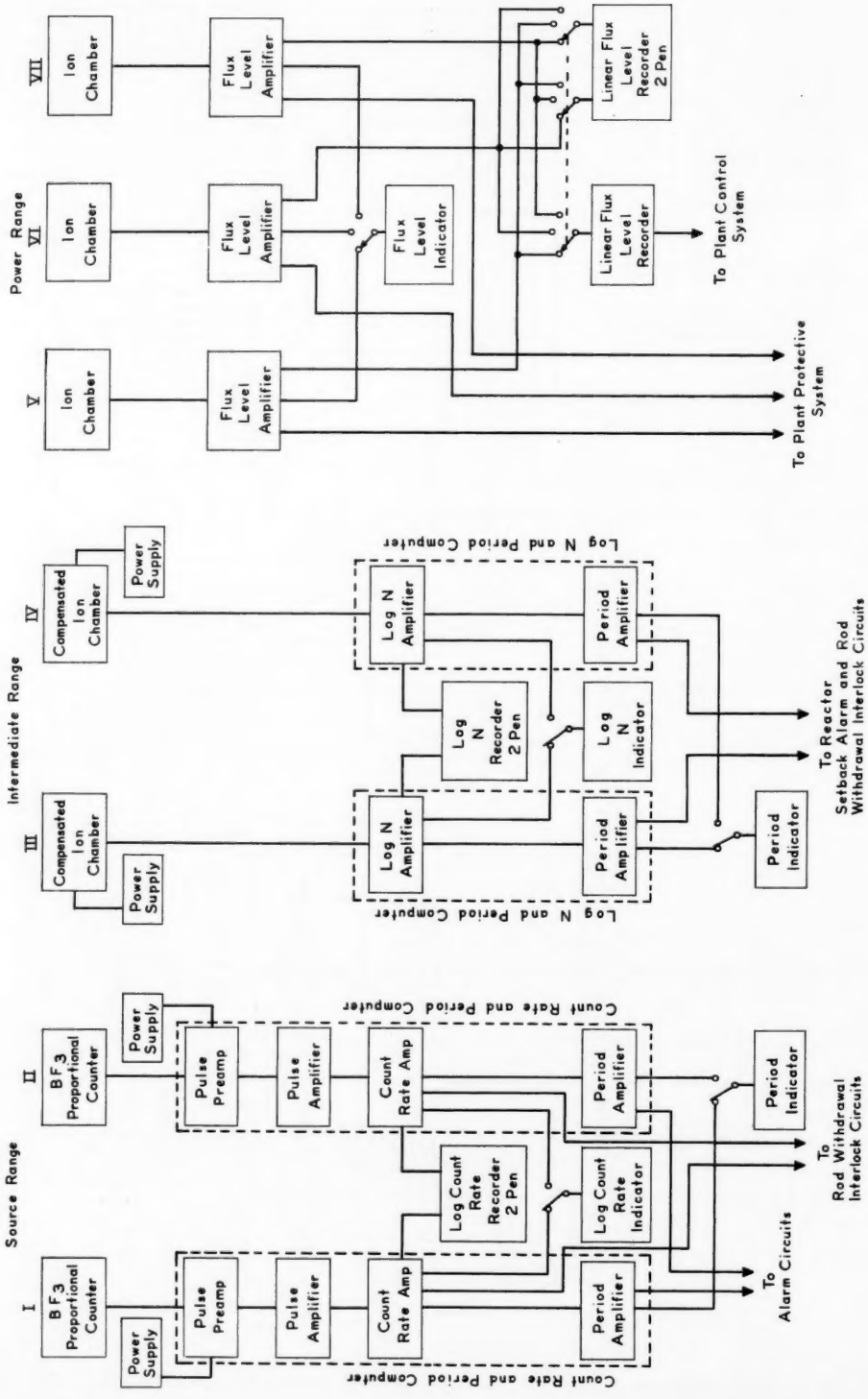

Fig. VIII-9 Block diagram[9] of nuclear instrumentation system, Piqua Nuclear Power Facility.

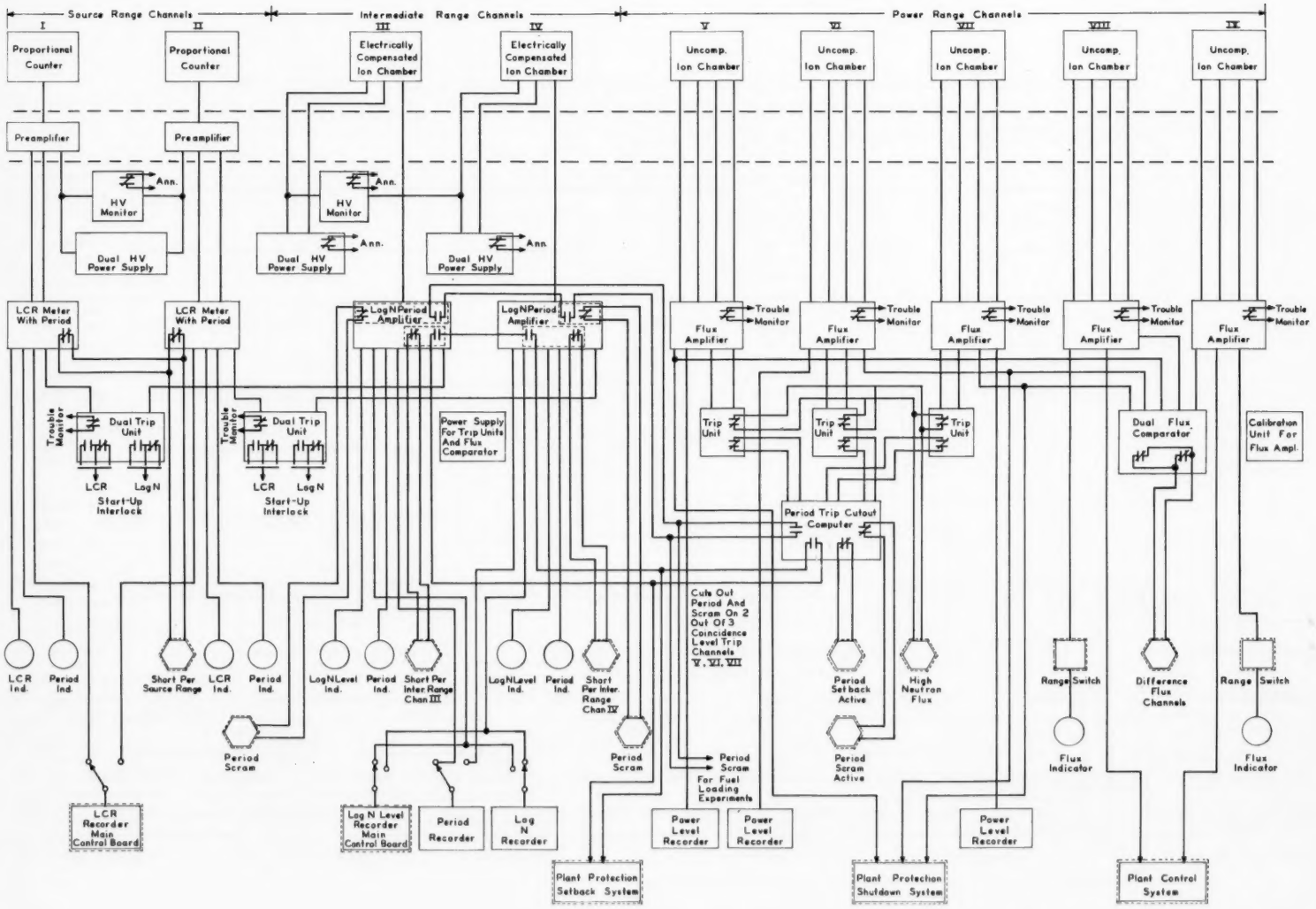

Fig. VIII-10 Block diagram[10] of nuclear instrumentation system, Sodium Graphite Reactor (SGR).

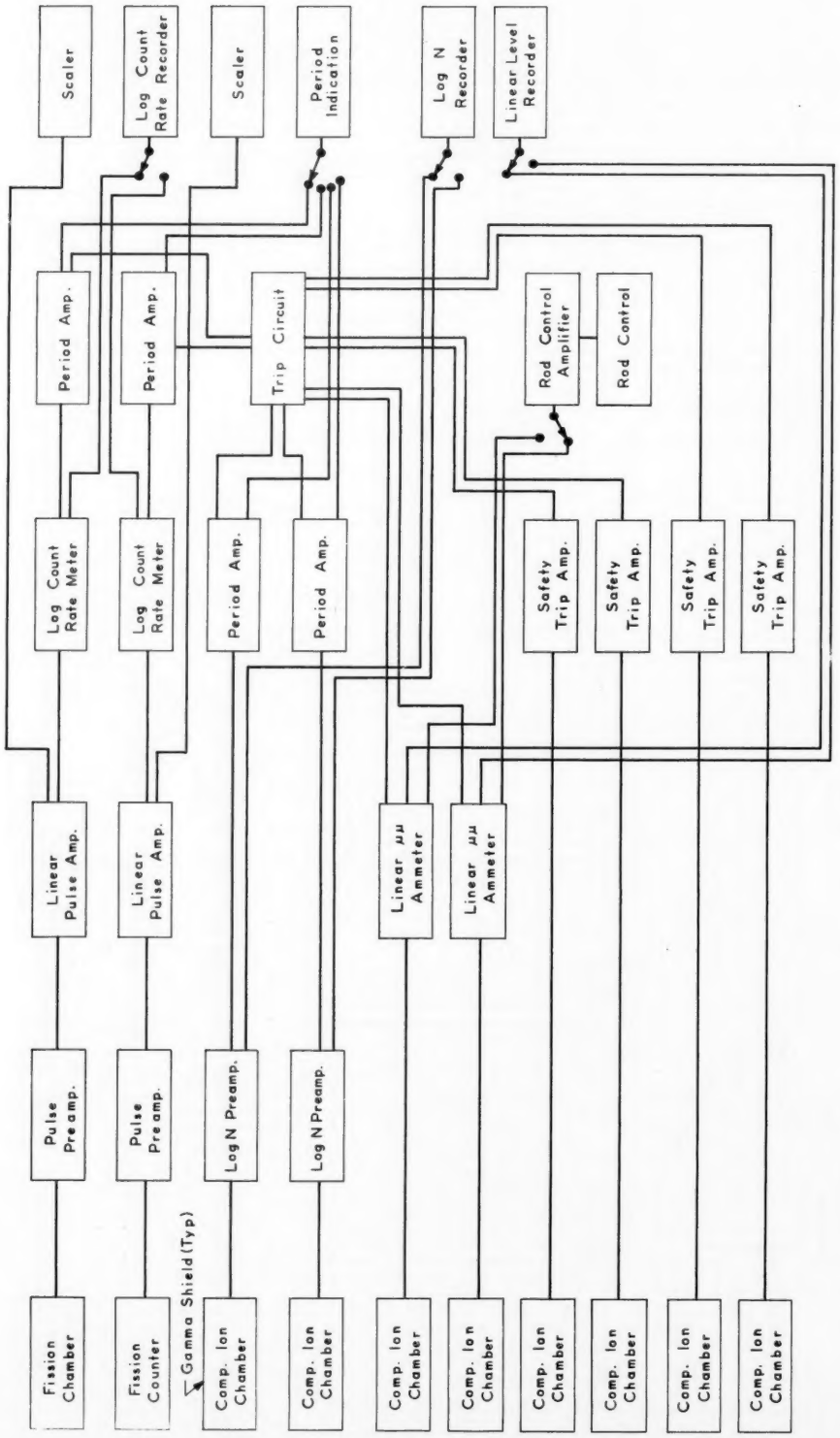

Fig. VIII-11 Block diagram[11] of nuclear instrumentation system, Experimental Breeder Reactor No. 2 (EBR-II).

Table VIII-1 NUCLEAR INSTRUMENTATION SYSTEMS INFORMATION*

Reactor location (name)	Reactor designer	1 Total no. of channels	2 No. and type of detectors: Source range	3 No. and type of detectors: Intermediate range	4 No. and type of detectors: Power range	5 Low-level period amplifier	6 Low-level period trip	7 Period information recorded	8 Galvo. chain included	9 Type of automatic power-level control
Pressurized-water reactors:										
Parr, S. C. (CVTR)[1]	Westinghouse Electric Corp.	8	2 BF_3's	3 CIC's	3 UIC's	Yes	Yes	No	No	Demand following (thermodynamic comparator)
Ft. Greely, Alaska (SM-1A)[2]	Alco Products, Inc.	7	1 BF_3 1 FC	2 CIC's	3 UIC's	Yes	Yes	Yes	No	Negative temperature coefficient
Sundance, Wyo. (PM-1)[3]	Martin Co.	7	2 BF_3's	2 CIC's	3 UIC's	Yes	Yes	Yes	No	
Boiling-water reactors:										
Pleasanton, Calif. (VBWR)[4]	General Electric Co.	6	2 boron-lined counters	4 CIC's		No	No	Yes	Yes	Subject to experiment
Humboldt Bay, Eureka, Calif.[5]	General Electric Co.	7	2 BF_3's	2 CIC's	3 CIC's	Yes	No	No	No	None
Big Rock Point, Mich.[6]	General Electric Co.	7	2 BF_3's	2 CIC's	3 CIC's	Yes	No	No	No	None
Punta Higuera, Puerto Rico (BONUS)[7]	General Nuclear Engineering Corp.	10	2 BF_3's	2 CIC's	2 CIC's 4 UIC's	Yes	No	Yes	Yes(2)	None (bypass control)
Sioux Falls, Minn. (Pathfinder)[8]	Allis-Chalmers Mfg. Co.	8	3 BF_3's	1 CIC (2 CIC's)	2 UIC's	Yes	Yes	Yes†	No	
Organic-cooled reactors:										
Piqua, Ohio[9]	Atomics International	7	2 BF_3's	(2 CIC's and 3 UIC's)		Yes	No	No	No	Demand following
Liquid-metal-cooled reactors:										
Hallam, Nebr. (SGR)[10]	Atomics International	9	2 BF_3's	2 CIC's	5 UIC's	Yes	No	Yes	No	Demand following‡
NRTS, Idaho (EBR-II)[11]	Argonne National Laboratory	10	2 FC's	(8 CIC's)		Yes	Yes	No	No	Constant flux

*Key to abbreviations: BF_3 = boron trifluoride gas-filled proportional counter; FC = fission chamber; CIC = compensated ion chamber; UIC = uncompensated ion chamber.

†Pathfinder period information can be recorded on a utility recorder.

‡The Hallam-plant automatic power-level controller provides compound control of regulating-rod position, primary and secondary sodium pump speeds, feed-water valve, attemperator valve, and turbine governor. A neutron-flux signal is apparently used as part of the regulating-rod position control. Three additional in-core channels are provided for flux mapping during critical experiments.

NUCLEAR SCIENCE ABSTRACTS

The U. S. Atomic Energy Commission, Division of Technical Information, publishes *Nuclear Science Abstracts (NSA)*, a semimonthly journal containing abstracts of the literature of nuclear science and engineering.

NSA covers (1) research reports of the U. S. Atomic Energy Commission and its contractors; (2) research reports of government agencies, universities, and industrial research organizations on a world-wide basis; and (3) translations, patents, books, and articles appearing in technical and scientific journals.

Complete indexes covering subject, author, source, and report number are included in each issue. These are cumulated quarterly, semiannually, and annually providing a detailed and convenient key to the literature.

Availability of *NSA*

SALE *NSA* is available on subscription from the Superintendent of Documents, U. S. Government Printing Office, Washington 25, D. C., at $22.00 per year for the semimonthly abstract issues and $15.00 per year for the four cumulated-index issues. Subscriptions are postpaid within the United States, Canada, Mexico, and all Central and South American countries, except Argentina, Brazil, British and French Guiana, Surinam, and British Honduras. Subscribers in these Central and South American countries, and in all other countries throughout the world, should remit $27.50 per year for subscriptions to semimonthly abstract issues and $17.50 per year for the four cumulated-index issues.

EXCHANGE *NSA* is also available on an exchange basis to universities, research institutions, industrial firms, and publishers of scientific information. Inquiries should be directed to the Division of Technical Information Extension, U. S. Atomic Energy Commission, P. O. Box 62, Oak Ridge, Tennessee.

TECHNICAL PROGRESS REVIEWS may be purchased from Superintendent of Documents, U. S. Government Printing Office, Washington 25, D. C. for $2.00 per year for each subscription or for $0.55 per issue. The use of the coupon below will facilitate the handling of your order.

POSTAGE AND REMITTANCE: Postpaid within the United States, Canada, Mexico, and all Central and South American countries except as hereinafter noted. Add $0.50 per year, or $0.15 per single issue, for postage to all other countries, including Argentina, Brazil, British and French Guiana, Surinam, and British Honduras. Payment should be by check, money order, or document coupons, and MUST accompany order. Remittances from foreign countries should be made by international money order, or draft on an American bank, payable to the Superintendent of Documents, or by UNESCO book coupons.

order form

SUPERINTENDENT OF DOCUMENTS
U. S. GOVERNMENT PRINTING OFFICE
WASHINGTON 25, D. C.

Enclosed:
document coupons ☐ check ☐ money order ☐

Charge to Superintendent of Documents No. _____

Please send a one-year subscription to

☐ REACTOR MATERIALS
☐ POWER REACTOR TECHNOLOGY
☐ NUCLEAR SAFETY
☐ REACTOR FUEL PROCESSING

(Each subscription $2.00 a year; $0.55 per issue.)

SUPERINTENDENT OF DOCUMENTS
U. S. GOVERNMENT PRINTING OFFICE
WASHINGTON 25, D. C.

(Print clearly)

Name _____

Street _____

City _____ Zone ____ State _____